Design, Test, and Evaluation of a High Powered 4 DOF Prosthetic Leg for Transfemoral Amputees

Brandyn T. Greczek

Dissertation submitted to the Faculty of the
Virginia Polytechnic Institute and State University
in partial fulfillment of the requirements for the degree of

Master of Science
in
Mechanical Engineering

Alan T. Asbeck, Chair
Alexander Leonessa
Maury A. Nussbaum

May 7th, 2019
Blacksburg, Virginia

Keywords: Transfemoral, Transtibial, Prosthesis, High Power

Design, Test, and Evaluation of a High Powered 4 DOF Prosthetic Leg for Transfemoral Amputees

Brandyn T. Greczek

(ABSTRACT)

A high powered 4 DOF prosthesis for transfemoral amputees is presented in this paper. The prosthesis utilizes series elastic actuators with high powered hobby grade helicopter motors capable of providing 2880 W of power each for knee and ankle pitch and ankle roll. In addition, a yaw motor with a planetary gearbox combination is used for yaw actuation providing up to 21 Nm of torque. The prosthesis was designed to accommodate a variety of activities including, but not limited to, walking, running, and stair climbing.

Design, Test, and Evaluation of a High Powered 4 DOF Prosthetic Leg for Transfemoral Amputees

Brandyn T. Greczek

(GENERAL AUDIENCE ABSTRACT)

A high powered prosthesis for transfemoral amputees is presented in this paper. Four control mechanisms, three of which are in series with springs to reduce the total power requirement of the motors, are used on the prosthesis to provide power to all motions of the leg. The prosthesis is capable of providing powered motion for knee and ankle pitch, ankle roll, and ankle yaw, i.e. ankle rotation from side to side. The prosthesis was designed to handle a variety of activities including, but not limited to, walking, running, and stair climbing.

Acknowledgments

I would like to thank my committee chairman Dr. Alan Asbeck, for making me a part of the Assistive Robotics Lab. I would also like to thank Dr. Leonessa and Dr. Nussbaum for serving on my advisory committee. To my lab mates that helped me with my project, I thank Taylor Pesek for his invaluable suggestions in programming and debugging, Athulya Simon and Michael Heng for wearing the prosthesis for initial testing and data collection, and of course my family for their constant encouragement and motivation throughout my graduate endeavors, thank you.

Contents

List of Figures

List of Tables

List of Abbreviations

ABA Able Bodied Adapter

$BLDC$ Brushless Direct Current

CAD Computer Aided Design

DOF Degree of Freedom

EMI Electro Motive Interference

g gravitational acceleration constant

Hz Hertz

$I2C$ Inter-Integrated Circuit

IMU Inertial Measurement Unit

kg kilogram

Kv Motor velocity constant RPM/V

m meters

MCU Microcontoller Unit

mm millimeters

N Newtons

PCB Printed Circuit Board

rad radians

RAM Random Access Memmory

RC Remote Control

ROM Range of Motion

RPM rotations per minute

SEA Series Elastic Actuator

TF Transfemoral

TT Trasntibial

USB Universal Serial Bus

V Volts

W Watts

Attribution

I contributed extensively to the design, prototyping, and initial testing of the high powered 4 DOF prosthetic leg described in this thesis. I was fully responsible for the selection of the sensors used for instrumenting the leg, the selection of the motors for each DOF that would satisfy the joint power requirements, and implementing, integrating, and programming the prosthesis with the selected electronics. In addition, I am responsible for the modeling of the inertial forces of the prosthesis which will be integrated into a more advanced controller architecture for future use.

I was also responsible for calculating the required data rates for data logging of the sensor data to be used for data analysis, using both I2C and Serial communication. I also created a MATLAB script which takes the logged data, post processes it, and plots all of the parameters for easy gait analysis. My final contribution is this thesis, documenting all of the design choices for the prosthesis, and any future changes that must be made for further testing of the prosthesis.

Chapter 1

Introduction

In the United States alone there are approximately 1.9 million amputees, of those about 18.5% of them are trans-femoral amputees (TFA) [1]. The loss of limbs may be caused by vascular degeneration or traumatic injury among others [2]. In addition, 32% to 84% are negatively affected by traumatic amputations, e.g. due to a car crash, and include depression, post traumatic stress disorder (PTSD), and/or phantom limb phenomenon [3]. Amputation also limits and makes more difficult the ability to perform everyday tasks, and as a result, may hinder the affected individual's body image, and potentially their self-esteem [4]. Therefore, a prosthesis that can give amputees back their mobility, no matter the type of physical activity they are performing, is much needed.

There are two types of lower limb amputations, trans-femoral (TF) amputation, i.e. above the knee amputation, and trans-tibial (TT) amputation, i.e. below the knee amputation. In addition, this may be either a unilateral (one limb amputated) or bilateral amputation (both limbs amputated). Depending on the severity of the amputation, a bilateral trans-femoral amputation being the most severe; amputees compensate using their intact limbs which leads to asymmetries in their gait. The joints used for compensation include their hip, knee, pelvis, and/or trunk, which leads to medical conditions such as osteoarthritis in the joints as a result of their gait compensation [5, 6, 7, 8, 9, 10]. However, compensation with multiple healthy joints leads to an increase in metabolic energy expenditure ranging from 10-60%, when compared to able-bodied individuals depending on the type of gait,

i.e. walking, running, stair climbing, sloped ascent; level of the amputation, i.e. TT, knee disarticulation, TF, and hip disarticulation; and the length of the residual limb, i.e. stump length [11, 12, 13, 14].

1.1 Motivation

Lower limb prosthetic devices for both TF and TT amputees have greatly improved over the past decade, resulting from technological improvements in sensory feedback systems and power electronics. However, before powered lower limb prostheses were available most lower limb prostheses were unpowered or energetically passive, meaning that they can store or dissipate energy, but not generate it. Prostheses comprised of fully passive components are limited in their ability to provide a natural gait to the user, and being passive in nature, require the prosthetic wearer to compensate with their intact limbs. In addition, these prostheses do not adapt well to changes in terrain since they offer no powered degrees of freedom (DOF) or sensory feedback system to adjust to these changes. Therefore, passive prostheses cannot accurately duplicate the gait cycle used by able-bodied individuals, they lack powered degrees of freedom and sensory feedback, and are not suitable for changes in terrain, figure 1.1 [15]. Recently though, fully powered prostheses have become commercially available which generate net positive power to the user to better mimic the gait of a biologically intact limb. In addition, most powered prostheses lack the power to generate the net positive power required for activities such as stair climbing and running.

Figure 1.1: Image of an unpowered prosthetic leg used for trans-femoral amputees.

1.2 Contribution

The aim of this work is to present a prosthetic wearer with a leg that can accurately mimic a biological leg, in this paper we present a four DOF prosthesis able to produce powered motions in the sagittal plane, frontal, and transverse plane (pitch, roll, and yaw) in the ankle in addition to sagittal plane motion (pitch) in the knee. The actuators responsible for knee and ankle pitch and ankle roll are powered by a brushless direct current (BLDC) motor connected to a ball screw via a timing belt and pulley system. The yaw DOF actuator uses a planetary gearbox and motor combination connected to a center shaft via a timing belt and pulley system. These actuators provide the power and required range of motion (ROM) for all degrees of freedom to ascend and descend stairs as well as run at 2.7 m/s (6 mph) in addition to walking.

To replicate natural human motion, load cells, joint encoders, motor encoders, and current sensors were implemented to control series elastic actuators (SEAs) which incorporate high powered helicopter remote control (RC) motors. The use of RC helicopter motors as opposed to a more commonly used motor, e.g. Maxon EC-40, makes the prosthesis affordable, robust, and reliable. The use of high powered helicopter motors also provides ample power for any of the desired physical activities the amputee would like to perform.

An able-bodied leg is able to detect when body weight force and forces beyond that are being applied, e.g. during a weighted squat. To replicate this behavior, two controllers were implemented, a middle-level torque reference controller (impedance controller), and a lower level force controller used to add current when needed to the impedance controller's signal based on the present joint forces. These controllers were based on that of Sup (2008) [16]. The use of these two controllers working together makes the leg more biomimetic in nature and allows for smoother control when large forces, body weight and beyond, are imparted

on the joints.

This paper describes the initial testing of the prosthesis on an able-bodied individual using an able-bodied adapter. The tests conducted include walking at a moderate speed of 0.67 m/s (1.5 mph) while testing for basic gait functionality, i.e. joint angle and torque trajectory tracking. During the tests both the yaw DOF and roll DOF were kept at 0°; however, the roll DOF experienced slight deviations from 0° due to unforeseen asymmetric loading conditions. The results of the treadmill tests are presented.

Finally, since the prosthesis is expected to last for a full day of physical activity, the effects of using high powered motors for motion control have been analyzed to determine the power consumption and expected battery life of the prosthesis. In addition, the prosthesis discussed in this work has several novel features,

- First prosthesis to incorporate a fully powered yaw DOF.
- High powered motors to perform high force tasks greater than body weight.
- First analysis of optimizing a series elastic actuator to minimize power consumption during all of walking, running, and stair climbing.

1.3 Thesis Organization

The structure of this document is as follows. Chapter 2 provides an overview of the current technology commercially available and the latest research at Universities for powered prosthetic limbs for TF amputees. Chapter 3 presents an overview of the system and the calculations that were performed prior to component selection for the prosthesis. Namely, the calculations for determining the minimum motor power required given joint power requirements, optimizing the series elastic (SE) elements of the SEA for energy return, yaw DOF torque requirements, and finite element analysis (FEA) on critical components. Chapter 4 details the mechanical design of the prosthesis, discussing the reasons for the design choices made in selecting motors, ball screws, SE spring elements, and the yaw actuator. Chapter 5 details the electrical, communication, and control systems of the prosthesis. Namely, it details the design of the circuit boards used in the system, the inter-integrated circuit (I2C) and universal asynchronous receiver-transmitter (UART) communications, and controllers used for automation. In addition, it discusses the kinematic modeling of the prosthesis. Chapter 6 presents the results from the 0.67 m/s (1.5 mph) treadmill walking tests. Chapter 7 discusses the results of the tests in further detail evaluating the prosthesis's performance. Chapter 8 concludes the work and chapter 9 discusses the future work which must be completed before further testing of the prosthesis.

Chapter 2

Background

With advances in battery technology, small and powerful motors, hydraulics, and pneumatics, powered prostheses are becoming more common. Now, there are commercially available fully powered lower limb prostheses for TF and TT amputees with different forms of actuation, including pneumatic, hydraulic, motor/gearbox and/or series elastic actuation [16, 17, 18]. These prostheses adapt to the terrain and the desired motion of the user by actively varying the damping of the powered joints on the fly via microprocessors. Endolite has a large selection of prostheses for both TF and TT amputees, including standalone knee and ankle actuators which use hydraulics and/or pneumatics for actuation. Endolite's "Linx" full limb system offers four microprocessor control, Bluetooth connectivity for calibrating the prosthesis to the user, is built for an active lifestyle, and uses hydraulic actuators for operation, figure 2.1a [19]. Ottobock also offers a wide range of stand-alone active knee and ankle prostheses as well as three full limb integrated knee ankle prostheses. Ottobock's "Helix 3D" is a fully functioning microprocessor controlled leg which offers both knee and ankle actuation in addition to pelvic rotation via hydraulic actuation, as shown in figure 2.1b [20, 21].

a

(a) Endolite LiNX full leg system for TFAs.

b

(b) Ottobock's Helix 3D full leg system including pelvic rotation for hip disarticulation.

Several research institutions have created prostheses for TF and TT amputees that accommodate more demanding forms of human locomotion aside from walking and sloped ascent/descent including, stair climbing, running, and potentially jumping. In addition, the incorporation of the roll DOF to the ankle and its effects on human gait is being explored [16, 22, 23]. AMBER Lab at Caltech has created the AMPRO3 microprocessor controlled prosthesis for TFAs which includes knee and ankle pitch as well as an unpowered compliant passive ankle roll DOF. AMPRO3 uses planar torsional springs as their SEA elements for the powered degrees of freedom, and a nonlinear optimization based controller for prosthesis control. The prosthesis is currently undergoing initial testing with walking and sloped ascent/descent locomotion. Figure 2.2 shows the AMPRO3 prosthesis [23]

The SPARKy 3 microprocessor controlled ankle prosthesis uses parallel ankle actuators to generate motion in both the sagittal and frontal planes of motion, i.e. ankle pitch and roll. The prosthesis uses SEAs with dual Maxon EC-30 motors and die springs as the SE element.

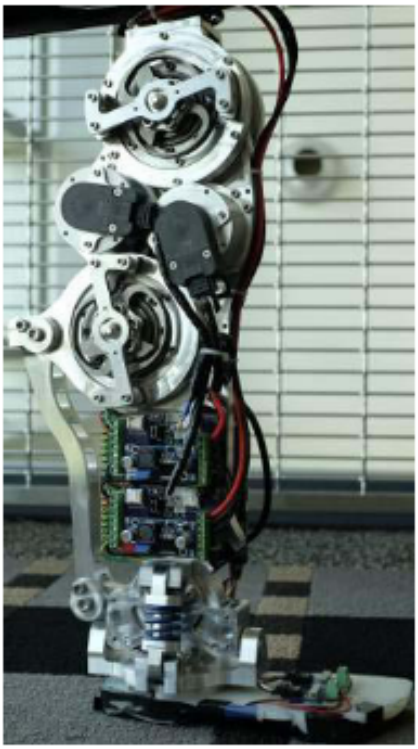

Figure 2.2: AMBER Lab's AMPRO3 prosthesis for TFAs.

The SPARKy 3 is designed to be a high powered ankle capable of all forms of human ankle locomotion including running, and jumping, with a peak power output of 1500 W. Testing of the ankle in running, and jumping has yet to be performed with the SPARKy 3, though walking, sloped ascent/descent, stair climbing, and jogging have been tested on the previous versions. Figure 2.3 shows the latest design, SPARKy 3 [22, 24].

Vanderbilt University has produced a fully powered microprocessor controlled knee and ankle prosthesis for TFAs which uses SEAs with Maxon EC-30 motors and die springs as the elastic element. For control, a multi-level controller is used which includes, a high-level user intent controller, a middle-level finite state impedance controller which varies the stiffness and damping coefficients for each state, and a low-level force controller. This prosthesis has been tested for walking, sloped ascent/descent, running up to 2.5 m/s (5 mph), and stair climbing. Figure 2.4 shows the Vanderbilt University prosthesis [16, 25, 26].

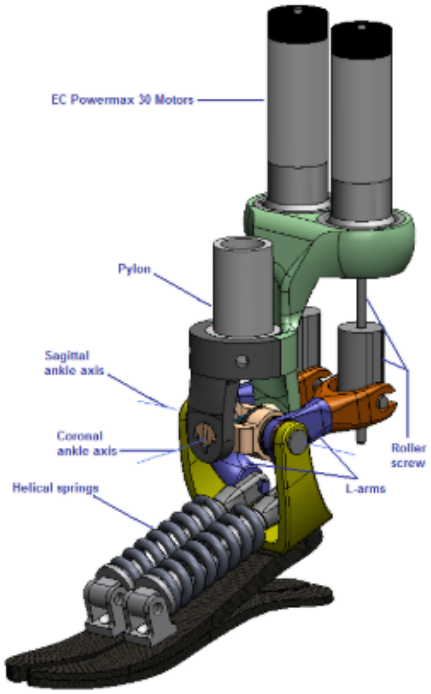

Figure 2.3: SPARKy 3 powered 2 DOF prosthetic ankle for TTAs.

The development of the prostheses presented from both the commercial and research fields show that this area of product development and research is still highly active, and that much work has yet to be done to mimic human locomotion completely. In addition, the prostheses presented show that both stair climbing and running are more difficult to achieve since these modes of human locomotion require larger joint torques, and therefore a higher motor power output [27, 28]. Lastly, no prior work has been done concerning the addition of the transverse plane of motion of the ankle, i.e. the yaw DOF, to a prosthesis in order to study its effects on the gait cycle. Though no prostheses are available which incorporate yaw motion, data from studies on the human gait show that yaw does play a significant role in providing a more natural, symmetric, and stable gait. During level walking alone, the ankle moves around 2° (internal axial rotation) and -6° (external axial rotation) in the transverse plane (yaw). Figure 2.5 shows the motions of all three degrees of freedom of the ankle, i.e. frontal, transverse, and sagittal planes [29, 30]. If all degrees of freedom are not permitted

Figure 2.4: Vanderbilt Universities fully powered prosthetic leg for TFAs.

by the prosthesis, the wearer's hip and knee joints must accommodate those motions, which may contribute to osteoarthritis [5].

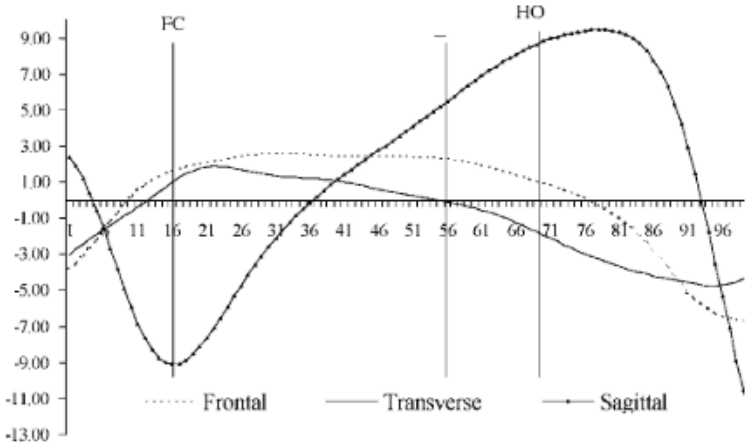

Figure 2.5: The range of motion of each of the degrees of freedom of the ankle. The yaw is the transverse plane of motion.

Chapter 3

System Overview and Design Requirements

3.1 System Overview

The prosthesis described in this work was designed to be a testbed capable of performing all forms of physical activity. The prosthesis uses SEAs for knee pitch, ankle pitch and roll, and a geared motor for the yaw DOF with no SE element. BLDC motors and lithium batteries were chosen over other forms of actuation (pneumatic, hydraulic, etc.) since they provide the needed power for walking, running, and stair climbing, and do not require heavy accessories, e.g. pneumatic pumps, for actuation. The SEAs for both the knee and ankle joints use large diameter ball screws to allow for back-drivability and a large ROM for each of the joints ($>$ 90° for the knee and $>$ 60° for the ankle). The yaw DOF with its geared motor allows for a ROM of ±15°. Figure 3.1 shows the final CAD model of the prosthesis described in this work.

The microprocessor used to perform all of the computations for control of the prosthesis is the TIVA C Series TM4C123GH6PM microcontroller, figure 3.2. Table 3.1 gives the specifications of the microcontroller. One microcontroller is used for each DOF with a Master module commanding each over I2C. In addition, the Master Tiva transmits joint angles, speeds, forces, and motor current to a computer via serial communication. The

communication may be expanded to send over IMU data, and motor accelerations as well if needed for data analysis. Using this information the Master module sends equilibrium angles to the Slaves at a specified time once certain conditions in the gait cycle have been met, thereby making the prosthesis passive in nature. This allows the actuators to generate the forces required by each of the joints to complete the gait cycle while still allowing the user to maintain control over the prosthesis.

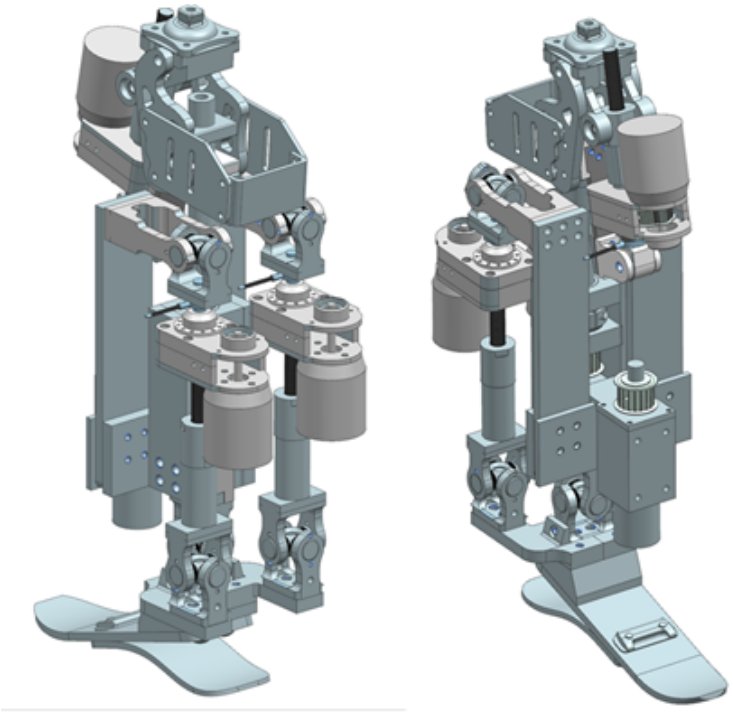

Figure 3.1: Final CAD model of the prosthesis described in this work.

Features	*Description*
MCU	32-bit ARM® Cortex™-M4 80-MHz processor core
Flash (KB)	256
RAM (KB)	32
Dimensions (mm)	63.5 x 50.8

Table 3.1: Tiva C TM4C123GH6PM Specifications

Motor and ball screw sizing for each joint was based on the most demanding gait. The most demanding gait for the ankle is running in which the velocities and torques were the largest.

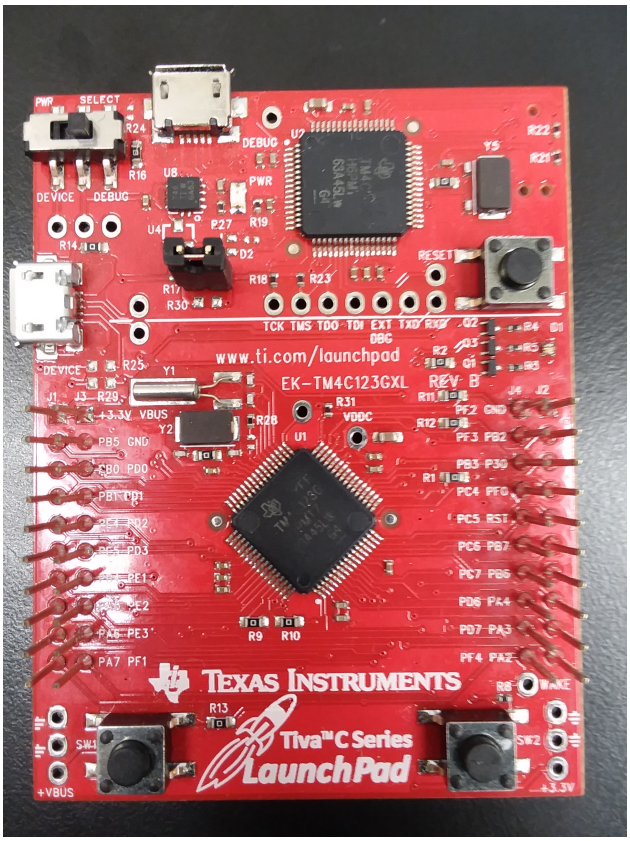

Figure 3.2: TM4C123GH6PM Tiva C Series Microcontroller used for robotic manipulation and control of leg.

For the knee the largest joint velocity occurs during stair climbing, and the largest torque occurs during running, as shown in Table 3.3. However, for the transverse plane of motion of the ankle (yaw) only walking data is available, and therefore, the yaw ROM was designed for this specification, $\pm 15°$. In addition, for the yaw motion, a simple calculation for the torque requirement gave an estimate of 17.5 Nm at the ankle during level walking, as explained in greater depth in section 3.1.4. Lastly, table 3.2 shows the initial design requirements for the prosthesis [31]. Note that in table 3.2 there is a gap between the walking and running speeds. This gap is the transition gap between walking and running, which varies from person to person [32].

Metric	*Ideal Value*
Walking Speed(m/s)	1.0 - 1.51
Running Speed (m/s)	2 - 2.68
Support Walking & Running Forces (kg)	100 - 300
Power for Walking & Running (W)	1000 - 2700
Battery Life (hr)	1 - 4
Weight (kg)	6.80 - 9.07
Height (m)	0.483 - 0.559

Table 3.2: Design Requirements for the Prosthesis

Gait Mode	*Joint*	*Speed (rad/s)*	*Torque (Nm/kg)*
Walking [33]	Knee	-7.17	0.56
	Ankle	-5.13	1.41
Running [27]	Knee	7.00	1.52
	Ankle	-7.68	1.84
Stair Climbing [28]	Knee	13.18	1.27
	Ankle	6.69	1.17

Table 3.3: Speed and torque requirements for each joint. The requirements are for the pitch degree of freedom since this is the degree of freedom that requires the greatest effort.

For testing in a laboratory setting with an able-bodied individual, an able-bodied adapter (ABA) was created, figure 3.3. Being a prototype, the system is tethered to a computer for data logging; however, it may easily be untethered once an on-board data logger, e.g. Universal Serial Bus (USB) module or Bluetooth device is implemented, and the batteries are placed in a fanny pack style pouch for easy portability. For initial laboratory testing the batteries are placed on the prosthesis wearers back with the microcontrollers off to the side.

3.1.1 Calculations

The calculations for the various components of the prosthesis used to provide the needed power and withstand the stresses experienced by each joint for each gait mode are based on the findings in table 3.3. In particular, the highest stresses occur during the running gait at

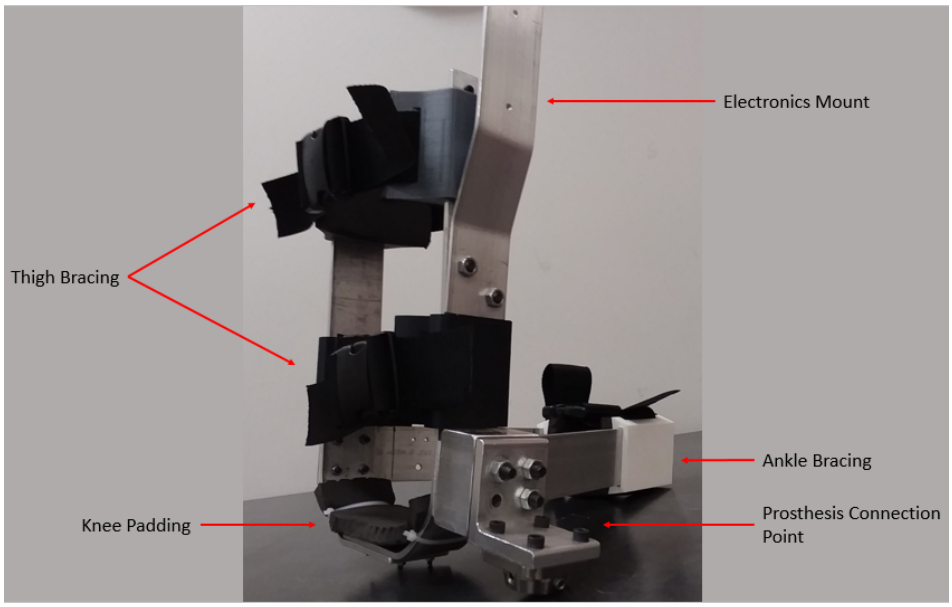

Figure 3.3: Final able bodied adapter used for initial testing of 4 degree of freedom high powered prosthetic leg.

2.68 m/s where upwards of 3 g, i.e. three times the force of gravity, may be felt, or >300 kg for a 100 kg individual, and therefore the structural components of the prosthesis were built to handle these loading conditions. [34, 35]. Note that sloped ascent/descent data was not analyzed since the actuators were built to accommodate both stair climbing and running which are more demanding on the joint power requirements, though the sloped ascent/descent data was available for use [33]. The data was fitted for a 100 kg individual, from which the maximum torque requirements for both the knee and ankle joints are 1.52 Nm/kg and 1.84 Nm/kg respectively. The maximum speed requirements for the knee and ankle were 13.18 rad/s and -7.68 rad/s respectively as seen in figures 3.4 and 3.5. These values for torque and speed were multiplied by safety factors of 1.3 and 1.5 respectively; however, they were lowered to 1.2 and 1.15, due to the capabilities of available motors, ball screws, and size and weight limitations as discussed in chapter 4. The maximum power requirement of each joint was then calculated by multiplying the resulting speed and torque together. The highest power requirement was 2751 W for the ankle in running, and 2494 W in stair climbing for

the knee. The appropriate ROM for knee pitch, and ankle pitch, roll, and yaw is roughly 0° to 90°, −30° to 30°, −35° to 35°, and −15° to 15° respectively. The calculations presented include speed and torque requirements for each gait mode, optimizing spring stiffness for the gait modes, the yaw DOF torque requirements, and finite element analysis (FEA).

3.1.2 Motor Sizing Calculations

Using data from Ounpuu (1994), Novacheck (1998), and Aldridge (2012) [27, 28, 36], speed vs. torque plots were generated to display the maximum power requirements of each of the joints with the selected actuator maximum power. Figures 3.4 and 3.5 show the maximum power requirements for the ankle and knee for each of the gait modes, i.e. walking, running, and stair climbing, compared to the actuator power. From these two figures, it is evident that the actuator is capable of meeting the needed power requirements for each of the gait modes, with a maximum power requirement for the knee of 400 W in stair climbing, and 800 W for the ankle in running.

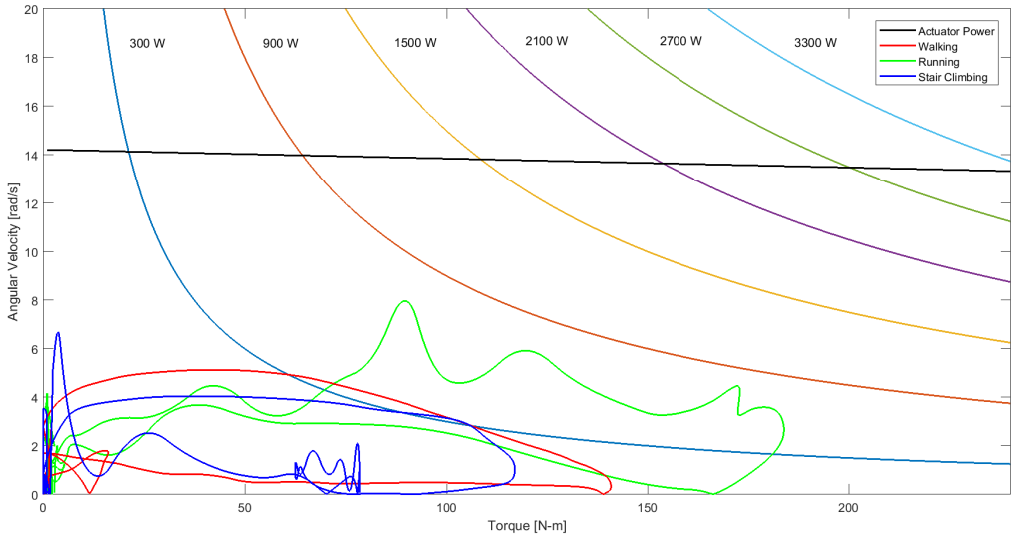

Figure 3.4: Speed vs. Torque curves for the three main gaits explored for the prosthesis's ankle degree of freedom. Running has the highest power requirement of the three gaits. The actuator power curve easily satisfies the joint requirements.

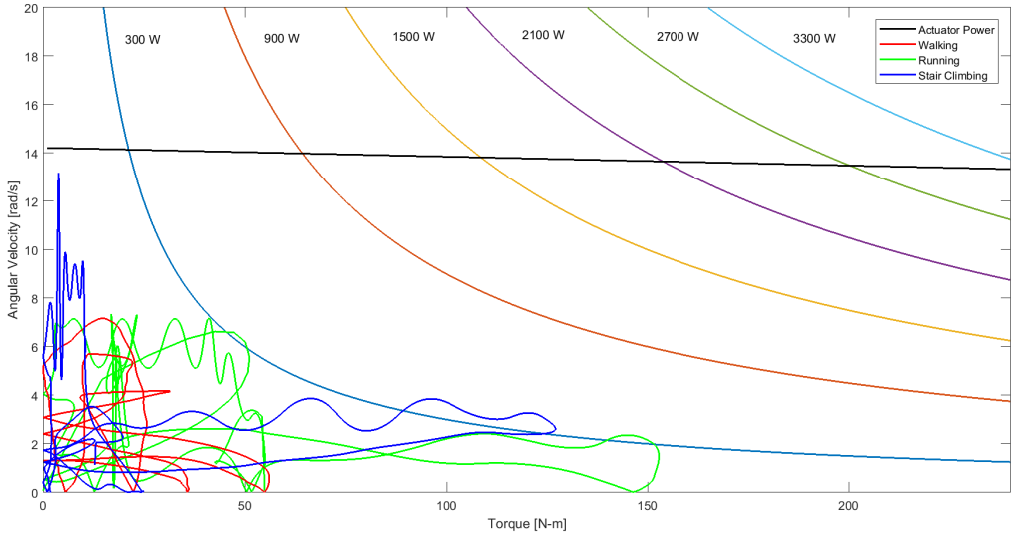

Figure 3.5: Speed vs. Torque curves for the three main gaits explored for the prosthesis's knee degree of freedom. Stair climbing has the highest power requirement of the three gaits. The actuator power curve easily satisfies the joint requirements.

3.1.3 Series Elastic Actuator Spring Calculations

Springs were placed in series with the actuators to reduce the total motor power requirement for the joint by absorbing and returning energy during motion, and to give a more natural feel to the knee and ankle joints. The spring type chosen for the SEA was a leaf spring, discussed in section 4.3. Calculations were carried out for spring stiffness optimization following the same procedure developed by Hollander (2006) [37]. A custom Matlab script was created to generate figure 3.6 which took into account the moment arm of the actuator, the mass of the individual (100 kg), and the period of the gait cycle. Figure 3.6 shows the results from the simulation for the power requirements of the motor with varying spring stiffnesses. Stiffness values were calculated for walking, running, and stair climbing with the stiffest value from the simulation chosen as the optimal value. The stiffness values for walking, running, and stair climbing are 160 kN/m, 148 kN/m, and 86 kN/m respectively, and therefore the stiffest value belongs to the walking gait. In addition, it may be seen that the curves for power consumption stay fairly constant as the stiffness of the spring is increased which indicates that any further increase in stiffness will not yield any additional gain in energy absorption or delivery. Lastly, if the spring stiffness is increased too far past the minimum power value, then the prosthesis would behave as though an infinite spring rate spring were inserted in its place, thus eliminating the benefits of having a SEA. With the optimal spring stiffness selected for each of the gait modes, calculations on the dimensions and deflection of the spring were performed. The leaf springs were modeled as cantilever beams, and the material selected by adjusting the length, width, height, arm length, and Young's modulus used in the calculation. Note that the desired spring stiffness was incorporated into the calculations via Hook's law, equation 3.1, and the total deflection was observed for changes in these parameters to match that calculated by equation 3.1. Figure 3.7 shows a diagram of the model used to perform the calculations, note that the arm length is h. Equations 3.2 - 3.4

are used in the spreadsheet for the calculation of the deflections at point R in figure 3.7. To expedite the material selection and calculations, a spreadsheet was used, appendix A section A.1. Ultimately it was determined that titanium would be the best material to use for the leaf springs.

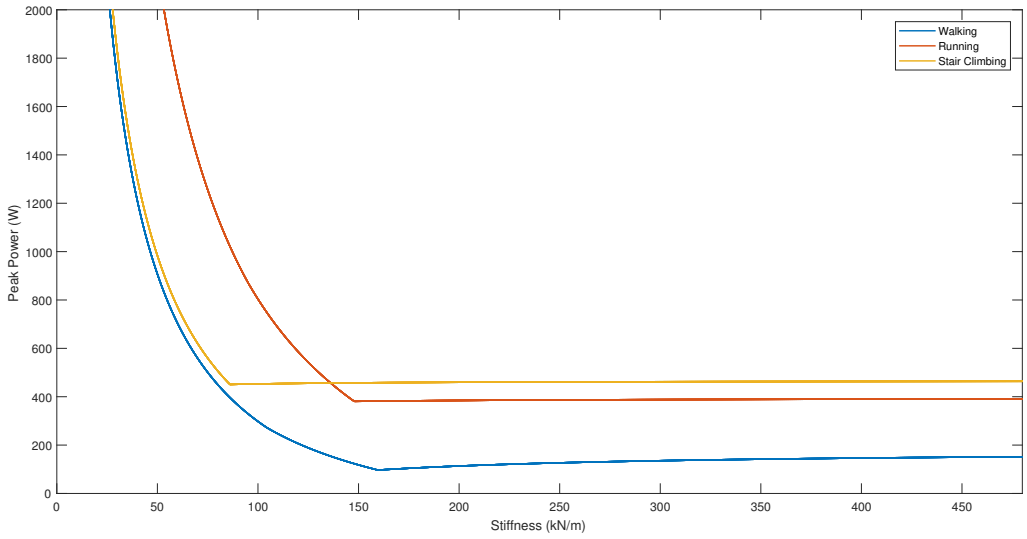

Figure 3.6: Motor power required as a function of spring stiffness. The stiffest spring rate was chosen to minimize the power requirement of the ankle motors. The stiffest condition belonged to the walking gait.

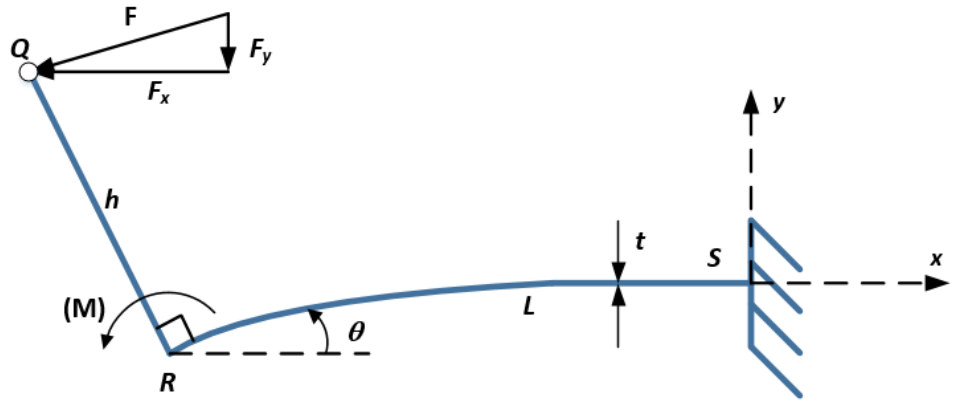

Figure 3.7: Diagram of cantilever beam model used for the leaf spring calculations.

$$F = k * \Delta x \tag{3.1}$$

$$\Delta R_{F_x} = \frac{F_x L}{EA} \tag{3.2}$$

$$\Delta R_{F_y} = \frac{F_y L^3}{3EA} \tag{3.3}$$

$$\Delta R_M = \frac{ML^2}{2EI} \tag{3.4}$$

Where E is the Young's modulus of the material, A is the cross sectional area of the beam, and L is the span of the beam. The results of these calculations gave a maximum deflection in the knee leaf spring of 5.68 mm, and a maximum leaf spring deflection in the ankle of 26.3 mm with both deflections occurring during the running gait.

3.1.4 Yaw DOF Calculations

For ankle yaw, a planetary gearbox (VEX Robotics VersaPlanetary 50:1) figure 3.8, was chosen for its simplicity in model integration and strength. A simple calculation was performed to estimate the torque required for yaw motion. For this calculation, a sine function was used to approximate ankle displacement during yaw. It was assumed that the ankle rotates at 1 Hz at an amplitude of 15°. Angular acceleration of the ankle yaw was determined by taking the second derivative of the estimation equation giving,

Figure 3.8: Versa planetary gearbox used for the yaw degree of freedom, with an overall gear reduction of 50:1.

$$- A\omega^2 sin(\omega * t) \tag{3.5}$$

where A is the amplitude of oscillation, ω is the frequency of oscillation, and t is time. The human body was then modeled as a cylinder with the full body weight on one foot coaxial with the cylinder. Under these assumptions, the moment of inertia for the human body was calculated using,

$$I = \frac{1}{2} m R^2 \tag{3.6}$$

Where m is the mass of the cylinder modeled human which in our case is 100 kg, and R is the radius of the cylinder being 0.15 m [38]. After calculating the ankle yaw torque, a safety factor of 1.5 was applied to give a final torque value for the yaw DOF of 17.5 Nm.

3.1.5 Finite Element Analysis

To ensure that all of the components used to build the prosthesis could handle the forces they are to experience, FEA was performed for verification of the prosthesis's structural integrity under heavy loads and impacts. The components tested were the leaf springs, long and short trunnions, and knee joint pivot, figure 3.9, so that potential points of failure would be identified and subsequently fortified or changed. These components were chosen as they are not only integral to the functionality of the prosthesis, but also because the failure of these components would be attributed to excessive forces beyond those designed for, and render the prosthesis inoperable.

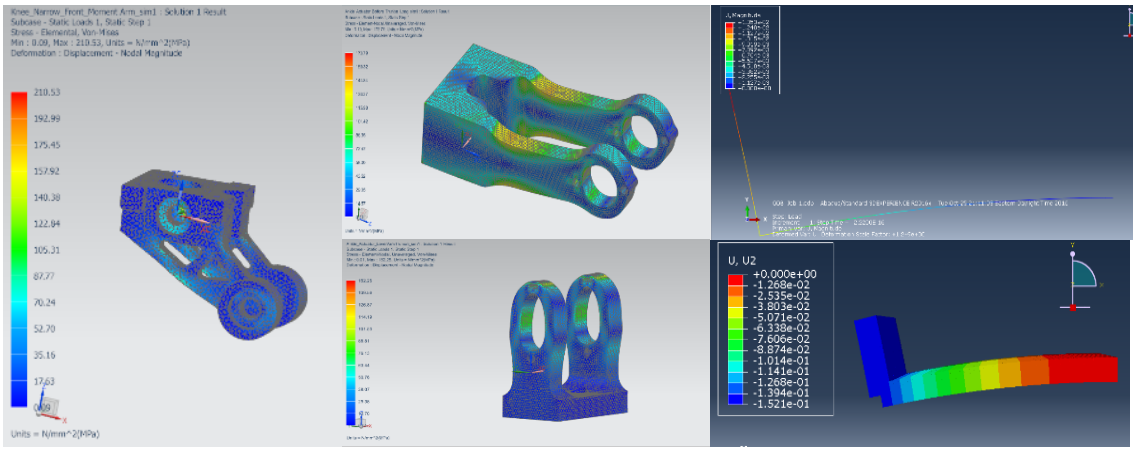

Figure 3.9: Left: The knee pivot which allows rotation of the knee joint. The knee pivot is also the main connection point to the prostheses adapter which connects to the residual limb. Top Middle: The long ankle trunnion which is connected to at the top of the leaf spring, which connects the leaf spring to the actuator, and is responsible for transferring the stored leaf spring energy to the ankle. Bottom Middle: The short ankle trunnion responsible for connecting the ankle actuator to the foot to allow for power transfer. There are a total of two of each trunnion on the prostheses. Top Right: The ankle leaf spring. Bottom Right: The knee leaf spring.

Chapter 4

Mechanical and Electrical Design

The prosthesis contains 4 DOF, 1 in the knee and 3 in the ankle. The knee uses a single linear actuator to rotate the knee to the desired angle, while the ankle uses a dual actuator system to create both pitch and roll. For pitch, both actuators act in an agonist fashion, with roll accomplished by moving in an antagonist fashion. The third DOF in the ankle, yaw, is controlled by a motor and gearbox system. Figure 4.1 depicts the 3 degrees of freedom of the ankle. Speed and torque requirements for each of the active joints of the prosthesis were derived from the body mass normalized data of Ounpuu (1994) and Novacheck (1998) for running at 3.2 m/s, Winter (2009) for level walking, and Aldridge (2012) for stair climbing [27, 28, 36, 39], as discussed in chapter 3. With the maximum power requirements and ROM for each joint determined, motors, ball screws, and leaf springs were then appropriately sized to satisfy the joint requirements.

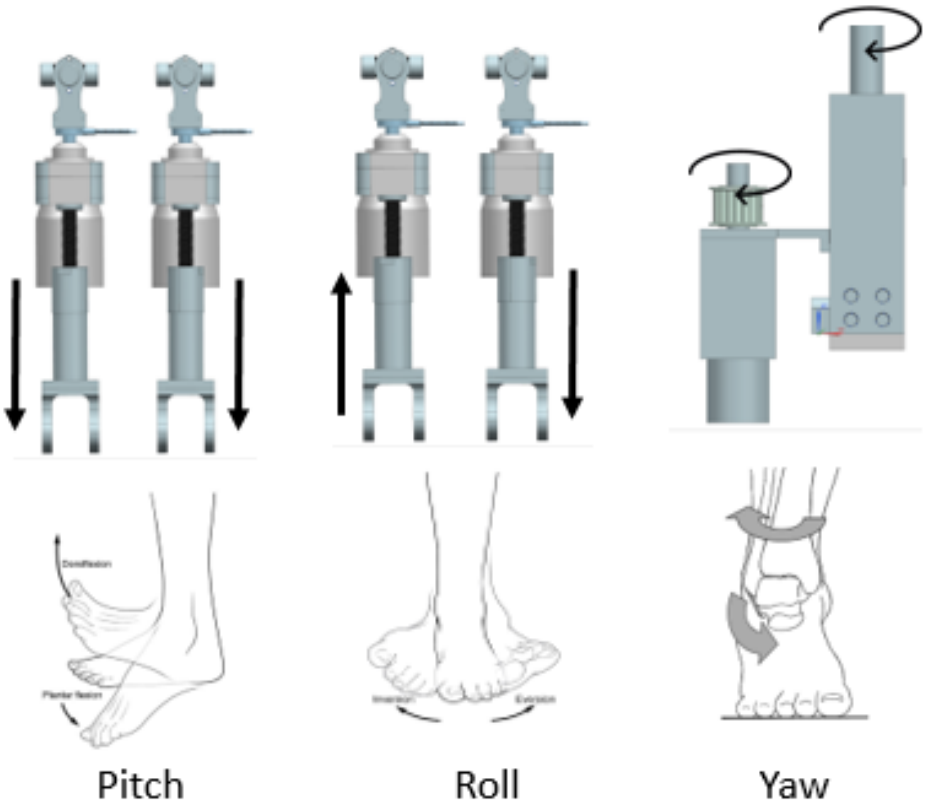

Figure 4.1: The three degrees of freedom of the ankle, i.e. roll, pitch, and yaw.

4.1 Motor Selection and Instrumentation

Given the large power requirements for each joint, motors typically used for controlling prostheses, e.g. Maxon EC-30, were not suitable without being overdriven which requires additional cooling, e.g. water cooling. Therefore, larger un-instrumented hobby grade motors were employed. A spreadsheet which calculated the maximum torques and speeds for motors given their max voltage, power, Kv, and a chosen gear reduction was created to determine which motors would satisfy the joint requirements, appendix A section A.2. The motor chosen for both joints was the RotorStar Brushless Outrunner Helicopter - 4962-480 Kv (700/.90 size heli) motor, capable of producing 3400 W at peak power output. In choosing a motor of this size as compared to the small Maxon EC-30 motors, we are introducing larger rotor inertia (calculated in section 5.3.2) which must be accounted for, as well as increasing the overall prosthesis weight, and therefore inertia. In addition, though the motors are capable of this power output, they are limited by the maximum current output of the motor controller (60 A), which gives a maximum motor power output of 2880 W. Figures 4.2 – 4.4 shows a portion of the spreadsheet used for the motor calculations, the chosen motor for knee and ankle actuation, and the motor chosen for yaw actuation, respectively.

For instrumentation, a hall effect sensor board was created for motor control, as shown in figure 4.5. The motor controller chosen for the input signal used a 120 electrical degree hall effect spacing, and paired with the chosen motor which had 14 pole pairs gave a hall effect mechanical degree spacing of 8.57° via [40]

$$\left(\frac{360\ mdeg}{3 * pp}\right) = \frac{m\ mdeg}{120\ edeg} \tag{4.1}$$

where *mdeg* is the mechanical degrees of the motor, *edeg* is the electrical degrees of the motor,

	RotorStar Brushless Outrunner Helicopter - 4962-480kv (700/.90 size heli)	GFORCE G180 BRUSHLESS OUTRUNNER MOTOR (C6374-200KV)	Alien 6374 Outrunner brushless motor 170KV 3200W	Turnigy Aerodrive SK3 - 6374-192kv Brushless Outrunner Motor	9235-100KV Turnigy Multistar Brushless Multi-Rotor Motor	Turnigy Aerodrive SK3 - 5065-236kv Brushless Outrunner Motor	Turnigy Aerodrive SK3 - 5065-320kv Brushless Outrunner Motor
Motor Voltage [V]	44.4	37	37	44.4	44.4	37	37
Motor Power [W]	2700	1100	1100	1300	1300	1100	1100
Kv [rpm/V]	480	200	170	192	100	236	320
Motor Current [A]	60.8	29.7	29.7	29.3	29.3	29.7	29.7
Kv [rad/Volt-sec]	50.265	20.944	17.802	20.106	10.472	24.714	33.510
Ke [N-m/Amp] = 1/Kv	0.020	0.048	0.056	0.050	0.095	0.040	0.030
No-load Speed [RPM]	21312	7400	6290	8524.8	4440	8732	11840
Torque [Nm]	**1.210**	**1.419**	**1.670**	**1.456**	**2.796**	**1.203**	**0.887**
Gear Ratio: []	50						
Torque * Gear Ratio [Nm]	**60.490**	**70.975**	**83.499**	**72.812**	**139.798**	**60.148**	**44.359**
Speed after gear ratio [rpm]	426.24	148	125.8	170.496	88.8	174.64	236.8
Price	$84.70	$85.00	£ 65.00	$79.96	$167.18	$56.86	$56.86
Weight (g)	448	750	750	858	674	530	531
Diameter (mm)	49	62.8		59	92	49	49
In Stock	Yes	Yes	Custom	Yes	Yes	No	No
Torque to Weight (Nm/g)	0.00270	0.00189	0.00223	0.00170	0.00415	0.00227	0.00167
Torque to Diameter (Nm/mm	0.0247	0.0226		0.0247	0.0304	0.0246	0.0181

Figure 4.2: A sample of the spreadsheet used for picking the proper motor that met all of the joint speed and torque requirements.

Figure 4.3: The Roto-Star 480 Kv hobby helicopter motor chosen for the knee and ankle pitch, and ankle roll degree of freedom.

and *pp* is the number of pole pairs in the motor. Mechanical degrees of the motor refers to the rotation of the shaft where one rotation equals 360°. Electrical degrees refers to the magnetic position of the rotor where 360 electrical degrees is accomplished when the rotor

Figure 4.4: The Mystery hobby drone motor used for the ankle yaw degree of freedom.

makes a full cycle from “North Pole“ to “South Pole“ to “North Pole“. Figure 4.5 shows the Eagle CAD drawing of the hall effect sensor board, and figure 4.6 shows the board installed on the motor.

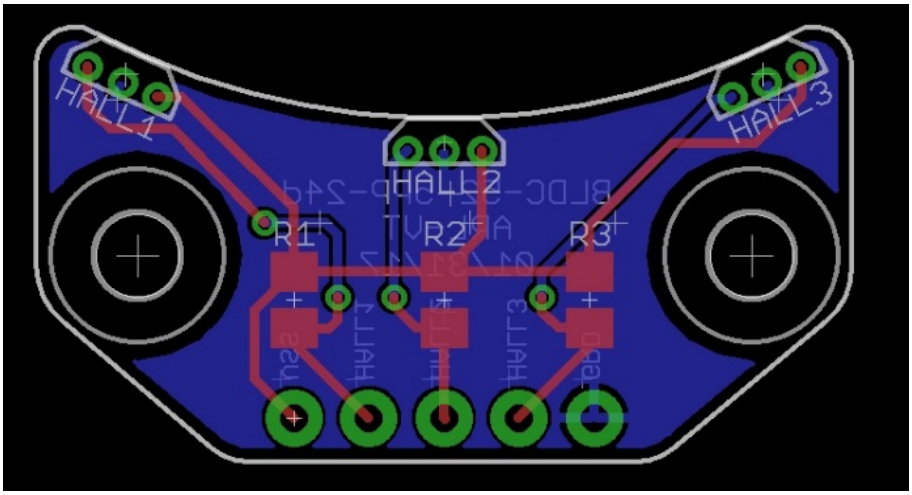

Figure 4.5: The hall effect sensor board used for enabling control of the hobby brushless DC helicopter motors.

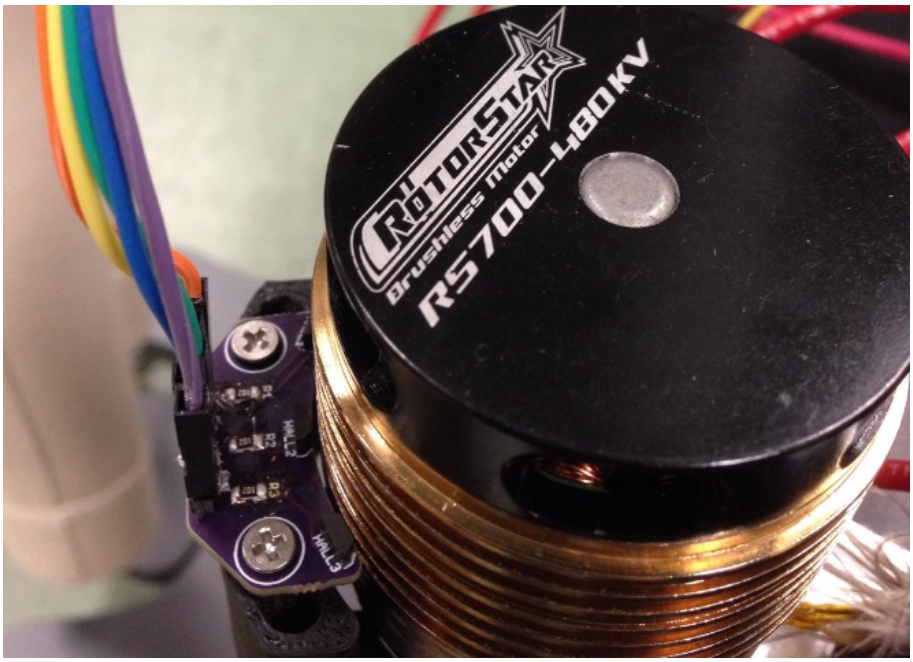

Figure 4.6: The hall effect sensor boards installed on the brushless helicopter motors.

4.2 Ball Screw Selection

Ball screws were chosen over a gearbox due to their higher efficiency (> 90% vs. 75%), smaller volume, and lighter weight. Ball screws were chosen using the power and force requirements for each joint, discussed in section 3.1.1 while considering the maximum allowable stresses on the ball screw. In addition, the ball screws needed to be back-drivable, meaning that they can reverse direction quickly during operation, and unpowered motion. Therefore, ball screws with a lead greater than 4 mm for our application were required. Ball screw selection was facilitated by the use of a spreadsheet, appendix A section A.3, which took the properties of each ball screw and the selected motor as inputs, with the output being the allowable stresses on the ball screw, and the maximum speed and torque expected for the joint given a ball screw pre-gearing and moment arm length. Ball screws that met both speed and torque requirements were highlighted in blue, green if the condition met only one of the joint requirements, and no highlighting if neither of the joint requirements were met. Figure 4.7 displays a portion of the spreadsheet used to determine the appropriate ball screws.

Ball Screw Pre-gearing	No Gearing	1:1.25 geared	1:1.5 geared	1:2 geared	1:2.5 geared	1:3 geared	1:3.5 geared	1:4 geared	
Rotational Speed (rpm)	21312	17049.6	14208	10656	8524.8	7104	6089	5328	Speed
Linear displacement (m/s)	1.7760	1.4208	1.1840	0.8880	0.7104	0.5920	0.5074	0.4440	
Linear Force (N)	1481.6	1852.0	2222.4	2963.2	3704.0	4444.8	5185.6	5926.4	Static Load
Peak Velocity (rad/s)									
Lever arm length (m)	No Gearing	1:1.25 geared	1:1.5 geared	1:2 geared	1:2.5 geared	1:3 geared	1:3.5 geared	1:4 geared	
0.02	88.80	71.04	59.20	44.40	35.52	29.60	25.37	22.20	
0.021	84.57	67.66	56.38	42.29	33.83	28.19	24.16	21.14	
0.022	80.73	64.58	53.82	40.36	32.29	26.91	23.06	20.18	
0.023	77.22	61.77	51.48	38.61	30.89	25.74	22.06	19.30	
0.024	74.00	59.20	49.33	37.00	29.60	24.67	21.14	18.50	
0.025	71.04	56.83	47.36	35.52	28.42	23.68	20.30	17.76	
0.026	68.31	54.65	45.54	34.15	27.32	22.77	19.52	17.08	
0.027	65.78	52.62	43.85	32.89	26.31	21.93	18.79	16.44	
0.028	63.43	50.74	42.29	31.71	25.37	21.14	18.12	15.86	
0.029	61.24	48.99	40.83	30.62	24.50	20.41	17.50	15.31	
0.03	59.20	47.36	39.47	29.60	23.68	19.73	16.91	14.80	
0.031	57.29	45.83	38.19	28.65	22.92	19.10	16.37	14.32	
0.032	55.50	44.40	37.00	27.75	22.20	18.50	15.86	13.88	
0.033	53.82	43.05	35.88	26.91	21.53	17.94	15.38	13.45	
0.034	52.24	41.79	34.82	26.12	20.89	17.41	14.92	13.06	
0.035	50.74	40.59	33.83	25.37	20.30	16.91	14.50	12.69	
0.036	49.33	39.47	32.89	24.67	19.73	16.44	14.10	12.33	
0.037	48.00	38.40	32.00	24.00	19.20	16.00	13.71	12.00	
0.038	46.74	37.39	31.16	23.37	18.69	15.58	13.35	11.68	

Requirements	
Required seed (rad/s)	14.22
Required Force (Nm)	182
Power at given values (W)	2588

Motor Inputs	
Motor Speed (rpm):	21312
Motor Speed (rad/s):	2231.8
Motor Torque (Nm):	1.21
Power at given values (W)	2700

Ball Screw Inputs	
Outer Diameter (m)	0.0150
Ball center-to-center dia. (m	0.0158
Minor Diameter (m)	0.0125
Mean Thread Diameter (m)	0.0138
Lead (m)	0.005
Friction Coefficient (μ)	0.003

Figure 4.7: A sample of the spreadsheet used for determining the proper gear ratios and for selecting the proper ball screw for the application.

The ball screws selected had a lead of 5 mm and a diameter of 12 mm which had sufficient back-drivability (a function of the ratio of ball screw lead to ball screw diameter) for the prosthesis was chosen to achieve the desired joint speeds and torques.

4.3 Series Elastic Spring Selection

To achieve a more biomimetic feel to the prosthesis by adding in compliance while also reducing the load requirement on the motor, SEAs were implemented. Therefore, the design of the actuators required a spring element in order to achieve this behavior. For the spring type, die springs, leaf springs, and torsional springs were considered for the design. Each spring design has their own pros and cons and have been used successfully in other prostheses. For example, the SPARKy 3 prosthetic ankle by Bellman and Sugar (2008) [22] uses die springs for compliance, the Bionic ankle-foot prosthesis by Herr (2008) [41], uses carbon-composite leaf springs, and the robotic knee prosthesis by Rouse (2016) [42] uses a torsional spring.

The decision surrounding which type of spring element to use came down to four criteria: robustness, ease of integration, compact packaging, and their effectiveness as a spring element for the forces that the prosthesis would experience during each gait cycle. The leaf spring design came out to be the most effective of the four spring types. To handle the amount of stress the leaf springs would experience, grade 5 titanium was chosen as the material of choice. The ankle assembly uses two leaf springs of dimension 125 mm x 40 mm x 6 mm, while the knee has only one leaf spring with dimensions 80 mm x 25 mm x 6 mm, see section 3.1.3 for the deflection calculations. Figure 4.8, shows both the knee and ankle leaf springs.

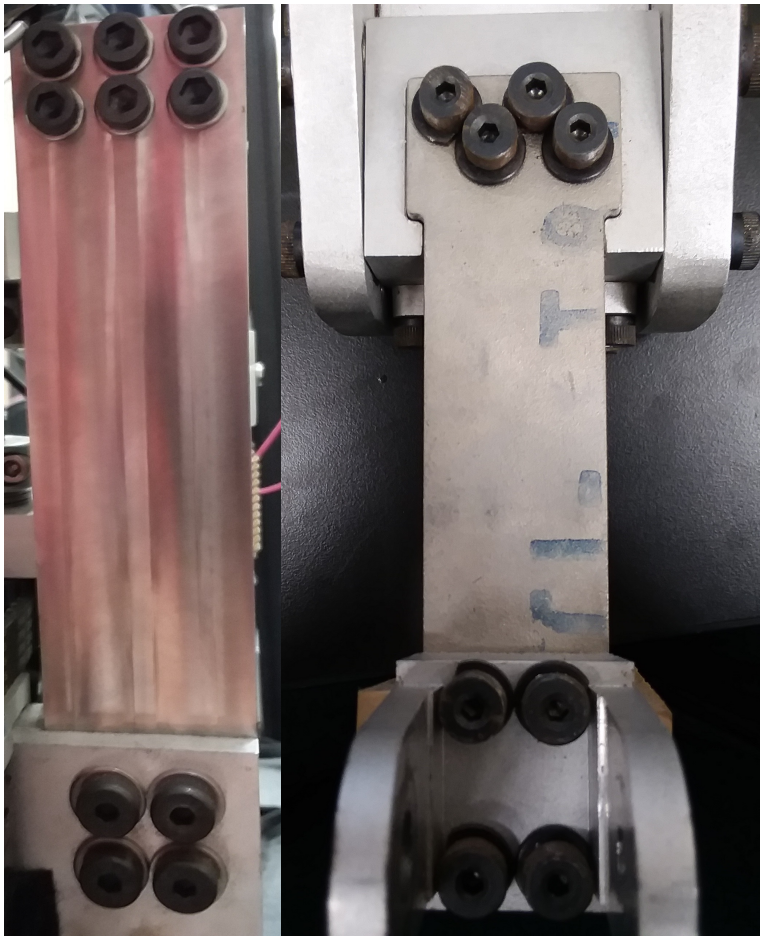

Figure 4.8: Left: Ankle actuator leaf spring. Right: Knee leaf spring.

4.4 Ankle Actuators

In order to achieve both roll and pitch in the ankle, parallel series elastic actuators were implemented, inspired by the design of Bellman and Sugar (2008) [22], and Virginia Tech's THOR and ESCHER humanoid robots [43]. This allowed for both the ankle pitch and roll to be controlled using the same two actuators instead of a single actuator dedicated to each DOF. This method of actuation for these two degrees of freedom gives more power to the ankle since two motors are working in conjunction with one another. The added power from two motors allows the prosthesis to be used for many different forms of human locomotion, beyond those discussed. The two actuators work both synchronously and asynchronously to generate the pitch and roll motions of the ankle respectively. Figure 4.9, shows each of the components on the linear SEAs.

The linear actuators include a BLDC hobby motor which inserts into a housing, and a timing pulley and belt provides a 2.5:1 gear reduction before the ball screw. As the ball screw spins, the ball nut which is attached to an adapter moves up or down the ball screw to transfer the motion to the trunnions which provide force to the moment arm to move the prosthetic foot.

Knee Actuator

The knee actuator shares an identical design to that of the ankle, with the only difference being the size of the leaf spring. Due to size restrictions and the forces that the knee experiences during the three primary gait cycles, the leaf spring was made smaller than those of the ankle. Figure 4.10, shows the CAD model of the knee actuator, its components, and sensor locations.

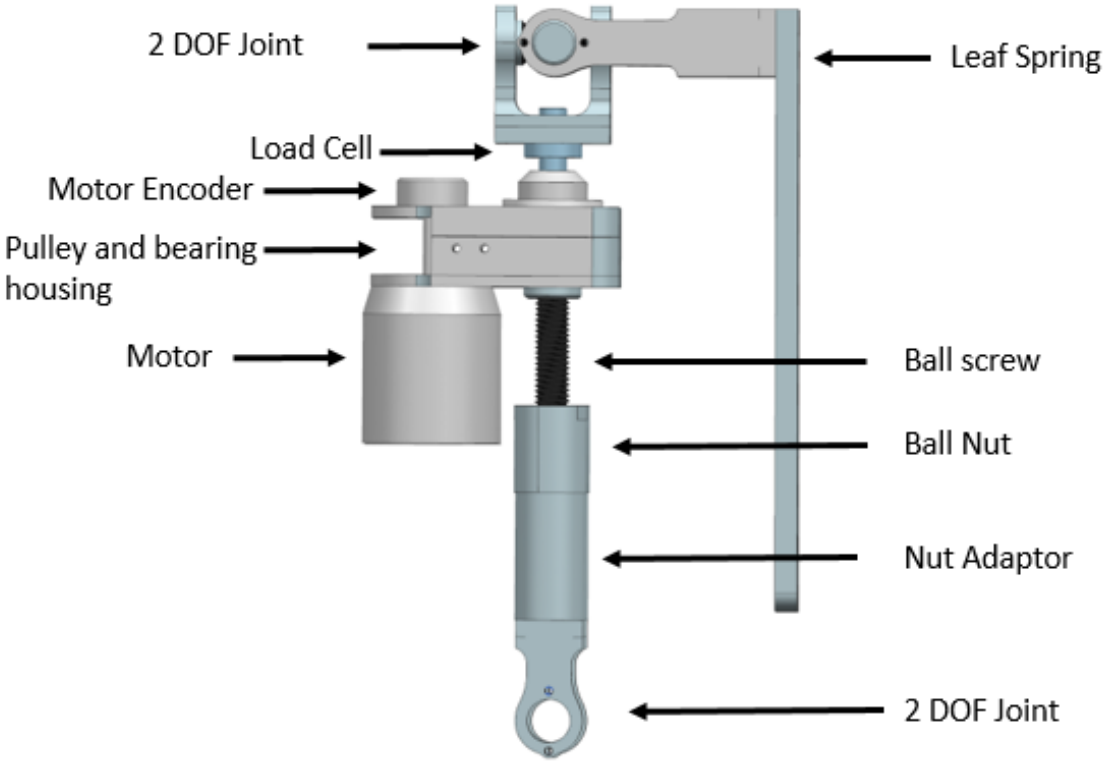

Figure 4.9: The ankle actuator used for powering both the second and third degrees of freedom of the ankle. There are two of these actuators present at the ankle joint.

4.4.1 Yaw Actuator

For the final DOF in the ankle (transverse motion, yaw) a separate geared motor actuator was implemented, figure 4.11. A geared motor was chosen for this DOF since it allowed for a more compact design, easily fit between the two parallel actuators of the ankle, as seen in figure 3.1, and provided greater torque to the joint than a direct drive motor would. The gearbox motor combination was chosen based on the yaw calculations, section 3.1.4. The gearbox chosen for the yaw is a two-stage planetary gearbox (Vex Robotics VersaPlanetary Gearbox), figure 3.8, with a 50:1 gear reduction which provides sufficient torque to the joint given the selected BLDC motor (Mystery Brushless Motor 5010-400 Kv), figure 4.4. This actuator is capable of providing 21 Nm of torque compared to the maximum joint torque

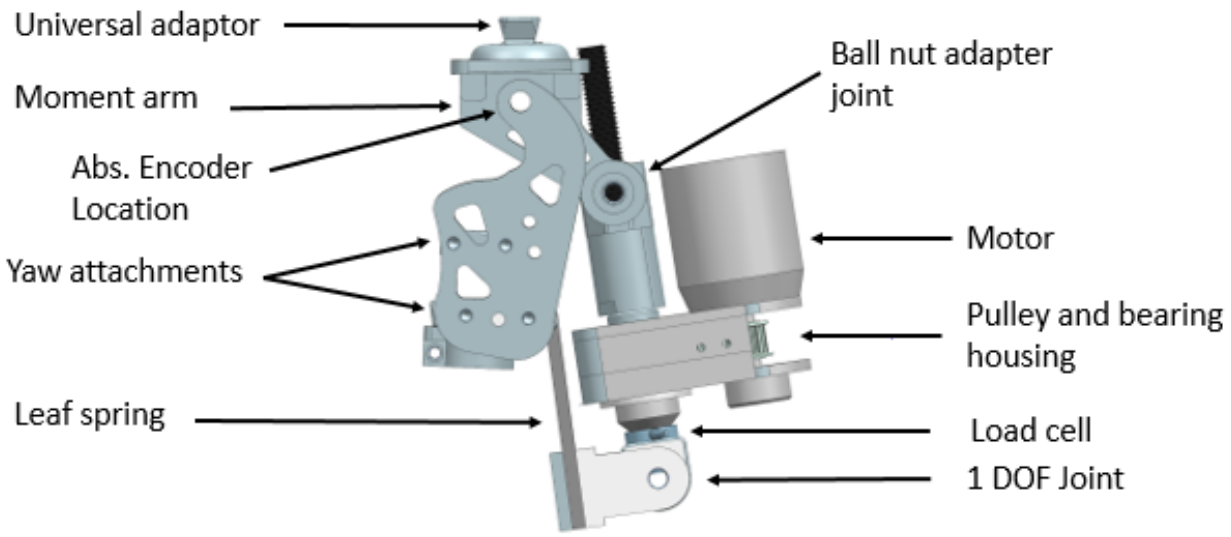

Figure 4.10: The Knee Actuator used for powering the first degree of freedom of the prosthesis. The linear actuator for the knee uses the same power transfer method as that discussed for the ankle above.

requirement of 17.5 Nm.

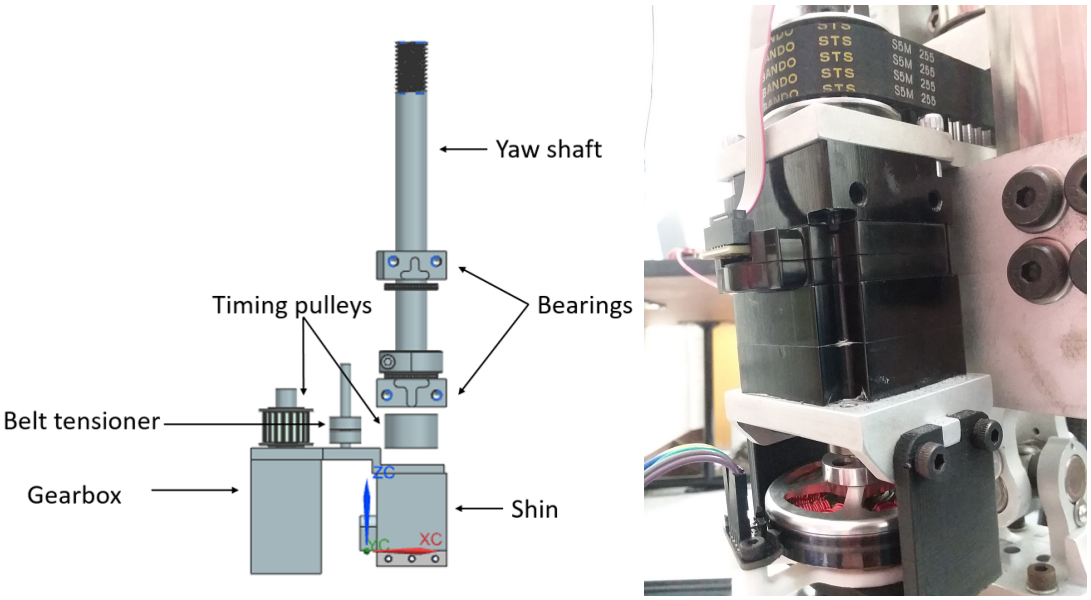

Figure 4.11: Left: The CAD model of the yaw actuator. Right: The final prototype of the yaw actuator. The yaw actuator is placed in between the two ankle actuators for a more compact design.

Figure 4.12 shows the completed ankle, and figure 4.13 shows the completed prosthesis

prototype used for testing and evaluation. The carbon fiber foot is bolted to the bottom of the ankle. The two rear actuators both have two degrees of freedom to produce the pitch and roll. The yaw actuator rotates the entire ankle assembly about the yaw shaft that runs up to and is secured to the knee.

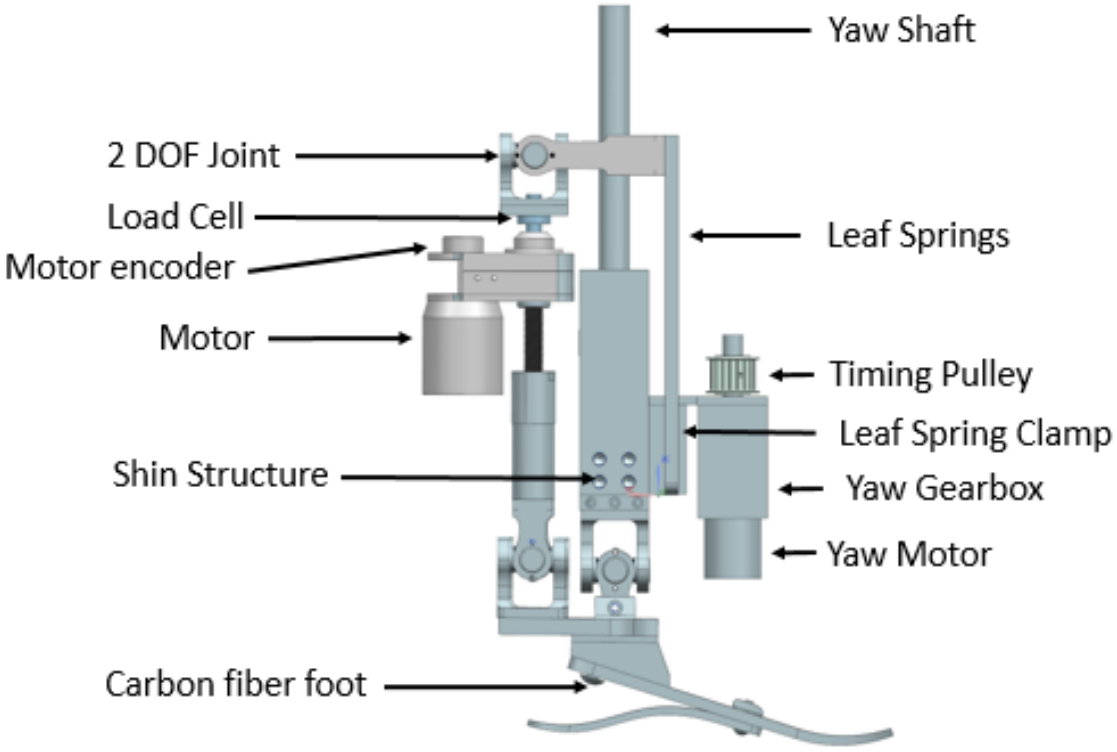

Figure 4.12: The completed ankle with the yaw actuator in between the two ankle actuators.

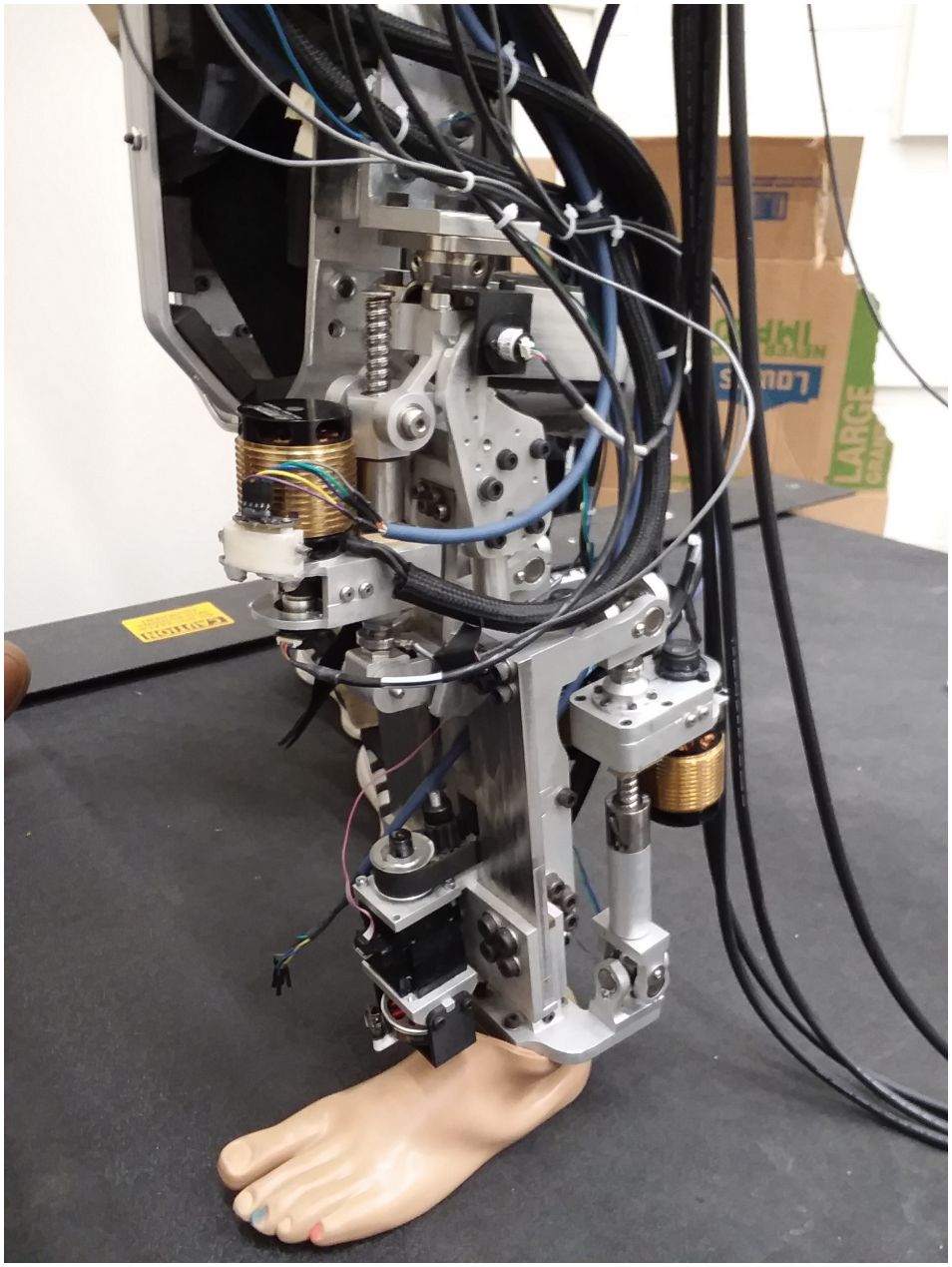

Figure 4.13: The finished prosthesis used for treadmill testing.

Chapter 5

Electronics, Communications, and Controls

5.1 Electrical System

To accurately replicate the gait cycle of an able-bodied individual, the prosthesis requires a system of sensors to provide feedback for operation. As determined through the gait cycle analysis research presented in chapter 3, the most important variables to measure are the joint torques, angles, and velocities. Absolute magnetic encoders (US Digital Part #MAE3) were selected to measure joint angles while single-axis load cells (Futek LCM200) were installed in series with the ball-screws to measure the axial forces on the ball screws which is directly proportional to the torque at the joint. Optical quadrature motor encoders were used to determine joint velocities, and inertial measurement units (IMUs) may be installed (are not currently installed) to measure joint accelerations for implementing the inertia modeling of the actuators and prosthesis, section 5.3.3. The IMUs may also be used for user intent recognition to determine what the user is attempting to do, i.e. walking to running, sit to stand, etc.

A network of Tiva microcontrollers interpret the sensor readings and control the actuators to achieve the desired motion. In total there are five Tiva microcontrollers, one for each DOF including one Master Tiva for sending commands to the Slave Tiva devices over I2C and for

logging data over Serial UART. The four Slave Tiva devices are outfitted with a prototyping shield which includes a load cell amplifier and an I2C communication connection point, and a separate joint and motor encoder shield. The Tiva board is then connected to the motor driver through a motor controller shield. In addition to the sensors listed above the motor controller shield has a current monitor connection point for sending an analog signal back to the Slave Tiva which is proportional to the current draw of the motors. The scaling is 20 A/V with a range of ±3 V, therefore; an additional scaling and offset circuit was created to scale the incoming signal to 0 – 3.3 V for the Tiva analog to digital converter (ADC).

The scaling and offset circuit uses op-amps and two resistor divider circuits, one for scaling and the other for offsetting the signal. Three op-amps were used in the design, one for buffering the input signal (TL972IP), and two additional op-amps for isolating the scaling and offset voltage divider circuit sections (MCP601). In addition, since the voltage supplied from the motor controller for the current reading is ±3 V, a charge pump DC-DC voltage converter (TC7660) was implemented to obtain a negative voltage from the positive supply as input to the Vss (negative supply voltage) rail of the TL972IP op-amp. Therefore, the TL972IP has a rail to rail voltage of approximately ±5 V, which is sufficient for the full ±3 V signal from the motor controller to pass through isolated from the scaling and offset circuit sections. Figure 5.1 shows the LTSpice simulation of the circuit, figures 5.2 and 5.3 show the eagle CAD circuit and board, and figure 5.4 shows the final circuit used in the system. Figure 5.5, shows all of these boards arranged in their stacked fashion, and figure 5.6 shows the final electrical system layout.

The Master Tiva is outfitted with a Master Shield, figure 5.7, which includes both 12 V and 5 V power regulators with connection points for each, four general purpose input output (GPIO) breakout pins, an additional UART module connection point, five I2C connection points, and two connection points for IMU sensors that work with the I2C standard (future

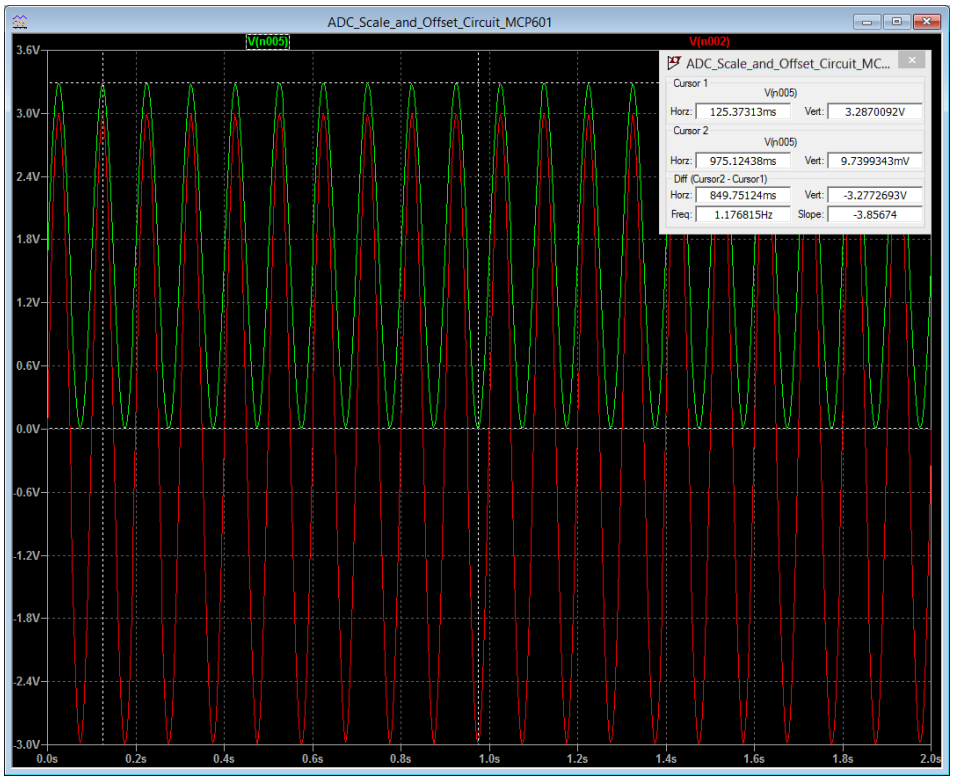

Figure 5.1: Simulation showing the scaling and offset performance of the op amp circuit. The red signal is the raw unconditioned signal coming from the motor controller. The green signal is the conditioned input to the microcontroller.

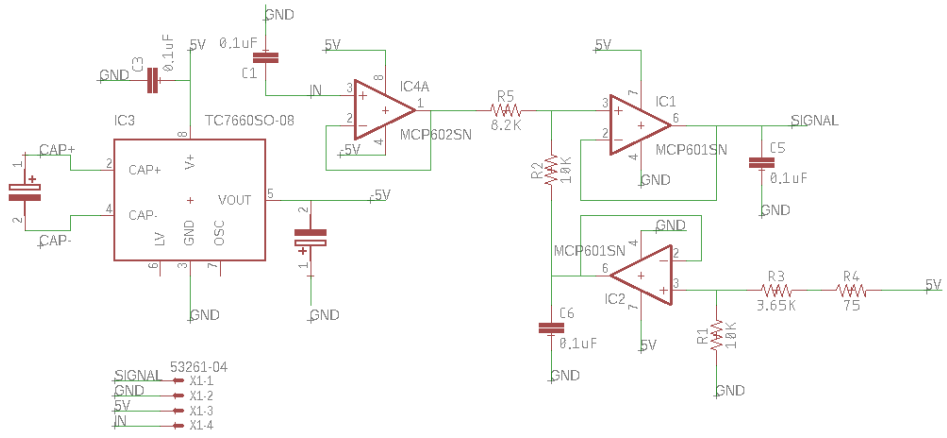

Figure 5.2: The circuit diagram of the printed circuit board used for scaling and offsetting the signal coming from the motor controller. Three op-amps are used to perform the signal conditioning in conjunction with a charge pump converter used to generate the negative voltage supply for the negative voltage rail of the TL972IP.

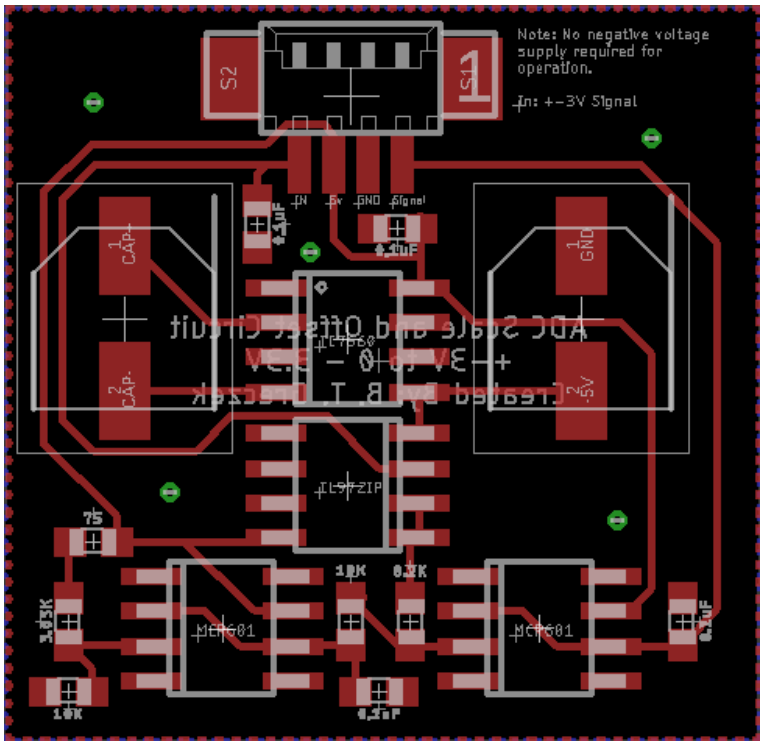

Figure 5.3: The printed circuit board layout of the scaling and offset circuit.

work). The Master Tiva is powered by three 4s Lipo Batteries in series for a total system voltage of 48 V. The voltage regulators then drop the 48 V to 5 V and 12 V with the 5 V used to power the Master Tiva and its sensors, and the 12 V power distributed to the Slave Tivas. A voltage regulator then regulates the 12 V signal down to 5 V to power the Slave Tiva and its sensors. The 12 V line to the Slave Tiva is needed as the excitation voltage for the load cell. In addition, an emergency stop has been added to the system as an additional safety precaution. Figure 5.8, is the block diagram of the electrical system, table 5.1 lists the sensors and their communication, and figure 5.9 depicts the data flow of the system.

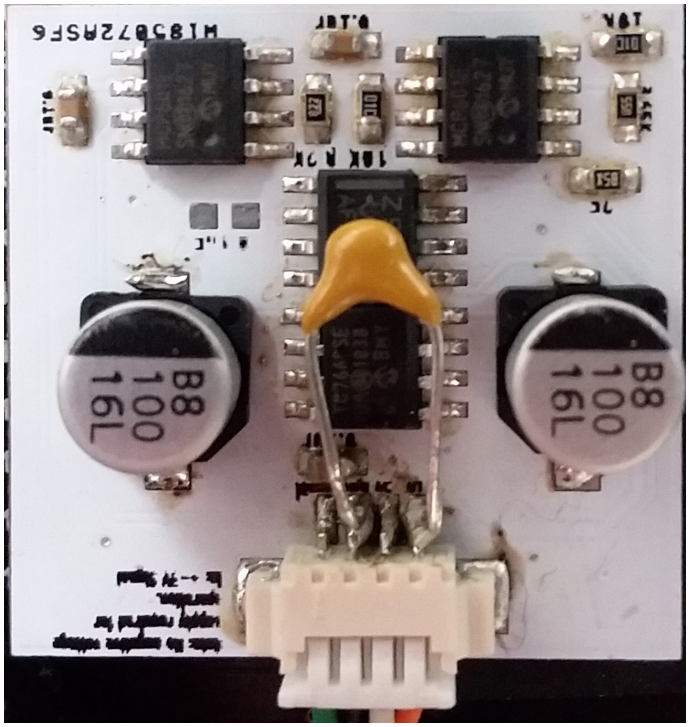

Figure 5.4: The final ADC circuit. The capacitor across ground and signal was added later. It had not been included in the board that had been purchased. The newer board version, depicted in the CAD files of the circuit now includes this capacitor.

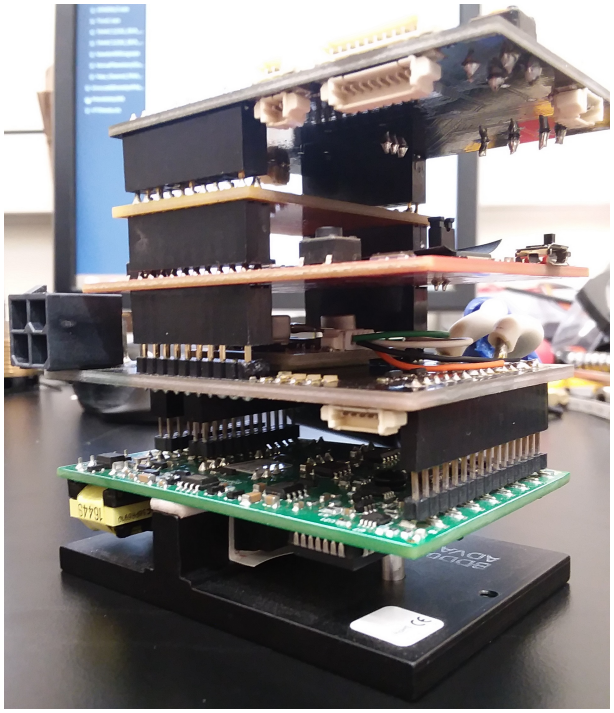

Figure 5.5: Electrical stack used for motion control of the prosthesis. The first board is used for power conversion, I2C communication, and load cell amplification. The second is used for absolute and optical encoders. The third is the TM4C microcontroller. The fourth is the motor controller shield, upon which lays the ADC conversion circuit.

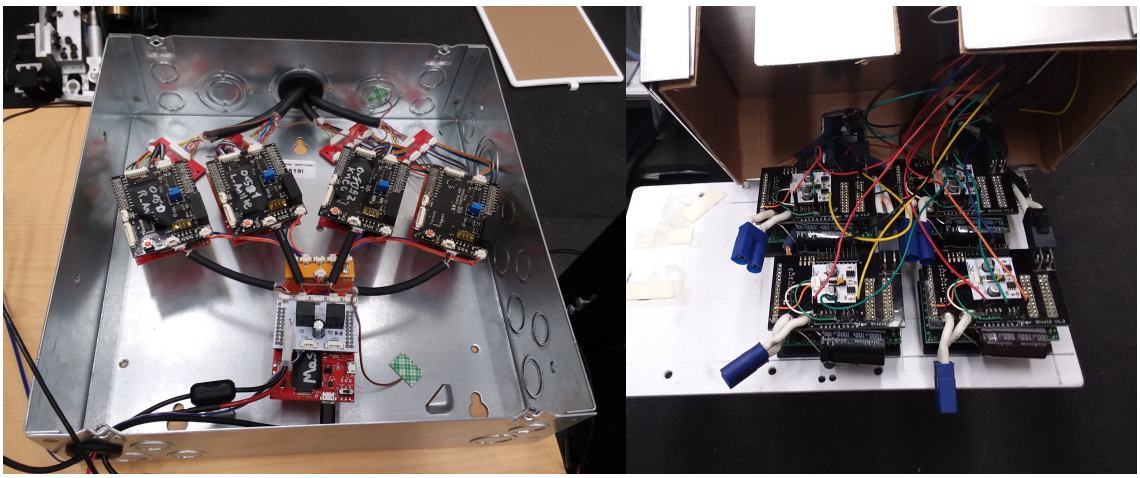

Figure 5.6: The layout of the electrical system used for testing the prosthesis. The aluminum box covering the power electronics and the microcontrollers is used to shield the signal electronics from electro-motive interference caused by the large current draw of the motors.

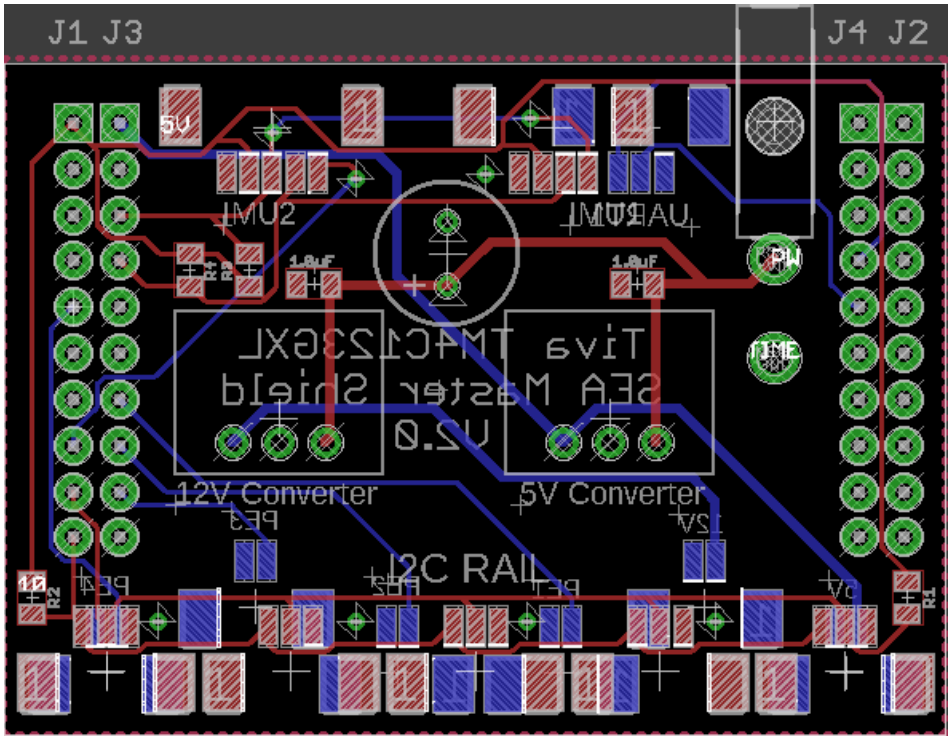

Figure 5.7: Master Shield board used to communicate with each Slave Tiva, and log data via Serial communication.

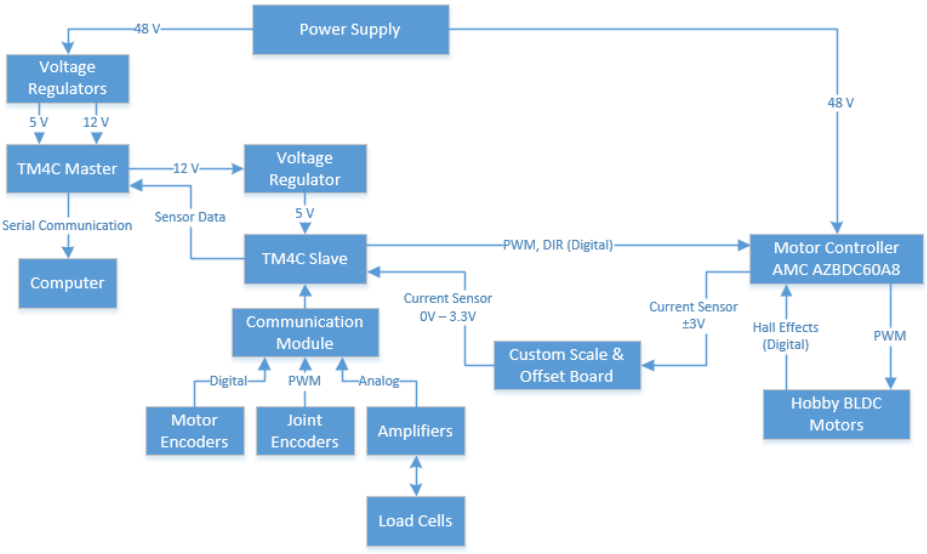

Figure 5.8: The electrical block diagram of the system.

Sensor Type	*Measurement*	*Model*	*Quantity*	*Comm. Protocol/Output Type*
Load Cell	Force (Knee; Ankle: Pitch/Roll)	Futek LCM200	3	Analog Voltage
Absolute Encoder	Joint Position	US Digital MAE3 Magnetic	4	10 bit PWM
Motor Encoder	Joint Velocity (Knee; Ankle: Pitch/Roll)	US Digital E4T Optical	3	Digital
Hall Effect Sensor	Motor Position/Control	Honeywell SS41-S	12	Digital
Microcontroller	Processing and Control	TI Tiva C Series	5	I2C, PWM, Analog…
Motor Controller	Motor PWM Signal Amplification & Current Sensing	AMC AZBDC60A8	4	PWM

Table 5.1: Sensors and Communication Protocols

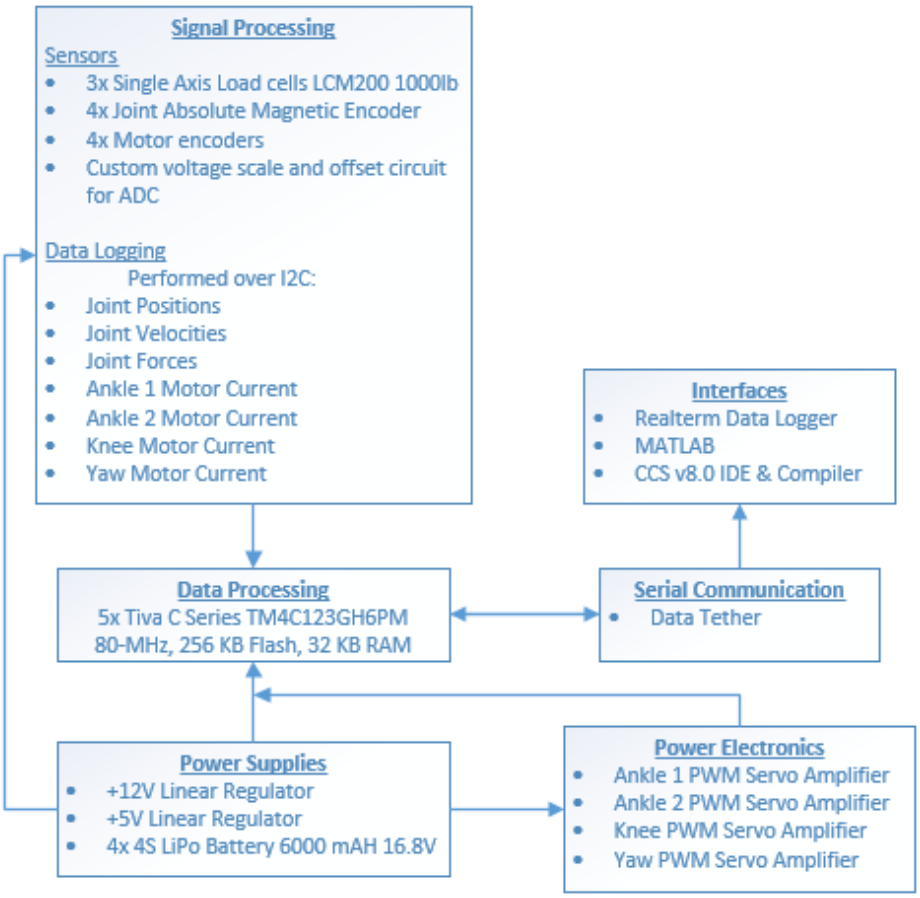

Figure 5.9: Flow diagram of signal inputs and outputs to the electrical system.

5.2 Communications System

I2C communication is one of the most important elements of the system, without which no functionality would be possible. The amount of data being transmitted between the Slave Tiva devices and the Master device is 32 bytes. The Master then logs these same 32 bytes over UART. Therefore, the total number of bytes sent in a single cycle is 64 bytes. Taking into account the possibility of sending tuning parameters to the Master and then to the Slave device, as well as the possibility of incorporating IMUs, totals upwards of 92 bytes of data. With a sampling rate of 500 Hz, this results in a required I2C speed of,

$$I2Cspeed = 10 * (92) * 500 = 460,000\ bps \tag{5.1}$$

including start and stop bits. Therefore, the I2C standard (100 kbps) and fast mode (400 kbps) are not fast enough for the required data transfer speeds needed, and so fast mode plus (1 Mbps) and high speed (3.34 Mbps) mode remained. The high-speed mode was chosen to ensure that any additional sensors added to the system could be easily incorporated into the communication protocol without extensive modification. In addition, the added speed allows for error checking and resending of data if a packet is missed by one of the Slave devices. Furthermore, the high-speed mode for I2C only applies to the data packets being sent and not the setup read/write packets which can only be sent at a maximum of 400 kbps. Therefore, taking this into account high-speed mode was the only viable option without risking loss of information upon transfer. However, using high-speed mode requires stronger pull-up resistors to accommodate the requirement of a faster signal rise time. In addition, the system capacitance must be small for the high-speed mode to work. Figure 5.10, shows an oscilloscope capture of the I2C data transfers taking place at high-speed mode. The reading on the oscilloscope shows that the data is being transferred

successfully and reliably; however, with a little bit of capacitance present on the I2C bus line. The capacitance of the bus line could be improved by reducing the number of boards present or shortening the I2C communication cable lengths.

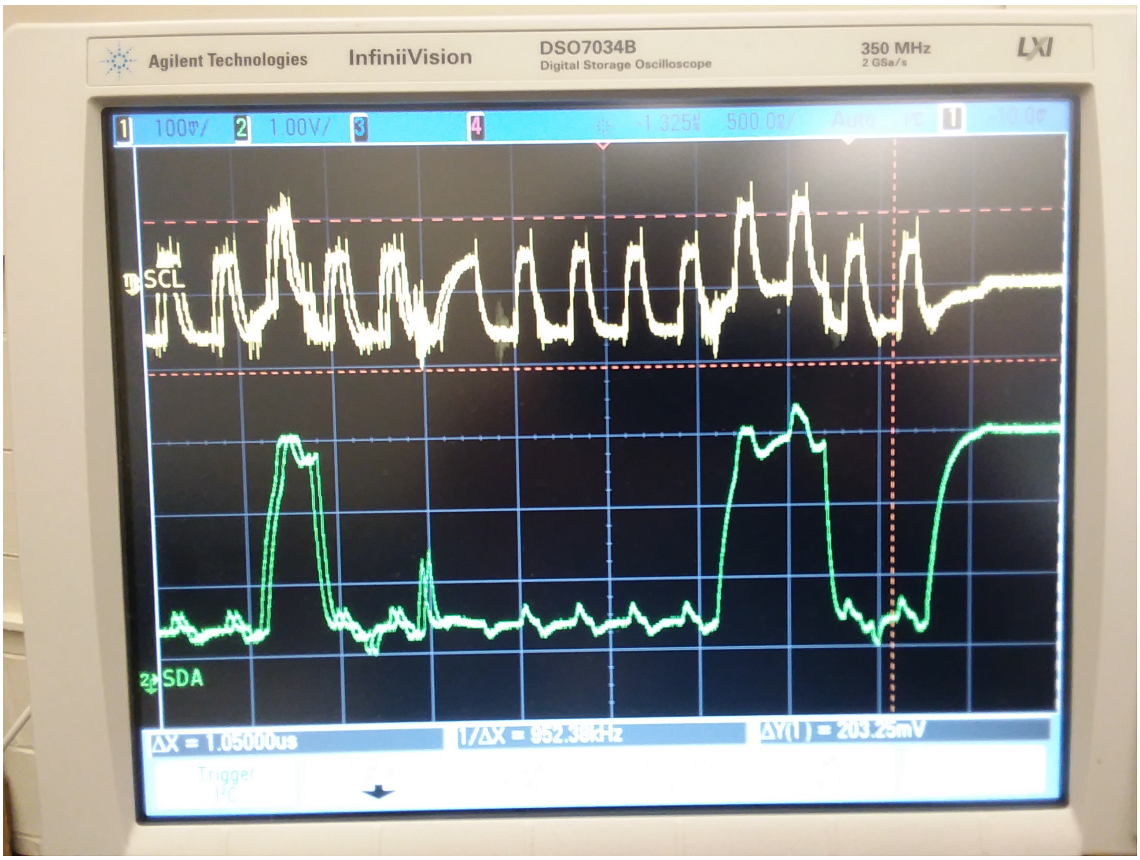

Figure 5.10: Oscilloscope capture of the I2C data communication between the Master and Slave Tiva devices. There is some slight capacitance in the signal as seen by the slew rate of the signal; however, the signal is good for reliable communication between devices.

The UART speed follows very closely to that of the I2C in that we are at most sending over 54 bytes of data from which we get a maximum speed for the UART module of,

$$UARTspeed = 10 * 54 * 500 = 270,000\ bps \tag{5.2}$$

Including start and stop bit with no parity bit. Therefore, the UART speed that would satisfy

this requirement and allow for sufficient time to perform the other tasks of the microcontroller was 921,600 bps. Figure 5.11, shows the Realterm data logging screen gathering data from the Master Tiva. The incoming data to Realterm is set to ASCII output format so that no additional conversion to hex or integer values is required. The data rate of 921,600 is too quick to allow the conversion on Realterm to take place without getting backlogged with data and freezing the program. Therefore, an external software, Hex Editor Neo, allows for the importing of an ASCII data file to be read. The file once interpreted, is imported into MATLAB for data analysis.

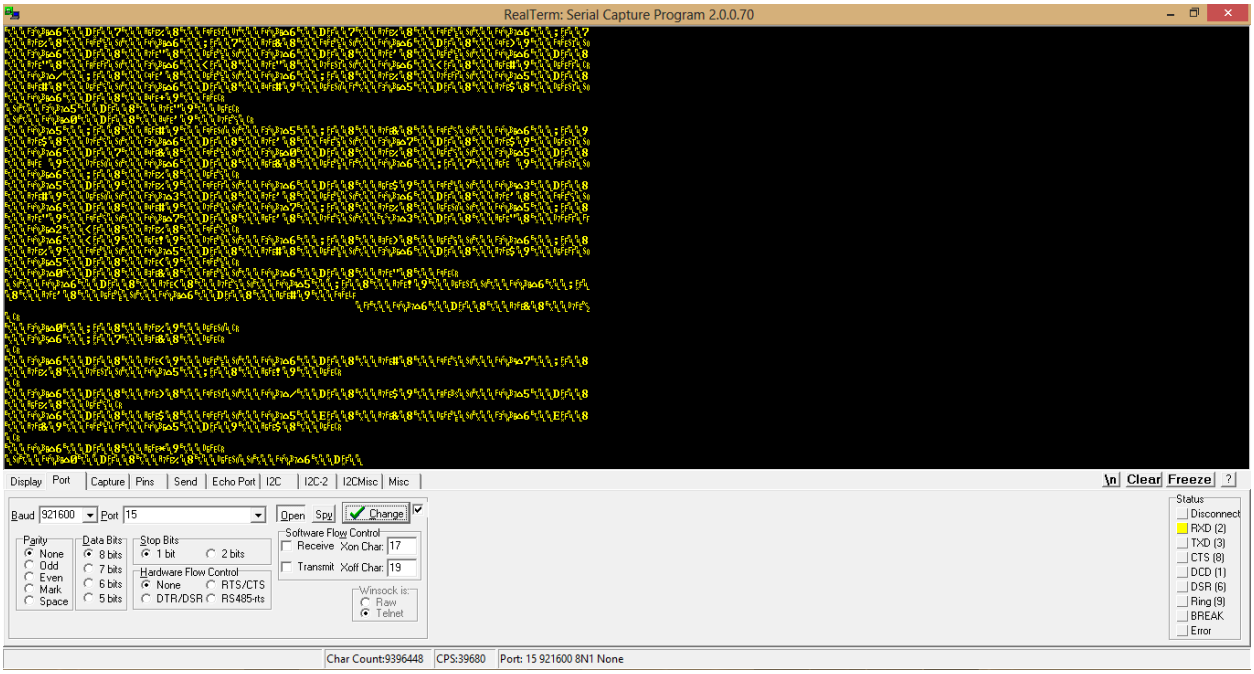

Figure 5.11: Realterm data logger program. Incoming characters are in ASCII format to maintain the desired data logging rate.

5.3 Control System

5.3.1 Torque Reference Controller

In order for the prosthesis to be passively responsive to disturbances while still maintaining predictable walking behavior, an impedance-based approach has been implemented, following that of Sup (2008) [16]. Using this approach each segmented portion of the gait cycle will have a unique stiffness and damping coefficient, which correspond to different joint torque commands for a given mode. The impedance model implemented is given,

$$\tau = k_1(\theta - \theta_e) + b\theta \tag{5.3}$$

Here, τ is torque, θ is the angle, θ_e is the equilibrium angle, k_1 is linear spring stiffness, and b is the linear damping coefficient. Using this approach, energy is delivered to the prosthesis by switching between modes, while keeping the prosthesis passive in nature, i.e. it will come to rest at a local equilibrium position, and only continue when the user initiates a transition. The switching criteria for gait mode transitions may be seen in figure 5.12, where the four modes are defined as stance flexion/extension, pre-swing, swing flexion, and swing extension.

This impedance model is used for each DOF including the roll, which needed to be tuned to work in conjunction with the pitch DOF since these two are dependent on each other. The two command signals, one for roll and the other for pitch, for the ankle were combined into a single equation which assigns different torque requirements to each of the actuators via the spring rate and damping coefficients until the roll angle is achieved. At this point, the torque commands to each of the actuators will be the same. To obtain the desired roll angle the coefficients for the roll actuation need to vary proportionally with the pitch DOF coefficients. This is a result of the two actuators having slightly different internal friction

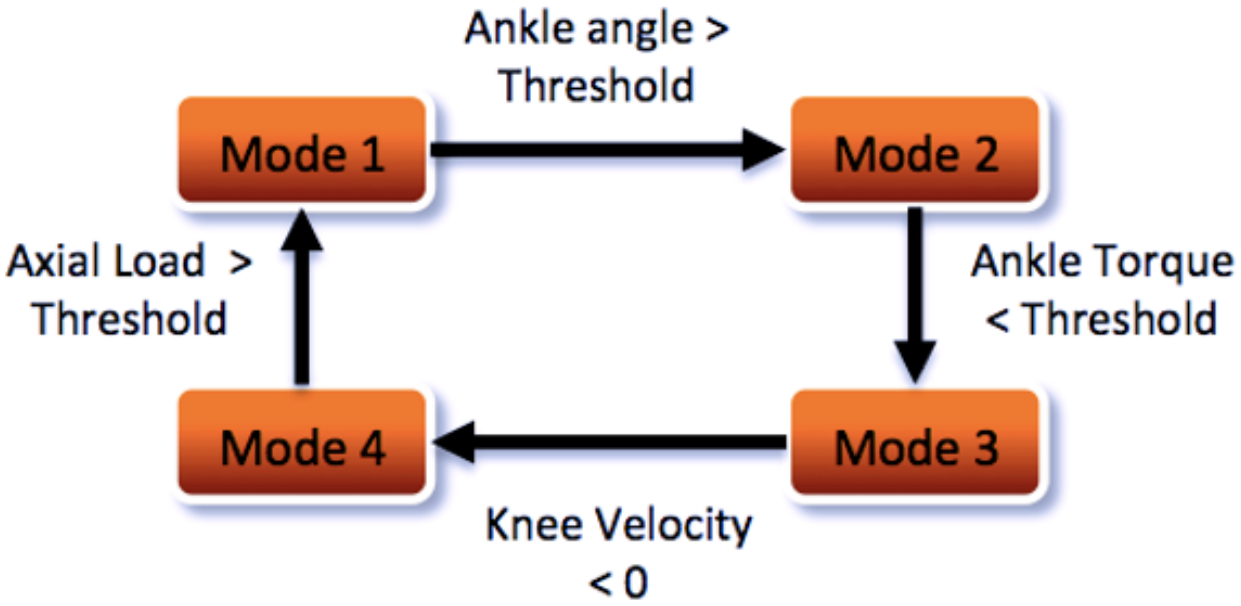

Figure 5.12: General switching criteria diagram for transitions between modes in the gait cycle.

and damping, and motor tunes. If the roll coefficients are left constant for large changes in pitch DOF coefficients, the actuators tend to drift out of sync with each other and fail to maintain the desired roll angle. A worst-case scenario occurs when the roll current is much greater than the pitch current. In this case, the actuators fail to move at all because the force holding them together dominates the motion and torque commands. The combined equation is,

$$\tau_{Total} = \tau_{Pitch} + \tau_{Roll} \tag{5.4}$$

Where the equations for the torque for each DOF is that of the impedance model. Using equation 5.4 for the ankle DOF we see that if one actuator is above the other than the roll torque will subtract from the pitch torque and slow the actuator down. Likewise, if one of the actuators is falling behind, the two torques will add and increase the speed of the

actuator to obtain the desired roll angle. In addition, a stance mode was added to allow the user to adjust to the prosthesis, and for the baseline parameters required for lifting their body weight to be tuned.

5.3.2 Ankle Kinematics

The impedance model, 5.4 is used for each DOF, however, the ankle requires additional calculations for proper control. Since this DOF operates using two parallel actuators, there are a few ways to approach the control of this system. One way is to couple both actuators together in pitch and roll so that both actuators only look at the current angle of the joints instead of their current location on the ball screw. The second option is to independently control them, and simply send them to locations on their respective ball screw that will achieve the desired roll and pitch angles of the ankle. The third option is to independently control them in pitch, and couple them in roll. The third option was chosen out of the three since it affords each actuator knowledge of its own location on the ball screw for control while maintaining the desired roll angle through the entire range of motion. The issues with the first option are that neither actuator knows the exact location of where they are on the ball screw, and as a result a crash into the top of the actuator is more likely to occur. An example of this would be to have the roll angle at a maximum while sending a pitch angle command other than zero to be attained. This would result in a crash, which may be avoided with additional safety functions in the program; however, is more difficult to implement. The issues with the second option are that neither actuator has any idea of the existence of the other, and therefore, any slight imbalance in the internal friction and damping of the actuators will result in unequal motion, thereby making stable control of the roll angle nearly impossible. Figure 5.13 shows the kinematic models used for determining the individual ball nut locations.

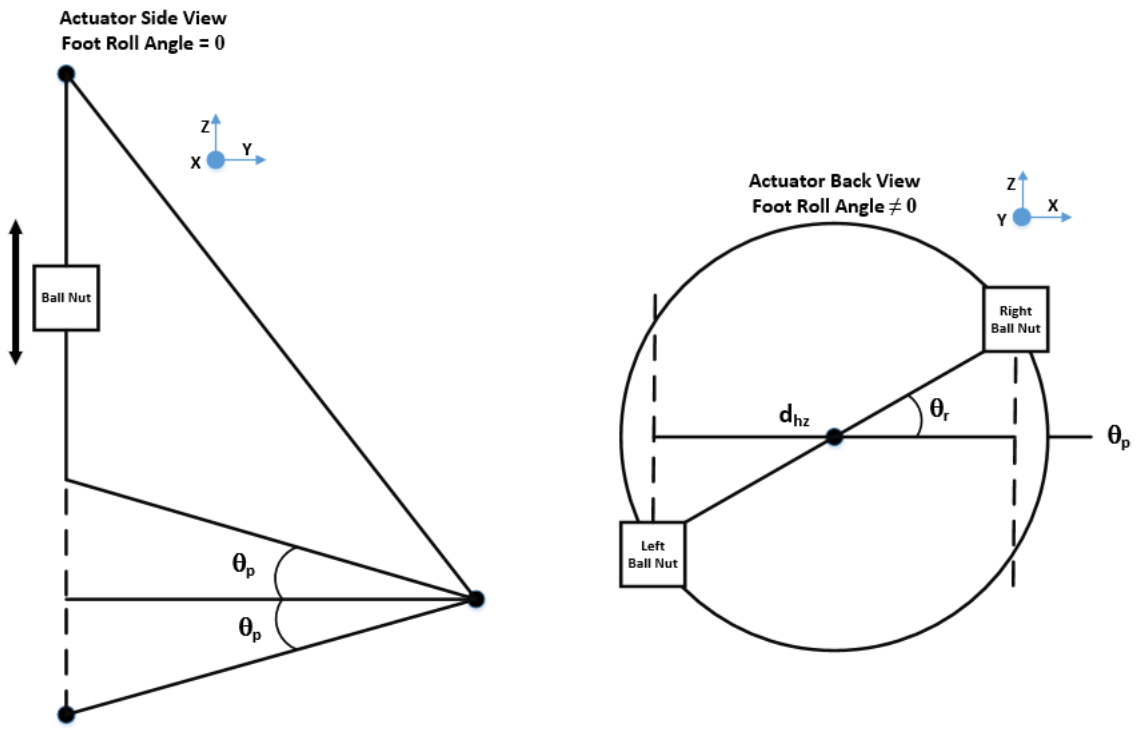

Figure 5.13: Kinematic model used for determining the individual ball nut locations.

From this model, we can derive the equations needed to relate the current joint positions, i.e. roll and pitch angles, to the locations of the left and right actuator ball nuts, equations 5.5 and 5.6. For these calculations, it was assumed that the actuators remain completely parallel to each other during the entire ROM. The equation for determining the ball nut locations is given,

$$D_{rb} = \theta_p \pm (0.5) * d_{hz} \cos\ (\theta_r) * \tan(\theta_r) \tag{5.5}$$

$$D_{lb} = \theta_p \mp (0.5) * d_{hz} \cos\ (\theta_r) * \tan(\theta_r) \tag{5.6}$$

In equations 5.5 and 5.6 the plus-minus sign corresponds to whether the prosthesis is being worn on a left or right foot. Note that D_{lb} and D_{rb} are the ball nut locations given as an angle; the angle at which the ankle pitch encoder would read if the other ball nut moved to

that same location. To validate the assumption made, the calculated ball nut position was compared against the pitch angle measurement from the absolute encoder at the joint and were within 0.5° of the absolute encoder position measurement. Using these same equations, the desired equilibrium angle was transformed to an equivalent ball nut location for each of the actuators for control using equations 5.7 and 5.8.

$$D_{rbe} = \theta_{pe} \pm (0.5) * d_{hz} \cos\ (\theta_{re}) * \tan(\theta_{re}) \tag{5.7}$$

$$D_{lbe} = \theta_{pe} \mp (0.5) * d_{hz} \cos\ (\theta_{re}) * \tan(\theta_{re}) \tag{5.8}$$

In equations 5.7 and 5.8 above D_{rbe} and D_{lbe} are the desired equilibrium angles of the ball nuts given θ_{re} and θ_{le} the desired roll equilibrium angle and θ_{pe} the desired pitch equilibrium angle. Lastly, d_{hz} is the horizontal distance between the ball nuts at 0° roll.

5.3.3 Force Controller

In addition to the torque reference controller (impedance controller) described above, a lower level force controller was implemented to supplement the actuation of the prosthesis. By incorporating a force controller, the prosthesis is able to move in a more natural way by compensating for the inherent friction and damping forces in the actuator and aiding in overcoming the inertial forces. The force controller is a simple PID controller which takes in the desired force to be applied to the ball screw via the torque reference signal and compares it to the present load on the ball screw. The signal leaving the force controller is the current input to the motor. By implementing the force controller the torque reference commands from the torque controller are more easily tracked by the leg during operation. Equation 5.9 is used in the force controller, note that the proportional gain is the only one used in the

controller.

$$Signal = K_p * (\frac{\tau_{total}}{MomentArm} - ForceSignal) \tag{5.9}$$

The force and torque reference controllers above are the ones used in the present system, and were used to obtain the walking data in chapter 6. However, inertial modeling was conducted to be used in a more advanced controller if needed once additional sensors are incorporated into the prosthesis, see chapter 9 section 9.3. The inertia for the system was computed using standard modeling equations for inertia. Sources of inertia in the actuator are the ball screw, ball screw pulley, and the motor shaft. Note that, another source of inertia is the ball nut; however, when compared to the loading conditions expected on the joint, e.g. $>$ 10 kg vs. 0.1 kg for the ball nut, is negligible, and handled by the joint force compensation described above. Values for inertia were derived from the NX CAD model of each of these components using the radius of gyration about the desired axis. Equation 5.10 for the inertia of a point mass at the end of a rod was chosen for the calculation,

$$I = m * r_g^2 \tag{5.10}$$

where m is the mass of the component and r_g is the radius of gyration about the desired axis as given by NX. The motor, being a hobby motor, had no documented rotor inertia, and therefore an NX model of the outrunner portion was created, figure 5.14, to obtain an estimate of the inertia.

Table 5.2, summarizes the results of these calculations.

The values calculated in table 5.2, are then translated to those seen at the motor. Equation 5.11, is used to calculate the additional torque requirements to overcome the rotational

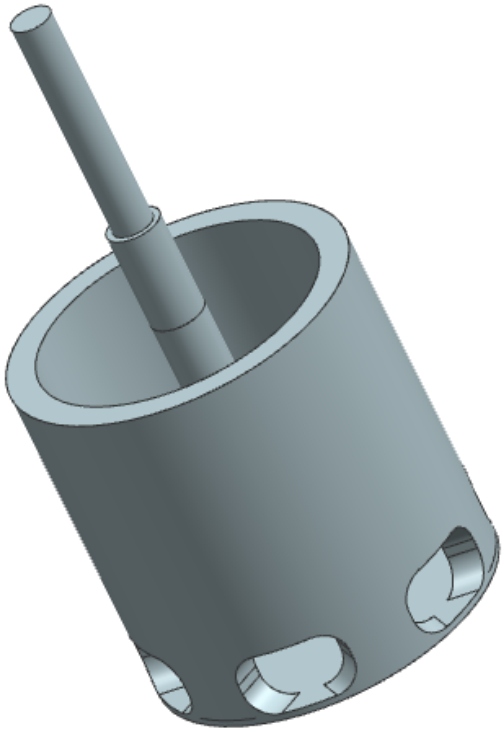

Figure 5.14: NX motor model used to calculate the moment of inertia of the motor.

Component	*Inertia [kg*m^2]*
Ball Screw Knee	$I_{BSK} = 1.277(10^{-6})$
Ball Screw Ankle	$I_{BSA} = 9.654(10^{-7})$
Ball Screw Pulley	$I_{plly} = 9.715(10^{-6})$
Motor	$I_{mtr} = 7.876(10^{-5})$

Table 5.2: Summary of Actuator Rotational Inertias

inertia.

$$\tau_{Ir} = (I_{mtr} + \frac{I_{BS} + I_{plly}}{PreGear^2}) * \alpha_{mtr} \tag{5.11}$$

In addition to the rotational inertia of the actuator components, the inertia of the prosthesis must also be taken into account. The prosthesis may be broken up into three separate cylindrical sections for modeling purposes, the sections being, the knee, the ankle, and the

foot. Each of these cylinders is connected to each other, all rotating about a single axis perpendicular to the length of the cylinders at the end of the knee cylinder model. Figure 5.15, depicts the model used for the inertia calculations of the prosthesis which is only applicable to the knee DOF program. Figure 5.16, depicts the model used for the calculation of the inertia for the yaw DOF which is only applicable to the yaw DOF program. Note that the only rotating sections of the prosthesis due to the yaw motion are the ankle and foot, depicted in the model. This calculation uses the same cylinder model for the ankle as that used for the knee inertia calculations.

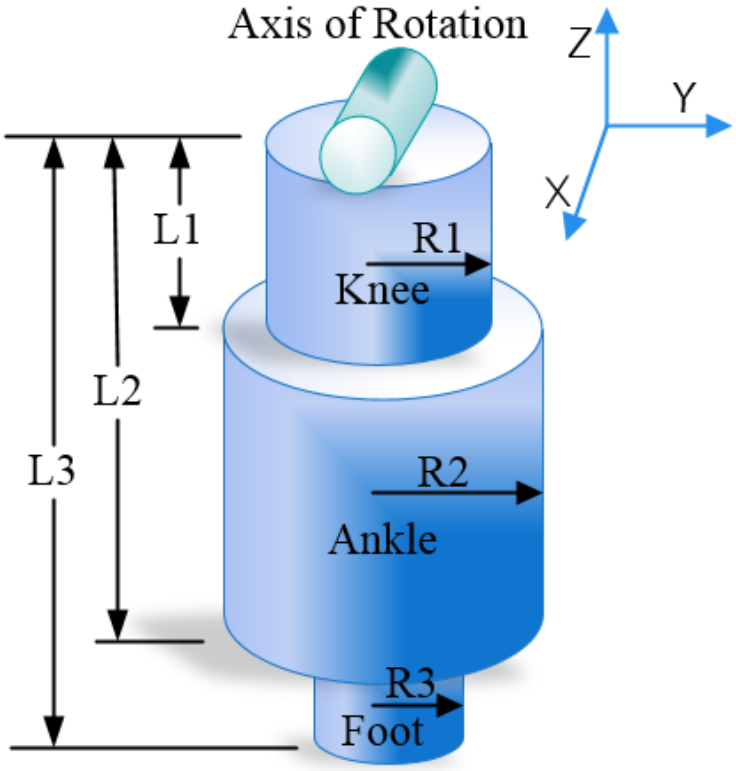

Figure 5.15: Model of prosthesis used for calculating the mass moment of inertia about the axis of rotation at the knee joint.

From the model of the leg above, the following inertia equations are derived,

$$I_{Knee} = \frac{1}{4} m_{Knee} R_1^2 + \frac{1}{3} m_{Knee} L_1^2 \tag{5.12}$$

$$I_{Ankle} = \frac{1}{4} m_{Ankle} R_2^2 + \frac{1}{3} m_{Ankle} (L_2 - L_1)^2 + m_{Ankle} L_1^2 \tag{5.13}$$

$$I_{Foot} = \frac{1}{4} m_{Foot} R_3^2 + \frac{1}{3} m_{Foot} (L_3 - L_2)^2 + m_{Foot} L_2^2 \tag{5.14}$$

Therefore, the total mass moment of inertia for the prosthesis is given by,

$$I_{Prosthesis} = I_{Knee} + I_{Ankle} + I_{Foot} \tag{5.15}$$

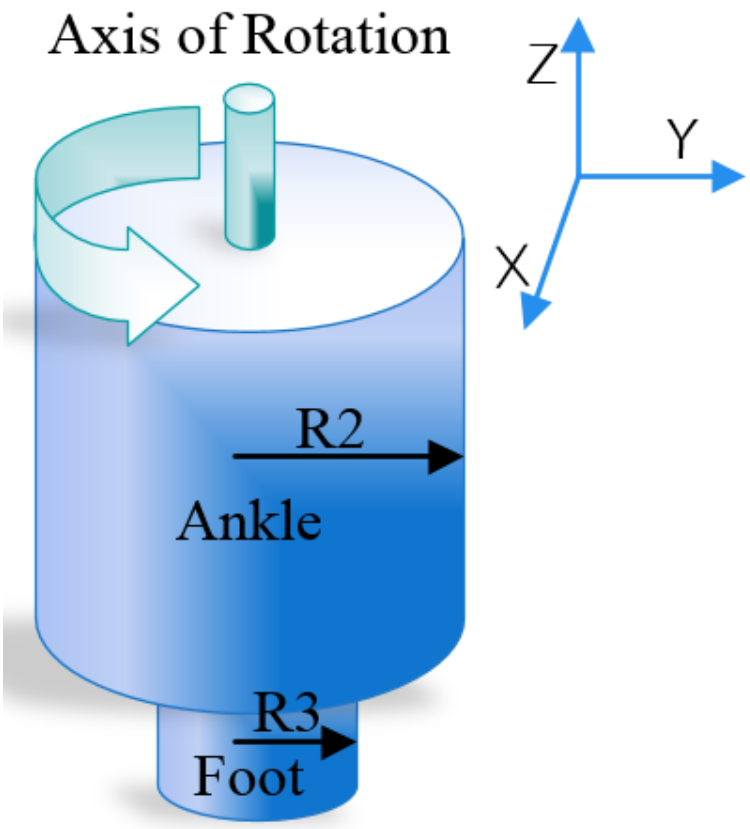

Figure 5.16: Model of prosthesis used for calculating the mass moment of inertia about the axis of rotation for yaw.

From the model of the prosthesis above, the following inertia equation is derived,

$$I_{Yaw} = \frac{1}{2} m_{Ankle} R_2^2 + \frac{1}{2} m_{Foot} R_3^2 \tag{5.16}$$

The results from these calculations are summarized in Table 5.3.

DOF	*Model [kg*m^2]*
Knee	$I_{Prosthesis} = 0.3788$
Yaw	$I_{Yaw} = 5.5(10^{-3})$

Table 5.3: Summary of prosthesis inertial modeling

Equation 5.17, may be used in the program for calculating the additional torque requirements

to overcome the inertia due to the prosthesis.

$$\tau_{Prosthesis} = \frac{I_{Prosthesis} * Lead}{GearRatio^2 * \eta_{BS}} * \alpha_{mtr} \tag{5.17}$$

Therefore, the total torque requirement due to inertial affects for the knee DOF is given by,

$$\tau_{Knee} = (I_{mtr} + \frac{I_{BS} + I_{plly}}{PreGear^2} + \frac{I_{Prosthesis} * Lead}{GearRatio^2 * \eta_{BS}}) * \alpha_{mtr} \tag{5.18}$$

Chapter 6

Results

The prosthesis was tested on a treadmill with able bodied individuals using an able bodied adapter. For these initial tests the yaw DOF was not used, and the roll DOF was kept at approximately 0°. Testing sessions lasted from 1 - 1.5 hours, to allow the user to become comfortable with walking in the ABA. The results presented below are for a walking speed of 0.67 m/s (1.5 mph), and show similar characteristics to that of a normal walking gait with a 1 second step period. In addition, the torque at each of the joints, the joint power, and the motor current draw and power to determine the battery life of the prosthesis are analyzed.

Gait Mode	Knee Impedance			Ankle Impedance		
	k (Nm/deg)	b (Ns/m)	θ (deg)	k (Nm/deg)	b (Ns/m)	θ (deg)
1	1.34	0.13	15	1.11	0.13	-1
2	1.34	0.13	11	1.34	0.13	-14
3	1.78	0.78	45	1.56	0.13	0
4	1.78	0.40	10	1.56	0.13	1

Table 6.1: Tuned parameters for the prosthesis at a walking speed of 0.67 m/s (1.5 mph).

6.1 Gait Replication

During the treadmill tests the equilibrium positions, spring stiffnesses, and damping coefficients were adjusted until a satisfactory gait was achieved. The final values for the equilibrium angles, spring stiffnesses, and damping coefficients are given in Table 6.1.

The final parameters listed in table 6.1 were tuned by observing the prosthesis during treadmill walking, user feedback, and data analysis. Once satisfactory parameters were achieved the prosthesis was able to walk reliably for a short span of speeds, e.g. 0.45 m/s - 0.67 m/s (1 - 1.5 mph) before parameters would need to be adjusted due to changes in gait at faster walking speeds, and for gait transitions in general, e.g. walking to running. The final walking gait achieved by the prosthesis for 0.67 m/s (1.5 mph) may be seen in Figure 6.1, and the nominal walking gait assuming a step period of 1 second may be seen in Figure 6.2 [33].

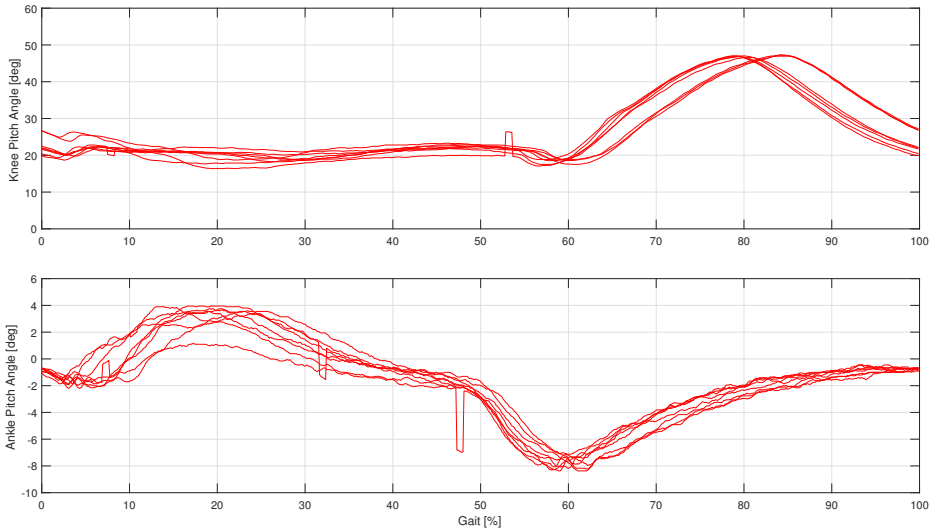

Figure 6.1: Gait pattern for the prosthesis at 0.67 m/s (1.5 mph) for eight consecutive strides.

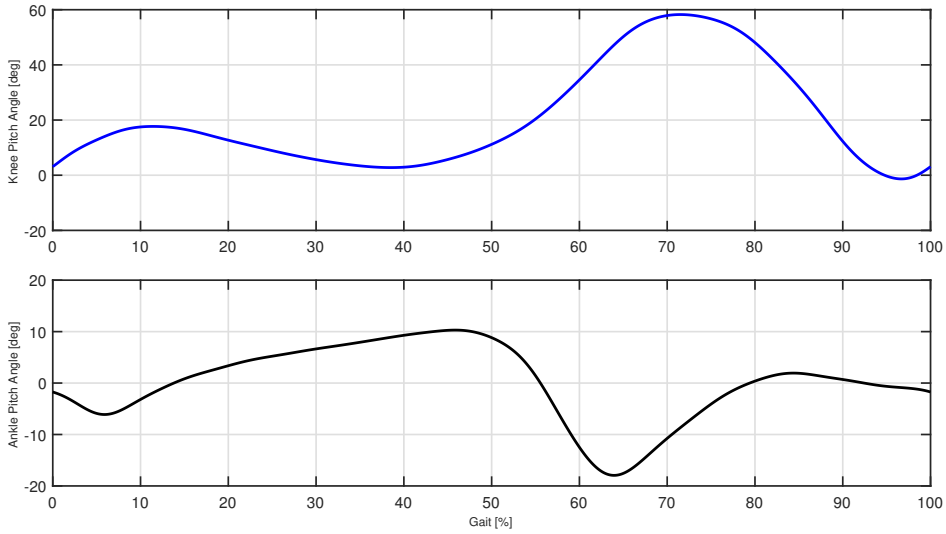

Figure 6.2: Normal walking gait pattern [33].

6.2 Joint Torques

Figure 6.3 shows the knee and ankle torques present throughout the gait cycle, and figure 6.4 shows the body weight normalized joint torques of a normal gait.

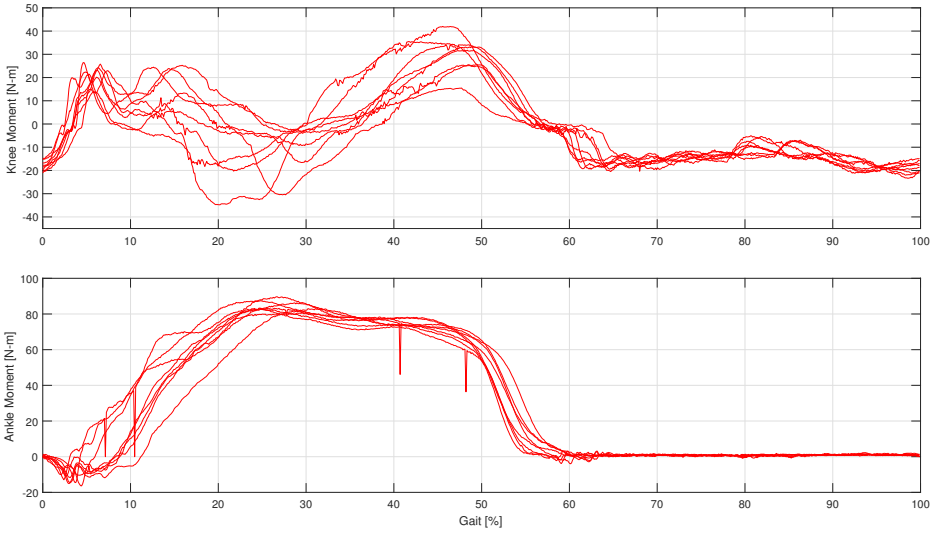

Figure 6.3: Gait joint torque pattern for the prosthesis at 0.67 m/s (1.5 mph) for eight consecutive strides.

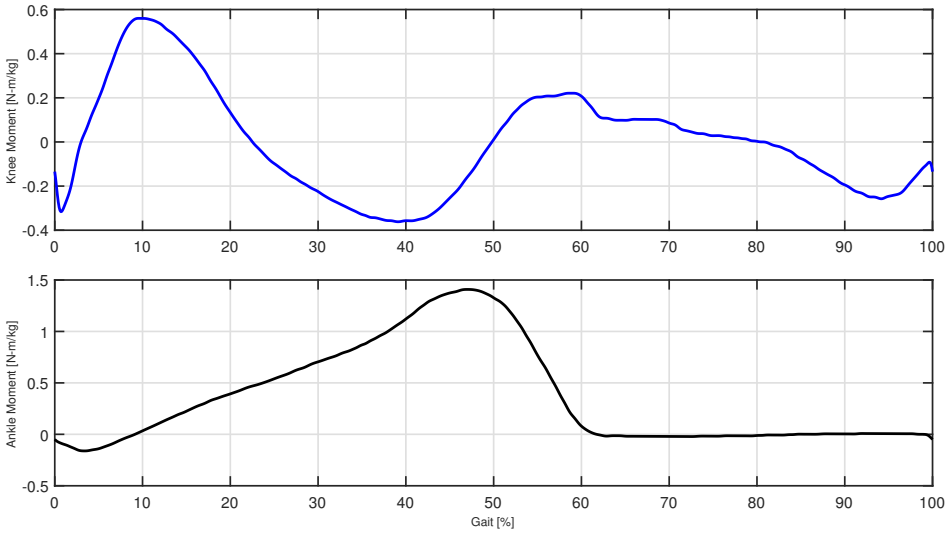

Figure 6.4: Body weight normalized joint torque pattern for normal walking gait.

From figure 6.3 we see that both the ankle and knee actuators apply the torque to the joint

where necessary in the gait cycle. The ankle experiences a slight increase in torque from 0 - 10% during stance flexion/extension reaching roughly -15 Nm with the maximum torque output occurring during toe-off at 20 - 60% reaching roughly 90 Nm. For the remainder of the gait cycle from 60 - 100% the torque remains constant at around 0 Nm. The knee experiences a somewhat large deviation in torque delivery from stride to stride due to several factors discussed in chapter 7 section 7.2. The torque delivery to the knee joint during stance flexion/extension from 0 - 36% peaks at 20 Nm at heel strike and then around -20 Nm leading into pre-swing, pre-swing from 37 - 60% peaks at 40 Nm, and swing flexion/extension from 60 - 100% peaks at -20 Nm.

6.3 Joint Powers

Both the knee and ankle joint powers throughout the gait cycle are presented in figure 6.5, with the joint powers of a normal gait shown in figure 6.6. The maximum power obtained by the prosthesis is 30 W for the knee and 25 W for the ankle. The maximum power given by the body weight normalized gait data for the knee is -1.145 W/kg, and 3.685 W/kg for the ankle.

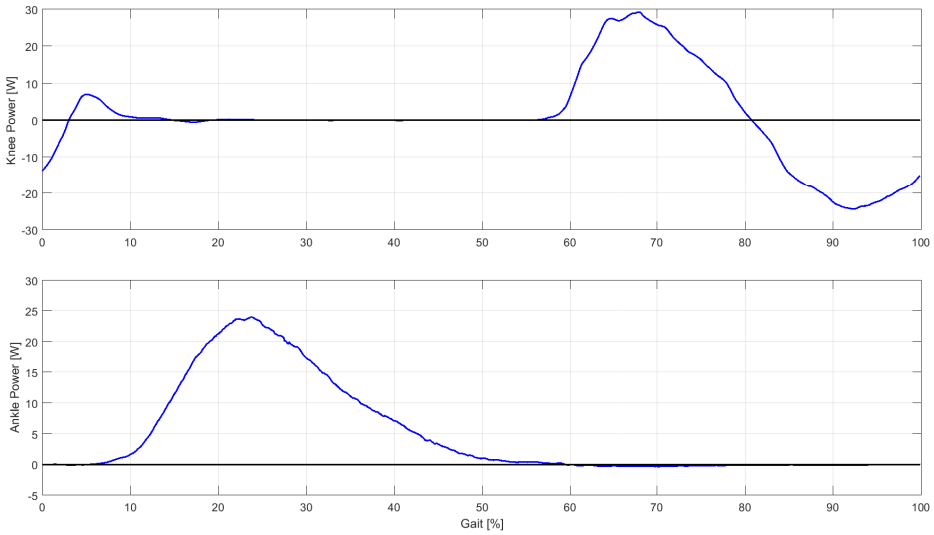

Figure 6.5: Averaged knee and ankle joint powers for the prosthesis for eight consecutive strides.

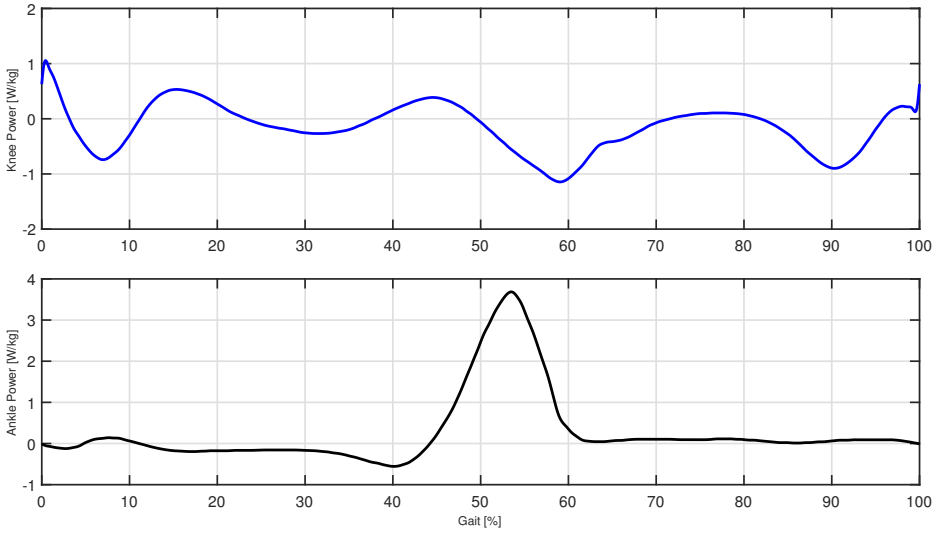

Figure 6.6: Body weight normalized joint powers for normal walking gait.

6.4 Battery Power Consumption

During the treadmill walking trials, batteries were used and data was gathered on the current draw of the motors. Figure 6.7 displays the average current draw for eight consecutive strides at a walking speed on 0.67 m/s (1.5 mph). The average current draw for the knee actuator is 5.10 A and that for the ankle is 13.78 A. In addition figure 6.8 shows the motor power during the gait cycle. The average power for the knee and ankle motors are 10.75 W and 7.11 W respectively.

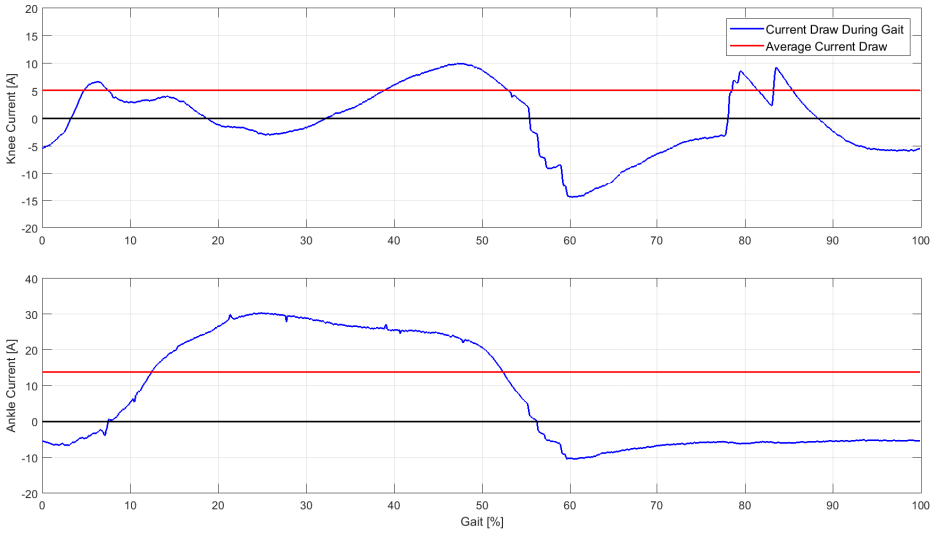

Figure 6.7: Averaged gait cycle current draw for knee and ankle actuators for eight consecutive strides.

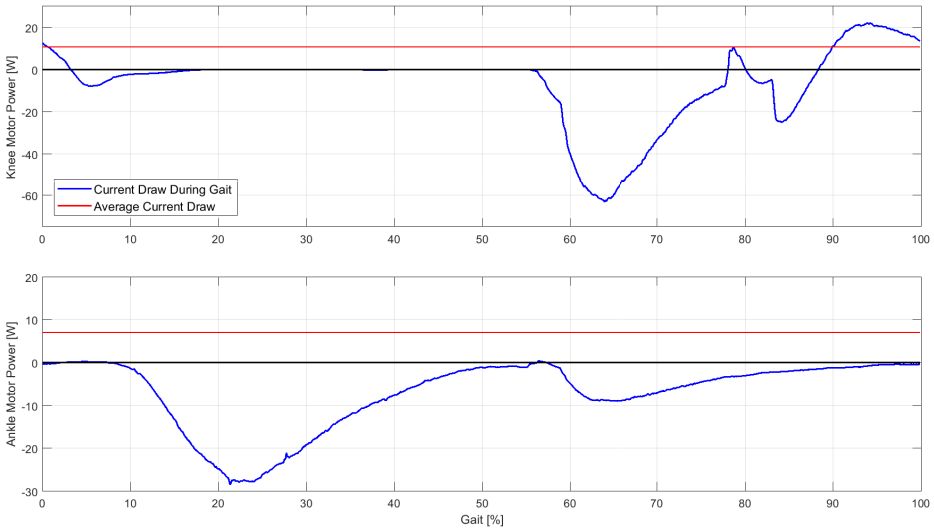

Figure 6.8: Averaged gait cycle motor power for knee and ankle actuators for eight consecutive strides.

Chapter 7

Discussion

For the treadmill tests an ABA was implemented with each test subject needing to become acclimated to it, and have the prosthesis tuned for their own particular gait. This was evident when conducting the tests with two different subjects, each requiring slightly different equilibrium angles, spring stiffnesses, and damping coefficients. The subjects also provided feedback on whether or not the ankle actuators were providing enough force during toe-off and if there was sufficient support from the leg throughout the stance flexion/extension phase of the gait. Once the prosthesis was tuned, the test subjects were comfortable with walking in the ABA; however, the ABA still caused issues at times due to the additional compliance, which would result in the subjects stumbling and therefore will need to be improved for future testing. Another area of complexity which needed tuning was the force controller's proportional gain for each of the ankle actuators. This needed to be done since there was a difference between the load readings on the right and left ankle actuators, which caused the roll to deviate from the desired angle, in our case for testing 0°. This though should not be a large area of concern when testing on an amputee since the force will be acting down the center line between the parallel actuators. In addition, during testing noise interference due to Electromagnetic Interference (EMI) caused the prosthesis's I2C communication to cut out frequently which rendered it nearly impossible to accommodate further testing. When the communication cut out, the Master module was no longer able to send data to the Slave devices which is critical for sending the new gait transition modes for continued operation.

In addition to the loss of communication with the Slave devices, the Master was no longer able to send data to the computer via UART for data logging. The data gathered is all that could be obtained before the communication cut out. However, multiple possible solutions to mitigate the EMI were attempted which included,

- Making the I2C communication protocol more robust in handling arbitration lost errors.
- Using shielded cabling with earth ground.
- Placing the motor controllers in an earth grounded aluminum box.
- Placing the microcontrollers in earth grounded aluminum boxes.
- Removing the microcontrollers from the prosthesis and placing them in a large earth grounded steel box with shielded cabling.

The last solution provided sufficient time to gather the test data from the treadmill tests presented in chapter 6.

7.1 Gait Replication

From the treadmill tests depicted in figure 6.1 above, we see that the prosthesis is capable of imitating the gait cycle with additional tuning of the parameters. From the data gathered there is a slight resemblance in the stance flexion/extension phase, around 0 - 36% of the gait, to that of a normal gait in the knee DOF; however, there is a greater resemblance in the ankle to a normal gait. Once the prosthesis enters into pre-swing, about 36 - 60% of the gait, there is a slight dip in the knee angle as is for a normal gait followed by the largest motion of the knee during walking, swing flexion and extension, 60 - 100% of the gait. During pre-swing the ankle goes into toe-off and pushes the prosthesis to continue the forward motion of the leg. Once the pre-swing phase is complete the ankle moves to 1° so that the foot is sufficiently elevated and clear of the floor for the swing extension phase of the knee. This also allows the foot to land on the heel instead of landing flat footed. One area of issue is the synchronization between the knee and ankle DOF when the knee is entering swing flexion later than the ankle, and therefore the power delivery to the user is not efficient and causes a slightly unnatural gait. All of the issues in the current gait pattern for the prosthesis may be mitigated with further tuning once the issues of noise interference have been resolved. See chapter 9 for details on resolving these issue.

7.2 Joint Torques

Following that of the gait pattern replication, it is important to replicate the joint torques accurately in order to minimize power consumption, and to provide positive work where necessary in the gait cycle. The joint torques were calculated using the load cell data gathered during testing and the known 50 mm moment arm for the joint. The torque delivery to the

ankle shows that the actuators are providing the torque where necessary in the gait cycle. For our test subjects, the normalized walking gait data would yield a maximum torque output of 36.41 Nm for the knee and 91.52 Nm for the ankle. The torque distribution matches what is expected when observing the phases of the gait cycle. Starting in stance flexion/extension the knee follows the characteristic pattern of the normal gait, but hits a lower maximum torque output of around 20 Nm than the expected 36.41 Nm. The knee then experiences a drop in torque output, around -20 Nm, due to the stance phases main function of being a support for the body weight of the user. Entering into pre-swing the knee begins to move more quickly as it prepares to enter into swing flexion/extension where it propels the user's body forward. At this point in the gait the torque output is lower since the leg is now free swinging in air where the load on the knee joint is low but the velocity is high. The ankle torque output in the stance flexion/extension phase is supposed to have a gradual increase in torque leading up to toe-off; however, for our prosthesis the onset of torque is more sudden in the stance flexion/extension support phase and is maintained through pre-swing where toe-off occurs. Once the gait cycle enters into swing flexion/extension the ankle torque drops to zero as expected and as seen in the normalized torque output in figure 6.4. This is due to the fact that the ankle is in the air as the knee completes its swing. Note that throughout the gait cycle the ABA adds compliance to the knee joint which has a marked effect on the ability of the knee actuator to follow the torque commands, particularly in the stance flexion/extension phase of the gait which is where the large deviations in torque output between consecutive strides of the gait cycle originate from.

7.3 Joint Power

The power output of the joints shows that both the knee and ankle joints are offset in their application of power, and therefore are not providing as much assistance during walking as possible. The maximum power output achieved by the knee DOF is offset from what is expected by approximately 10% occurring at 70% instead of 60% of the gait cycle. In addition the maximum power output is around 30 W whereas for our subjects it is expected to be around 74.43 W using the normalized gait data. This then suggests that most of the power is output during the swing flexion/extension phases of the gait where the velocity of the joint is at its highest. For the remainder of the gait cycle the power output of the knee joint stays around zero due to a very low velocity output during the stance flexion/extension phases of the gait. The ankle has a marked difference between what was achieved and what was expected when viewing the body weight normalized gait data. The maximum power output achieved by the ankle is only 25 W whereas the expected output is 239.5 W. In addition the application of the power to the ankle lasts from 10 - 50% of the gait cycle when it should last from about 45 - 60% of the gait cycle. Therefore, much work is needed in the tuning of the parameters to maximize the power delivery to the user during the walking gait, and to better synchronize the knee and ankle actuators throughout the gait cycle.

7.4 Battery Power Consumption

Ideally the batteries are to last for 1 - 4 hrs depending on the gait of the individual and the speed at which they are moving. As seen in figure 6.7 the average battery power consumption for the prosthesis during level walking at 0.67 m/s (1.5 mph) is 20.9 W, and indicates that the prosthesis will last for approximately 20 minutes, with three 6400 mAh 4s LiPos. This estimate is due to the large current draw of the motors as seen in figure 6.7. This then shows that the prosthesis must be tuned further in order to maximize the application of the torques when necessary. In addition, the use of large BLDC motors introduces a large rotor inertia which requires a higher current to initiate rotation of the shaft. However, as previously stated the largest factor affecting the large current draw of the motors are the tuning parameters for the torque controller. Therefore, the prosthesis is not capable of sustaining a full day of walking at reasonable speeds, let alone performing any strenuous activities such as running and jumping, though the leg is designed to be able to perform these tasks. In order to increase the functioning time of the prosthesis it is necessary to tune the parameters more precisely, which may be accomplished by making some changes to the electrical system as discussed in chapter 9.

Chapter 8

Conclusions

The prosthesis described in this work was built to be a high powered 4 DOF leg for TF amputees capable of performing a wide variety of high power tasks, e.g. running, squatting, and potentially jumping. The prosthesis successfully replicated certain characteristics of the walking gait of an able bodied individual with deviations in the angle and torque trajectories due to additional compliance in the ABA for the knee joint, and parameter tuning in both the knee and ankle joints. To achieve a more bio-mimetic feel the prosthesis utilizes SEAs which store and return energy to the joint during the gait cycle, and to reduce the total motor power required throughout the gait cycle. However, the SEAs need to be tested further to determine their effectiveness in reducing the motor power consumption throughout the gait cycle. Replicating the walking gait was achieved through the use of proper sensor selection which included, load cells placed in line with each ball screw on the linear actuators, absolute encoders placed at the ankle joint for roll, pitch, and yaw, and the knee joint for pitch, and incremental motor encoders for velocity calculations. In addition to the sensors used for enabling the prosthesis to perform locomotive tasks current sensors were implemented for future use to determine the effectiveness of the SEAs at returning energy back into the walking gait, and for motor power and battery consumption calculations. The average power for the knee and ankle motors were 10.75 W and 7.11 W respectively with a current draw of 5.10 A and 13.78 A for the knee and ankle respectively. The average power consumption of the motors shows that the prosthesis is capable of 20 minutes of walking without needing to

recharge the batteries. Therefore other activities which require higher power consumption than walking are currently not feasible without worrying about the batteries dying. The linear actuators use high power helicopter BLDC motors which provide 2880 W of peak power to the prosthesis for the given motor controller which can provide 60 A peak current output. The maximum power requirements for the prosthesis are 2751 W for the ankle in running and 2494 W in the knee for stair climbing. Hobby motors are not typically used in bio-medical applications due to their lack of precision in movement and high rotational inertia; however, we have shown that with proper sensor instrumentation they work well in providing the needed joint torques during walking and replicating the walking gait on a treadmill at 0.67 m/s (1.5 mph), but with further tuning required. The maximum torque output recorded for both the knee and ankle are 40 Nm and 90 Nm respectively. In addition, the benefits of using these motors are many which include the ability to perform a wide range of human locomotive tasks beyond those of walking, e.g. running, stair climbing, squatting, and potentially jumping, all of which have larger power requirements if they are to be performed successfully, and their cost as compared to the standard motors used, e.g. $90 vs $260. Further testing is to be done regarding if there are any added benefits by including the yaw DOF in the walking gait after some mechanical revisions are made to the yaw DOF. In addition, testing on the different types of human locomotion are to be studied in order to push the prosthesis to its upper limit and test how the system responds to activities requiring higher power outputs. Lastly, several revisions may be made to the electronics of the prosthesis, including reducing the number of microcontrollers used to control the prosthesis which may fit into a shielded box to be worn on the wearer's back or hip.

Chapter 9

Future Work

The prosthesis described in this work has been able to produce proof of concept results that show promise for this type of mechanical setup which uses parallel SEAs for ankle actuation and a single SEA for the knee. However, due to system complexity the ultimate goal of achieving a full description of how the gait cycle is affected by the addition of a powered yaw DOF, and the effects that the high powered motors have on allowing the prosthesis to achieve more demanding forms of human locomotion have been compromised. Therefore in this chapter an overview of the future work will be laid out which will describe steps that may be taken to improve the system for further testing of the novel features of the prosthesis. We start with the yaw DOF followed by the electronics system used including: the control system, PCBs, additional sensors to be added for better performance, and motor testing to determine the thermal constant of the motors used.

9.1 Yaw Actuator

The yaw actuator as a whole does not need much revision; however, the belt tensioner must be redesigned in order to maintain proper tension on the belt as the prosthesis is in motion. Currently the belt tensioner uses radial bearings with a single bolt that is mounted to the same platform as the yaw gearbox, and only has support at one end. Therefore as the tension in the belt is increased the bolt bends backwards and loses tension during operation. This backwards bending of the bolt also causes an uneven distribution of tension on the belt with only the bottom portion of the radial bearings making contact with the belt. The belt tensioner currently used may be seen in figure 9.1 with the bolt bending backwards. A revision of the belt tensioner would include support at both ends so when the tensioner is adjusted the bolt will not bend backwards during operation. In addition to the belt tensioner, a minor issue is that thread locker must be added to the timing pulley and nut which connect to the yaw shaft in order to prevent them from coming loose during operation.

Lastly, it is recommended that the motor used for yaw actuation be switched out for one which is more reliable. The Mystery motor currently being used was not able to be properly tuned as an ideal position for the hall effect sensor board could not be found. The motor was only capable of providing good acceleration and torque in one direction of rotation while the other direction suffered, thereby making the yaw DOF unreliable in its torque delivery and trajectory tracking during the walking gait.

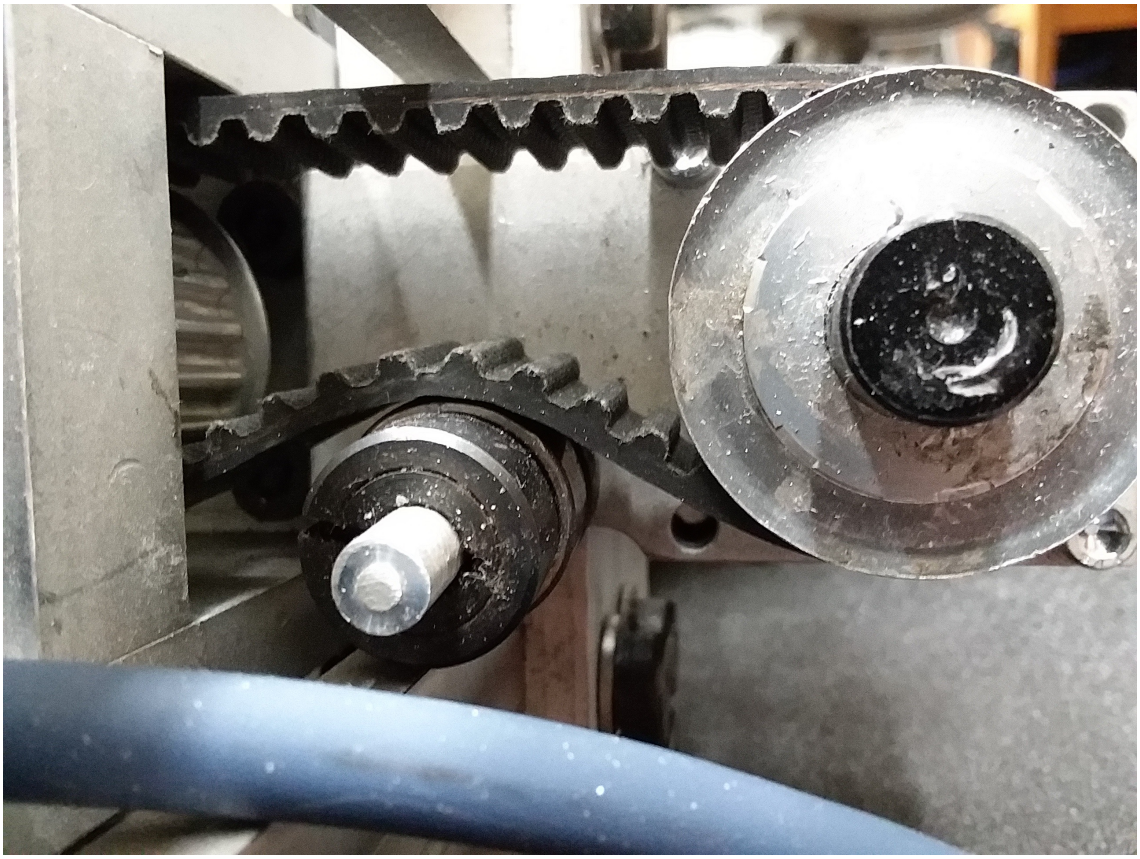

Figure 9.1: Current yaw belt tensioner on prosthesis.

9.2 Electronics - Control System

In addition to the yaw DOF issues discussed above the electronics will also need a revision due to the over-complexity of the system. Currently there are five microcontrollers controlling the system, one for each DOF and one Master module for sending gait cycle transition commands and for data logging. However, a more powerful controller such as a small on-board computer, e.g. a Raspberry Pi (figure 9.2), would be able to control each of the actuators and log data over UART to a laptop or desktop computer. By having only one module controlling all of the actuators the main issue of EMI would be eliminated since there would be no communication protocol between Master and Slave devices. In addition, the switching criteria for the actuators could be better synchronized since the actuators are controlled by one device, and the lack of delays due to bus recovery from EMI would increase gait mode transition speed. Very minimal additional hardware would be needed to make the change; however, depending on the on-board computer used a different programming language may be needed if it is not compatible with C or C++ based languages as used in Code Composer Studio (CCS). However, the current code may be used as a template for the order of processes regarding sensor signal reading and torque application for the new code.

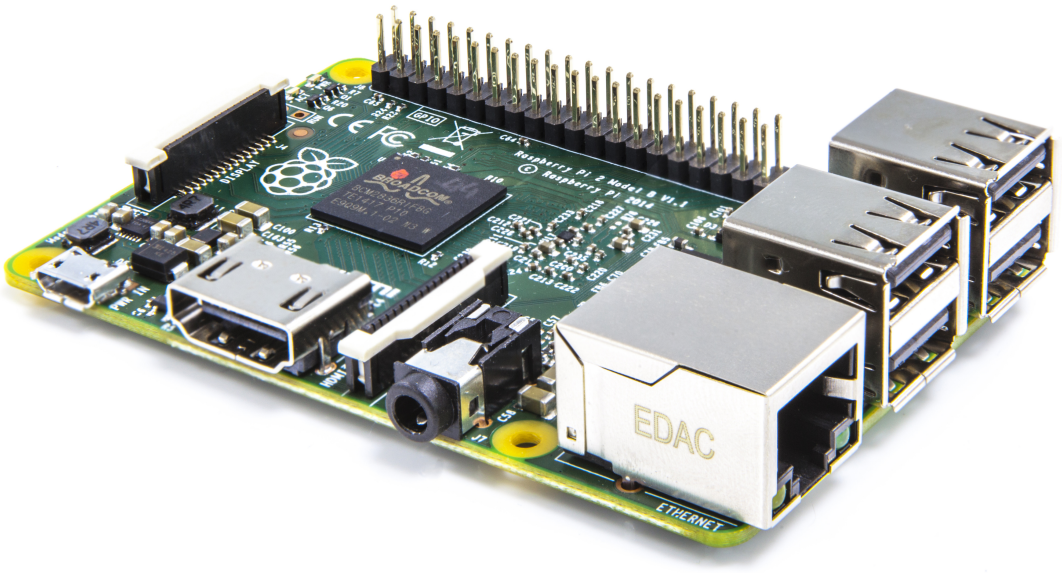

Figure 9.2: Raspberry PI board as potential on-board computer to replace current microcontroller system.

9.3 Electronics - Hardware

Along with the control system used, some of the hardware may be changed out to achieve better performance of the prosthesis. These changes are optional; however, would be beneficial for obtaining maximum performance. The force controller used in the prosthesis is a simple PID controller which uses the load cell readings as one input and the desired torque command from the torque controller converted to an axial force on the ball screw as the other. Currently the load cell signals are being amplified using a pre-made amplifier board; however, the amplifier board has a voltage offset of 2.5 V which limits the range of the present system and decreases the resolution of the load cell readings. A separate load cell amplifier board with adjustable voltage offset is recommended for future use regardless of whether or not the current microcontroller controls system is used. This board is also recommended if the new researcher(s) opt to replace the present control system with a single on-board computer (highly recommended approach). The recommended amplifier board has already been made by a previous researcher and need only be populated, figure 9.3. The board however, has yet to be tested to its full potential.

If the present control system is deemed insufficient for the prosthesis to perform other forms of human locomotion, moments of inertia for the prosthesis have been calculated as discussed in section 5.3.3 of the paper, and may be used if needed. Note that these values have not been thoroughly tested with the current prosthesis and may need some adjustment as incorporating inertia into controllers can be hazardous if the values are too large, i.e. cause uncontrollable behavior. If it is desired to use the inertia calculations, then IMUs must be added onto the prosthesis at the locations of the ankle, knee, and yaw joints. However, one IMU at the ankle joint is sufficient for all of the needed information, but with a little more math, figure 9.4. The one IMU approach though may be deemed more favorable over having one at each joint since there will be fewer wires to manage and less data to transfer over the

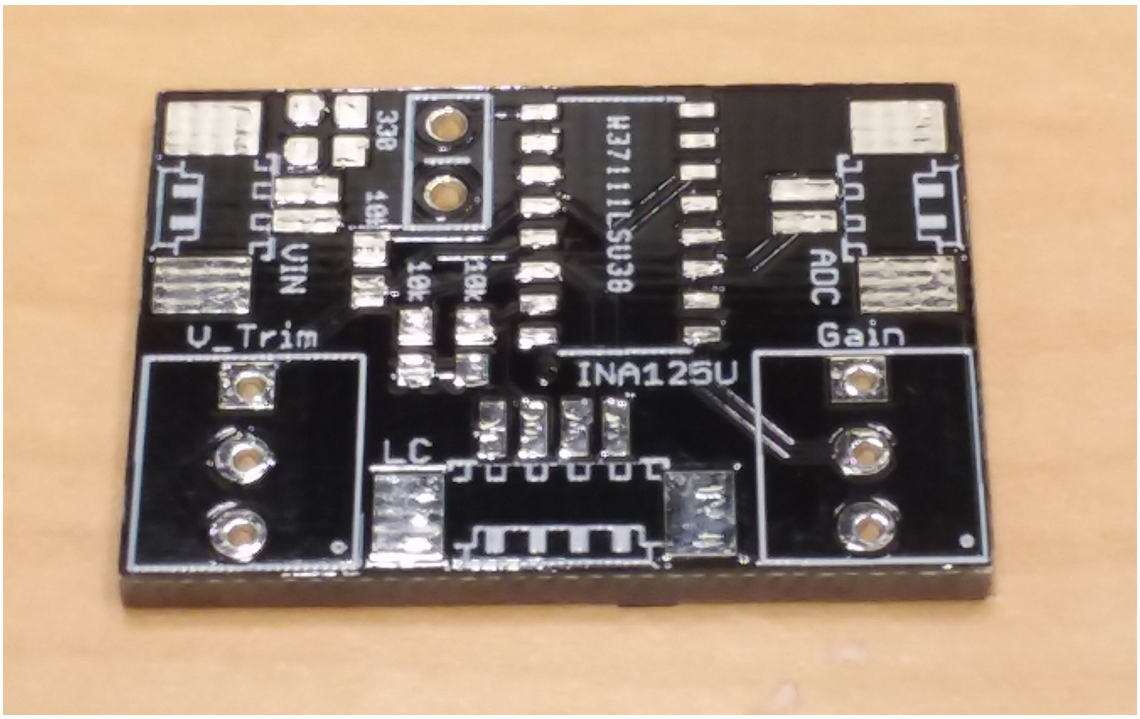

Figure 9.3: Load cell amplifier board.

IMUs communication protocol which will minimize loss of data due to noise interference.

In addition to the sensors currently employed on the prosthesis one other sensor may be added to increase the reliability of the gait transitions. The sensors which may be added are small force sensors in the foot. These force sensors do not need to be a load cell, but instead may be inexpensive force sensing resistors (figure 9.5) positioned at the heel and ball of the foot to sense, in conjunction with the actuator load cells, the heel strike and toe-off phases of the gait cycle. These would be a very simple addition to the prosthesis since it would only require setting up a few analog pins on the on-board computer for operation.

Lastly, to unlock the full potential of the BLDC helicopter motors used, a motor controller capable of higher current delivery is recommended. At present the motor controllers used are only capable of 60 A peak while the motors are capable of 75 A peak. If a new motor controller is desired, then it is recommended that the new motor controller have a current

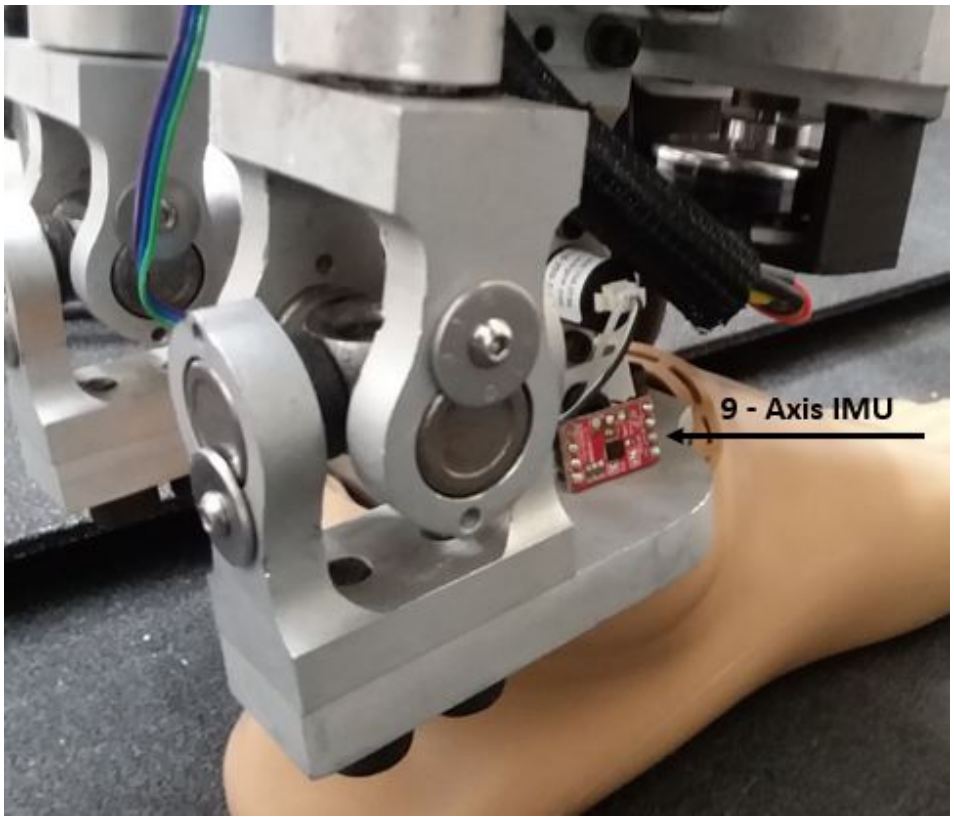

Figure 9.4: Approximate IMU placement on ankle to implement inertia modeling in future controller.

sensor output pin which will work with the ADC voltage range of the on-board computer so as to avoid making a custom PCB to scale and offset the current sensors voltage signal. Regarding the 75 A current rating for the motors, note that this is with cooling; however, for short bursts of operation which is characteristic of human locomotion cooling is less of an issue. That being said, experiments on these motors regarding their thermal constant to determine if cooling would be needed is recommended. This may be achieved by using a custom made motor mount (figure 9.6) to be connected to a lathe tool holder with the motor shaft connected to the lathe's three jaw chuck via shaft collar and shaft. The motor may then be instrumented with a thermocouple and held at stall using varying current draws to determine the thermal constant.

Figure 9.5: Force sensing resistor to be placed in the foot for heel strike and toe-off detection.

Figure 9.6: Custom motor mount for lathe testing to determine the thermal constant of the BLDC helicopter motors used in the prosthesis.

Bibliography

[1] H. Liu, C. Chen, M. Hanson, R. Chaturvedi, S. Mattke, and R. Hillestad, "Economic Value of Advanced Transfemoral Prosthetics," tech. rep., 2017.

[2] K. Lamb, "Amputation."

[3] A. Sahu, R. Sagar, S. Sarkar, and S. Sagar, "Psychological effects of amputation: A review of studies from India," *Industrial Psychiatry Journal*, vol. 25, no. 1, pp. 4–10, 2016.

[4] L. A. Holzer, F. Sevelda, G. Fraberger, O. Bluder, W. Kickinger, and G. Holzer, "Body image and self-esteem in lower-limb amputees," *PLoS ONE*, vol. 9, no. 3, pp. 1–8, 2014.

[5] R. Gailey, "Secondary Conditions Related to Prosthetic Users and Ten Steps to Reduce the Risk of Injury," *Safety and Fitness for All*, vol. 18, no. 5, pp. 14–15, 2008.

[6] Amputees Federation of New Zealand Incorporated, "Care of your back, hip, knees and shoulders," 2013.

[7] S. Michaud, S. Gard, and D. Childress, "A preliminary investigation of pelvic obliquity patterns during gait in persons with transtibial and transfemoral amputation Stephanie," *Journal of Rehabilitation Research and Development*, vol. 37, no. 1, pp. 1–10, 2000.

[8] H. Goujon-Pillet, E. Sapin, P. Fodé, and F. Lavaste, "Three-Dimensional Motions of Trunk and Pelvis During Transfemoral Amputee Gait," *Archives of Physical Medicine and Rehabilitation*, vol. 89, no. 1, pp. 87–94, 2008.

[9] S. Jaegers, J. Arendzen, and H. de Jongh, "Prosthetic Gait of Unilateral Transfemoral Amputees: A Kinematic Study," *Archives of Physical and Medicine and Rehabilitation*, vol. 76, no. 8, pp. 736–43, 1995.

[10] D. Sanderson and P. Martin, "Lower extremity kinematic and kinetic adaptations in unilateral below-knee amputees during walking," *Gait and Posture*, vol. 6, no. 2, pp. 126–136, 1997.

[11] R. L. Waters, J. Perry, D. Antonelli, and H. Hislop, "Energy Cost of Walking of Amputees: The Influence of Level of Amputation," *Journal of Bone and Joint Surgery*, vol. 58, no. A, pp. 42–46, 1976.

[12] Inger-Marie Starholm, Terje Gjovaag, and Anne Marit Mengshoel, "Energy expenditure of transfemoral amputees walking on a horizontal and tilted treadmill simulating different outdoor walking conditions," *Prosthetics and Orthotics International*, vol. 34, no. 2, pp. 184–195, 2010.

[13] R. Gailey, M. Wenger, M. Raya, N. Kirk, K. Erbs, P. Spyropoulos, and N. M.S., "Energy expenditure of trans-tibial amputees during ambulation at self-selected pace," *Prosthetics and Orthotics International*, vol. 18, pp. 84–91, 1994.

[14] C. Huang, J. Jackson, N. Moore, P. Fine, K. Kuhlemeier, G. Traugh, and P. Saunders, "Amputation: energy cost of ambulation.," *Archives of Physical Medicine and Rehabilitation*, vol. 60, no. 1, pp. 18–24, 1979.

[15] R. Eveleth, "The Future of Farmer Prosthetics," 2014.

[16] F. Sup, A. Bohara, and M. Goldfarb, "Design and Control of a Powered Transfemoral," no. 1973, 2008.

[17] "Endolite Catalogue," 2012.

[18] S. Huang, J. Wensman, and D. Ferris, "An Experimental Powered Lower Limb Prosthesis Using Proportional Myoelectric Control," *Journal of Medical Devices*, vol. 8, no. 2, 2014.

[19] Endolite, "LiNX - The Multi-Award Winning Integrated Limb System."

[20] Ottobock, "Helix 3D Hip Joint System," p. 2, 2013.

[21] Ottobock, "Genium - Bionic Prosthetic System," tech. rep., 2018.

[22] R. D. Bellman, M. A. Holgate, and T. G. Sugar, "SPARKy 3: Design of an active robotic ankle prosthesis with two actuated degrees of freedom using regenerative kinetics," in *Proceedings of the 2nd Biennial IEEE/RAS-EMBS International Conference on Biomedical Robotics and Biomechatronics, BioRob 2008*, pp. 511–516, 2008.

[23] H. Zhao, E. Ambrose, and A. D. Ames, "Preliminary results on energy efficient 3D prosthetic walking with a powered compliant transfemoral prosthesis," in *Proceedings - IEEE International Conference on Robotics and Automation*, pp. 1140–1147, IEEE, 2017.

[24] T. Sugar, "SPARKy – Spring Ankle with Regenerative Kinetics," tech. rep., 2010.

[25] A. M. Huff, B. E. Lawson, S. Members, and M. Goldfarb, "A Running Controller for a Powered Transfemoral Prosthesis," no. 1, pp. 4168–4171, 2012.

[26] A. H. Shultz, S. Member, B. E. Lawson, S. Member, and M. Goldfarb, "Running With a Powered Knee and Ankle Prosthesis," vol. 23, no. 3, pp. 403–412, 2015.

[27] T. F. Novacheck, "The biomechanics of running," vol. 7, pp. 77–95, 1998.

[28] J. M. Aldridge, J. T. Sturdy, and J. M. Wilken, "Gait & Posture Stair ascent kinematics and kinetics with a powered lower leg system following transtibial amputation §," *Gait & Posture*, vol. 36, no. 2, pp. 291–295, 2012.

[29] C. J. Nester, D. Ph, and A. F. Findlow, "Transverse Plane Motion at the Ankle Joint," pp. 164–168, 2003.

[30] C. L. Brockett, "Biomechanics of the ankle," *Orthopaedics and Trauma*, vol. 30, no. 3, pp. 232–238.

[31] J. N. Laplante and T. P. Kaeser, "The continuing evolution of pedestrian walking speed assumptions," *ITE Journal (Institute of Transportation Engineers)*, vol. 74, no. 9, pp. 32–40, 2004.

[32] A. THORSTENSSON and H. ROBERTHSON, "Adaptations to changing speed in human locomotion: speed of transition between walking and running," *Acta Physiologica Scandinavica*, vol. 131, no. 2, pp. 211–214, 1987.

[33] A. N. Lay, C. J. Hass, and R. J. Gregor, "The effects of sloped surfaces on locomotion : A kinematic and kinetic analysis," *Journal of Biomechanics*, vol. 39, pp. 1621–1628, 2006.

[34] P. Cavanagh and M. Lafortune, "Ground Reaction Forces in Distance Running *," *Journal of Biomechanics*, vol. 13, no. 5, pp. 397–406, 1980.

[35] J. Nilsson and A. Thorstensson, "Ground reaction forces at different speeds of human walking and running.," *Acta Physiologica Scandinavica*, vol. 136, no. 2, pp. 217–227, 1989.

[36] S. Ounpuu, "THE BIOMECHANICS OF WALKING AND RUNNING," *Clinics in Sports Medicine*, vol. 13, no. 4, 1994.

[37] K. W. Hollander, R. Ilg, T. G. Sugar, and D. Herring, "An Efficient Robotic Tendon for Gait Assistance," *Journal of Biomechanical Engineering*, vol. 128, no. 5, p. 788, 2006.

[38] J. Lim, H. Choi, E. K. Roh, H. Yoo, and E. Kim, "Assessment of airflow and microclimate for the running wear jacket with slits using CFD simulation," no. August, 2015.

[39] D. A. Winter, *The Biomechanics and Motor Control of Human Movement*. Hoboken, NJ: John Wiley & Sons, Inc., fourth ed., 2009.

[40] J. Storey, "Hall Effect Sensor Placement for Permanent Magnet Brushless DC Motors," 2011.

[41] S. K. AU and H. M. Herr, "Powered Ankle-Foot Prosthesis," *IEEE Robotics & Automation Magazine*, pp. 52–59, 2008.

[42] E. Rouse, L. Mooney, and L. Hargrove, "The design of a lightweight, low cost robotic knee prosthesis with selectable series elasticity," in *6th IEEE RAS/EMBS International Conference on Biomedical Robotics and Biomechatronics (BioRob)*, p. 1063, 2016.

[43] C. Knabe, R. Griffin, J. Burton, G. Cantor-Cooke, L. Dantanarayana, G. Day, O. Ebeling-Koning, E. Hahn, M. Hopkins, J. Neal, J. Newton, C. Nogales, V. Orekhov, J. Peterson, M. Rouleau, J. Seminatore, Y. Sung, J. Webb, N. Wittenstein, J. Ziglar, A. Leonessa, B. Lattimer, and T. Furukawa, "Team VALOR's ESCHER: A Novel Electromechanical Biped for the DARPA Robotics Challenge," *Journal of Field Robotics*, vol. 34, no. 5, 2017.

Appendices

Appendix A

Spreadsheets

A.1 Leaf Spring Calculations Spreadsheet

$$\Delta x_a = \frac{-F_x l}{EA}$$

	Span (mm)	Width (mm)	Thickness (mm)	Arm length(mm)	Youngs Modulus E	Moment of Inertia	Force
Case 2	50	40	8	48	1.138E+11	1.70667E-09	4400
	55	40	8	48	1.138E+11	1.70667E-09	4400
	60	40	8	48	1.138E+11	1.70667E-09	4400
	65	40	8	48	1.138E+11	1.70667E-09	4400
	70	40	8	48	1.138E+11	1.70667E-09	4400
	75	40	8	48	1.138E+11	1.70667E-09	4400
	80	40	8	48	1.138E+11	1.70667E-09	4400
	85	40	8	48	1.138E+11	1.70667E-09	4400
	90	40	8	48	1.138E+11	1.70667E-09	4400
	95	40	8	48	1.138E+11	1.70667E-09	4400
	100	40	8	48	1.138E+11	1.70667E-09	4400
	105	40	8	48	1.138E+11	1.70667E-09	4400
	110	38	8	50	1.138E+11	1.62133E-09	4400
	135	50	8.5	50	1.138E+11	2.55885E-09	7000

$$\Delta_{ym} = \frac{-F_x h l^2}{2EI} \qquad \Delta_{yb} = \frac{-F_y l^3}{3EI}$$

Slope (rad)	Deflection at R (Rx) mm	Deflection at R (Ry) mm	Deflection at Q (Qx) mm	Deflection at Q (Qy) mm
0.054371705	0.006041301	1.359292619	2.614597413	1.430225916
0.059808875	0.006645431	1.644744069	2.875760208	1.730568918
0.065246046	0.007249561	1.957381371	3.136838183	2.059514247
0.070683216	0.007853691	2.297204525	3.397823639	2.417061421
0.076120387	0.008457821	2.664213533	3.658708879	2.803209916
0.081557557	0.009061951	3.058408392	3.919486207	3.217959166
0.086994728	0.009666081	3.479789104	4.180147932	3.661308564
0.092431898	0.010270211	3.928355668	4.440686366	4.13325746
0.097869069	0.010874341	4.404108084	4.701093825	4.633805163
0.103306239	0.011478471	4.907046353	4.961362628	5.16295094
0.108743409	0.012082601	5.437170475	5.221485098	5.720694016
0.11418058	0.012686731	5.994480448	5.481453565	6.307033575
0.131159814	0.01399038	7.213789774	6.553194511	7.643246008
0.16226095	0.019538923	10.95261415	8.097032393	11.60938666

Absolute Deflection at Q (mm)	Bending Stress at R (Mpa)
2.980212376	495
3.35631726	495
3.752512854	495
4.169819108	495
4.609136198	495
5.071255596	495
5.556871164	495
6.066589868	495
6.60094186	495
7.160389761	495
7.745337091	495
8.356135811	495
10.06794755	542.7631579
14.15414399	581.3148789

A.2 Hobby Motors Selection Spreadsheet

Quick motor calculations *Choosing motors using a maximum current draw of 30A from motor controller

	RotorStar Brushless Outrunner Helicopter - 4962-480kv (700/90 size heli)	GFORCE G180 BRUSHLESS OUTRUNNER MOTOR (C6374-200KV)	Alien 6374 Outrunner brushless motor 170KV 3200W	Turnigy Aerodrive SK3 - 6374-192kv Brushless Outrunner Motor	9235-100KV Turnigy Multistar Brushless Multi-Rotor Motor	Turnigy Aerodrive SK3 - 5065-236kv Brushless Outrunner Motor	Turnigy Aerodrive SK3 - 5065-320kv Brushless Outrunner Motor	Turnigy G160 Brushless Outrunner 290kv (160 Glow)
Motor Voltage [V]	44.4	37	37	44.4	44.4	37	37	37
Motor Power [W]	2700	1100	1100	1300	1300	1100	1100	1100
Kv [rpm/V]	480	200	170	192	100	236	320	290
Motor Current [A]	60.8	29.7	29.7	29.3	29.3	29.7	29.7	29.7
Kv [rad/Volt-sec]	50.265	20.944	17.802	20.106	10.472	24.714	33.510	30.369
Ke [N-m/Amp] = 1/Kv	0.020	0.048	0.056	0.050	0.095	0.040	0.030	0.033
No-load Speed [RPM]	21312	7400	6290	8524.8	4440	8732	11840	10730
Torque [Nm]	**1.210**	**1.419**	**1.670**	**1.456**	**2.796**	**1.203**	**0.887**	**0.979**
Gear Ratio: []	50							
Torque * Gear Ratio [Nm]	**60.490**	**70.975**	**83.499**	**72.812**	**139.798**	**60.148**	**44.359**	**48.948**
Speed after gear ratio [rpm]	426.24	148	125.8	170.496	88.8	174.64	236.8	214.6
Price	$84.70	$85.00	£ 65.00	$79.96	$167.18	$56.86	$56.86	$75.83
Weight (g)	448	750	750	858	674	530	531	632
Diameter (mm)	49	62.8		59	92	49	49	63
In Stock	Yes	Yes	Custom	Yes	Yes	No	No	Yes
Torque to Weight (Nm/g)	0.00270	0.00189	0.00223	0.00170	0.00415	0.00227	0.00167	0.00155
Torque to Diameter (Nm/mm)	0.0247	0.0226		0.0247	0.0304	0.0246	0.0181	0.0155
Volume (mm^2)	3038			5074		3496		

KEDA 63-64 190KV Brushless Outrunner 10S 2000W	RotorStar Brushless Outrunner Helicopter - 4956-520kv (600/.50 size heli)	Turnigy Aerodrive SK3 - 5055-280kv Brushless Outrunner Motor	NTM Prop Drive Series 28-26A 1200kv / 286w (short shaft version)	Multistar 2206-2150KV 3~4S 320w FPV Racing Motor "The Baby Beast"	Multistar Elite 5010-274KV Multi-Rotor Motor	6340-230KV Turnigy Multistar Brushless Multi-Rotor Motors Set (2 pcs)	NTM Prop Drive Series 35-42A 1250Kv 600W	Multistar Elite 5010-274KV Multi-Rotor Motor	4108-480KV Turnigy Multistar 22 Pole Brushless Multi-Rotor Motor With Extra Long Leads	MT2814	Multistar Elite 3508-268KV High Voltage Endurance Motor
37	44.4	37	14.8	14.8	29.6	22.2	15	29.6	14.4	29.6	32
1100	2200	1100	286	320	630	650	450	630	380	400	330
190	520	280	1200	2150	274	230	1250	274	480	400	268
29.7	49.5	29.7	19.3	21.6	21.3	29.3	30.0	21.3	26.4	13.5	10.3
19.897	54.454	29.322	125.664	225.147	28.693	24.086	130.900	28.693	50.265	41.888	28.065
0.050	0.018	0.034	0.008	0.004	0.035	0.042	0.008	0.035	0.020	0.024	0.036
7030	23088	10360	17760	31820	8110.4	5106	18750	8110.4	6912	11840	8576
1.494	**0.910**	**1.014**	**0.154**	**0.096**	**0.742**	**1.216**	**0.229**	**0.742**	**0.525**	**0.323**	**0.367**
74.710	**45.496**	**50.696**	**7.689**	**4.802**	**37.089**	**60.782**	**11.459**	**37.089**	**26.250**	**16.131**	**18.373**
140.6	461.76	207.2	355.2	636.4	162.208	102.12	375	162.208	138.24	236.8	171.52
$44.52	$75.62	$49.23				$172.09		$55.02	$31.86	$39.99	$39.99
670	394	369				322		211	111	163	163
63	49	49				63		58	27	59	59
Yes	Yes	No				Yes		Yes	Yes	Yes	Yes
0.00223	0.00231	0.00275				0.00378		0.00352	0.00473	0.00198	0.00225
0.0237	0.0186	0.0207				0.0193		0.0128	0.0194	0.0055	0.0062

	Mystery Brushless Motor 5010-400 Kv		
	26.1	14.8	
	400	265	
	475	400	
	15.3	17.9	
	49.742	41.888	
	0.020	0.024	
	12397.5	5920	
	0.308	**0.427**	
	15.405	**21.373**	
	247.95	118.4	
	$39.99	$39.99	
	163	163	
	59	59	
	Yes	Yes	
	0.00189	0.00262	
	0.0052	0.0072	

A.3 Ball Screw Selection Spreadsheet

Ball Screw Pre-gearing	No Gearing	1:1.25 geared	1:1.5 geared	1:2 geared	1:2.5 geared	1:3 geared	1:3.5 geared	1:4 geared
Rotational Speed (rpm)	16500	13200	11000	8250	6600	5500	4714	4125
Linear displacement (m/s)	1.1000	0.8800	0.7333	0.5500	0.4400	0.3667	0.3143	0.2750
Linear Force (N)	2286.0	2857.5	3429.0	4572.0	5715.0	6858.0	8001.0	9144.1

Peak Velocity (rad/s)								
Lever arm length (m)	No Gearing	1:1.25 geared	1:1.5 geared	1:2 geared	1:2.5 geared	1:3 geared	1:3.5 geared	1:4 geared
0.02	55.00	44.00	36.67	27.50	22.00	18.33	15.71	13.75
0.021	52.38	41.90	34.92	26.19	20.95	17.46	14.97	13.10
0.022	50.00	40.00	33.33	25.00	20.00	16.67	14.29	12.50
0.023	47.83	38.26	31.88	23.91	19.13	15.94	13.66	11.96
0.024	45.83	36.67	30.56	22.92	18.33	15.28	13.10	11.46
0.025	44.00	35.20	29.33	22.00	17.60	14.67	12.57	11.00
0.026	42.31	33.85	28.21	21.15	16.92	14.10	12.09	10.58
0.027	40.74	32.59	27.16	20.37	16.30	13.58	11.64	10.19
0.028	39.29	31.43	26.19	19.64	15.71	13.10	11.22	9.82
0.029	37.93	30.34	25.29	18.97	15.17	12.64	10.84	9.48
0.03	36.67	29.33	24.44	18.33	14.67	12.22	10.48	9.17
0.031	35.48	28.39	23.66	17.74	14.19	11.83	10.14	8.87
0.032	34.38	27.50	22.92	17.19	13.75	11.46	9.82	8.59
0.033	33.33	26.67	22.22	16.67	13.33	11.11	9.52	8.33
0.034	32.35	25.88	21.57	16.18	12.94	10.78	9.24	8.09
0.035	31.43	25.14	20.95	15.71	12.57	10.48	8.98	7.86
0.036	30.56	24.44	20.37	15.28	12.22	10.19	8.73	7.64
0.037	29.73	23.78	19.82	14.86	11.89	9.91	8.49	7.43
0.038	28.95	23.16	19.30	14.47	11.58	9.65	8.27	7.24
0.039	28.21	22.56	18.80	14.10	11.28	9.40	8.06	7.05
0.04	27.50	22.00	18.33	13.75	11.00	9.17	7.86	6.88
0.041	26.83	21.46	17.89	13.41	10.73	8.94	7.67	6.71
0.042	26.19	20.95	17.46	13.10	10.48	8.73	7.48	6.55
0.043	25.58	20.47	17.05	12.79	10.23	8.53	7.31	6.40
0.044	25.00	20.00	16.67	12.50	10.00	8.33	7.14	6.25
0.045	24.44	19.56	16.30	12.22	9.78	8.15	6.98	6.11
0.046	23.91	19.13	15.94	11.96	9.57	7.97	6.83	5.98
0.047	23.40	18.72	15.60	11.70	9.36	7.80	6.69	5.85
0.048	22.92	18.33	15.28	11.46	9.17	7.64	6.55	5.73
0.049	22.45	17.96	14.97	11.22	8.98	7.48	6.41	5.61
0.05	22.00	17.60	14.67	11.00	8.80	7.33	6.29	5.50
0.051	21.57	17.25	14.38	10.78	8.63	7.19	6.16	5.39
0.052	21.15	16.92	14.10	10.58	8.46	7.05	6.04	5.29
0.053	20.75	16.60	13.84	10.38	8.30	6.92	5.93	5.19
0.054	20.37	16.30	13.58	10.19	8.15	6.79	5.82	5.09
0.055	20.00	16.00	13.33	10.00	8.00	6.67	5.71	5.00
0.056	19.64	15.71	13.10	9.82	7.86	6.55	5.61	4.91
0.057	19.30	15.44	12.87	9.65	7.72	6.43	5.51	4.82
0.058	18.97	15.17	12.64	9.48	7.59	6.32	5.42	4.74
0.059	18.64	14.92	12.43	9.32	7.46	6.21	5.33	4.66
0.06	18.33	14.67	12.22	9.17	7.33	6.11	5.24	4.58

Peak Torque (Nm)								
Lever arm length (m)	No Gearing	1:1.25 geared	1:1.5 geared	1:2 geared	1:2.5 geared	1:3 geared	1:3.5 geared	1:4 geared
0.02	45.72	57.15	68.58	91.44	114.30	137.16	160.02	182.88
0.021	48.01	60.01	72.01	96.01	120.02	144.02	168.02	192.03
0.022	50.29	62.87	75.44	100.58	125.73	150.88	176.02	201.17
0.023	52.58	65.72	78.87	105.16	131.45	157.73	184.02	210.31
0.024	54.86	68.58	82.30	109.73	137.16	164.59	192.03	219.46
0.025	57.15	71.44	85.73	114.30	142.88	171.45	200.03	228.60
0.026	59.44	74.30	89.15	118.87	148.59	178.31	208.03	237.75
0.027	61.72	77.15	92.58	123.44	154.31	185.17	216.03	246.89
0.028	64.01	80.01	96.01	128.02	160.02	192.03	224.03	256.03
0.029	66.29	82.87	99.44	132.59	165.74	198.88	232.03	265.18
0.03	68.58	85.73	102.87	137.16	171.45	205.74	240.03	274.32
0.031	70.87	88.58	106.30	141.73	177.17	212.60	248.03	283.47
0.032	73.15	91.44	109.73	146.30	182.88	219.46	256.03	292.61
0.033	75.44	94.30	113.16	150.88	188.60	226.32	264.03	301.75
0.034	77.72	97.16	116.59	155.45	194.31	233.17	272.04	310.90

0.035	80.01	100.01	120.02	160.02	200.03	240.03	280.04	320.04
0.036	82.30	102.87	123.44	164.59	205.74	246.89	288.04	329.19
0.037	84.58	105.73	126.87	169.17	211.46	253.75	296.04	338.33
0.038	86.87	108.59	130.30	173.74	217.17	260.61	304.04	347.47
0.039	89.15	111.44	133.73	178.31	222.89	267.46	312.04	356.62
0.04	91.44	114.30	137.16	182.88	228.60	274.32	320.04	365.76
0.041	93.73	117.16	140.59	187.45	234.32	281.18	328.04	374.91
0.042	96.01	120.02	144.02	192.03	240.03	288.04	336.04	384.05
0.043	98.30	122.87	147.45	196.60	245.75	294.90	344.05	393.19
0.044	100.58	125.73	150.88	201.17	251.46	301.75	352.05	402.34
0.045	102.87	128.59	154.31	205.74	257.18	308.61	360.05	411.48
0.046	105.16	131.45	157.73	210.31	262.89	315.47	368.05	420.63
0.047	107.44	134.30	161.16	214.89	268.61	322.33	376.05	429.77
0.048	109.73	137.16	164.59	219.46	274.32	329.19	384.05	438.91
0.049	112.01	140.02	168.02	224.03	280.04	336.04	392.05	448.06
0.05	114.30	142.88	171.45	228.60	285.75	342.90	400.05	457.20
0.051	116.59	145.73	174.88	233.17	291.47	349.76	408.05	466.35
0.052	118.87	148.59	178.31	237.75	297.18	356.62	416.05	475.49
0.053	121.16	151.45	181.74	242.32	302.90	363.48	424.06	484.63
0.054	123.44	154.31	185.17	246.89	308.61	370.33	432.06	493.78
0.055	125.73	157.16	188.60	251.46	314.33	377.19	440.06	502.92
0.056	128.02	160.02	192.03	256.03	320.04	384.05	448.06	512.07
0.057	130.30	162.88	195.45	260.61	325.76	390.91	456.06	521.21
0.058	132.59	165.74	198.88	265.18	331.47	397.77	464.06	530.36
0.059	134.87	168.59	202.31	269.75	337.19	404.62	472.06	539.50
0.06	137.16	171.45	205.74	274.32	342.90	411.48	480.06	548.64

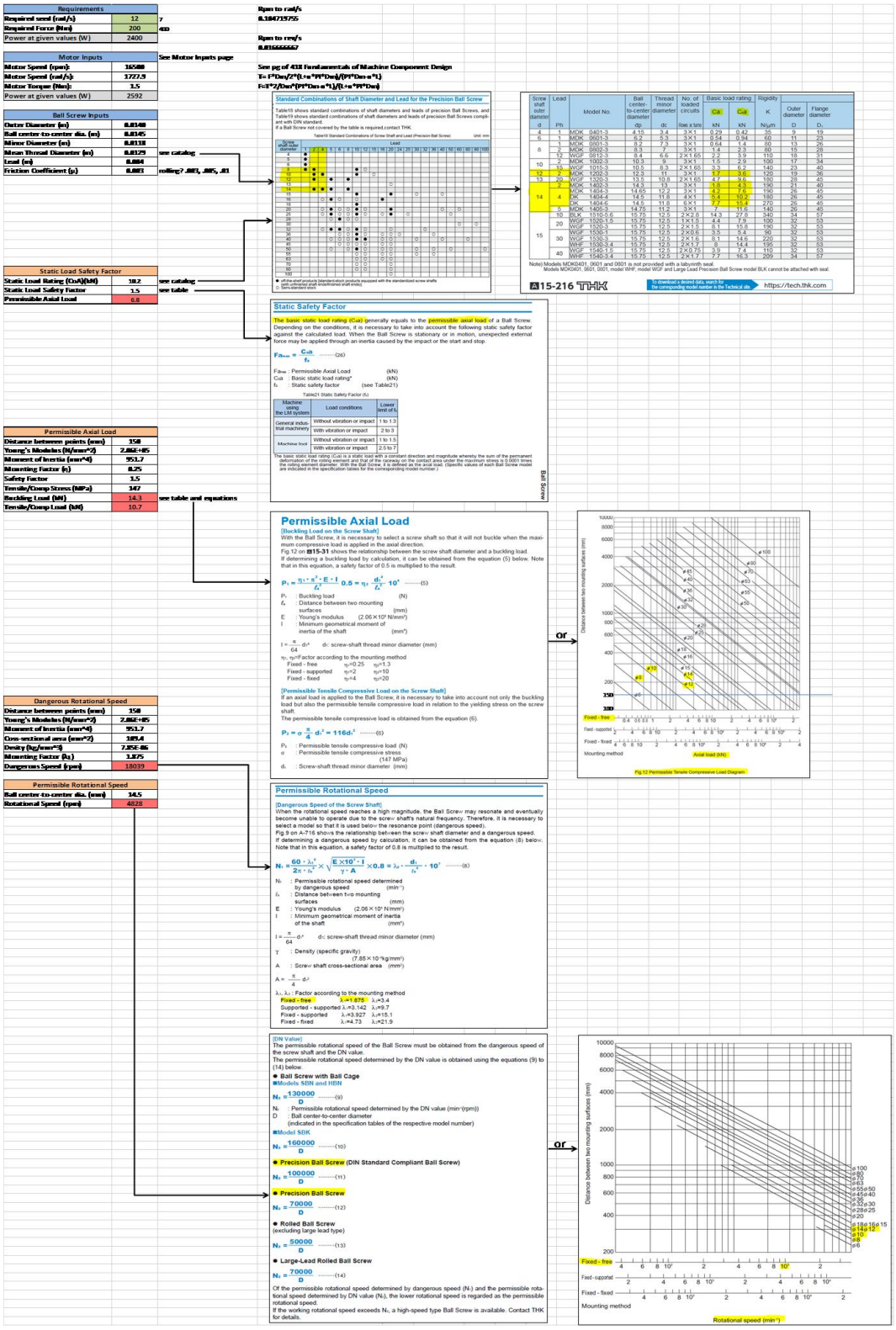
Requirements
Required speed (rad/s) 12
Required Force (Nm) 200
Power at given values (W) 2400
Motor Inputs
Motor Speed (rpm): 16588
Motor Speed (rad/s): 1737.3
Motor Torque (Nm): 1.5
Power at given values (W) 2592
Ball Screw Inputs
Outer Diameter (m) 0.0148
Ball center-to-center dia. (m) 0.0145
Minor Diameter (m) 0.0131
Mean Thread Diameter (m) 0.0139
Lead (m) 0.004
Friction Coefficient (μ) 0.007
Static Load Safety Factor
Static Load Rating (CoA)(kN) 10.2
Static Load Safety Factor 1.5
Permissible Axial Load 6.8
Permissible Axial Load
Distance between points (mm) 150
Young's Modulus (N/mm^2) 2.06E+05
Moment of Inertia (mm^4) 953.7
Mounting Factor (n) 0.25
Safety Factor 3.5
Tensile/Comp Stress (MPa) 147
Buckling Load (kN) 14.3
Tensile/Comp Load (kN) 10.7
Dangerous Rotational Speed
Distance between points (mm) 150
Young's Modulus (N/mm^2) 2.06E+05
Moment of Inertia (mm^4) 953.7
Cross-sectional area (mm^2) 189.4
Density (kg/mm^3) 7.85E-06
Mounting Factor (λ1) 1.875
Dangerous Speed (rpm) 18039
Permissible Rotational Speed
Ball center-to-center dia. (mm) 14.5
Rotational Speed (rpm) 4828
Rpm to rad/s
6.184715755
Rpm to rev/s
0.015555557
See pg of 418 Fundamentals of Machine Component Design
T= F*Dm/2*(L+π*F*Dm)/(F*Dm-π*L)
F=2*T/Dm*(F*Dm-π*L)/(L+π*F*Dm)
see Motor Inputs page
see catalog
rolling? .003, .005, .01
see catalog
see table
see table and equations
Standard Combinations of Shaft Diameter and Lead for the Precision Ball Screw
Table10 shows standard combinations of shaft diameters and leads of precision Ball Screws, and Table19 shows standard combinations of shaft diameters and leads of precision Ball Screws compliant with DIN standard.
If a Ball Screw not covered by the table is required,contact THK.
Table10 Standard Combinations of Screw Shaft and Lead (Precision Ball Screw) Unit: mm
Screw shaft outer diameter
Lead
1 2 4 5 6 8 8 10 12 15 16 20 24 25 30 32 36 40 50 60 80 100
4
5
6
8
10
12
14
15
16
17
18
20
25
28
30
32
40
45
50
55
63
70
80
100
● : All the shaft products (standard-shaft products and products equipped with the standardized screw shafts (with unfinished shaft ends/finished shaft ends)
○ : Semi-standard stock
Screw shaft outer diameter
Lead
Model No.
Ball center-to-center diameter
Thread minor diameter
No. of loaded circuits
Basic load rating
Rigidity
K
Outer diameter
Flange diameter
d
Ph
dp
dc
Ras x turns
Ca
Coa
kN
kN
N/μm
D
D1
4 1 MDK 0401-3 4.15 3.4 3×1 0.29 0.42 35 9 19
6 1 MDK 0601-3 6.2 5.3 3×1 0.54 0.94 60 11 23
1 MDK 0801-3 8.2 7.3 3×1 0.64 1.4 80 13 26
8 2 MDK 0802-3 8.3 7 3×1 1.4 2.3 80 15 28
12 WGF 0812-3 8.4 6.6 2×1.65 2.2 3.9 110 18 31
10 2 MDK 1002-3 10.3 9 3×1 1.5 2.9 100 17 34
10 WGF 1010-3 10.5 8.3 2×1.65 3.3 6.2 140 23 40
12 2 MDK 1202-3 12.3 11 3×1 3.2 3.6 120 19 36
13 20 WGF 1320-3 13.5 10.8 2×1.65 4.7 9.6 180 28 45
2 MDK 1402-3 14.3 13 3×1 3.8 4.3 190 21 40
MDK 1404-3 14.65 12.2 3×1 4.2 7.6 190 26 45
14 4 BK 1404-4 14.5 11.8 4×1 5.4 10.7 180 26 45
DK 1404-6 14.5 11.8 6×1 7.7 15.4 270 26 45
6 MDK 1405-3 14.75 11.2 3×1 7 11.6 140 26 45
10 BLK 1510-5.6 15.75 12.5 2×2.8 14.3 27.8 340 34 57
WGF 1520-1.5 15.75 12.5 1×1.5 4.4 7.9 100 32 53
20 WGF 1520-3 15.75 12.5 2×1.5 8.1 15.8 190 32 53
WGF 1530-1 15.75 12.5 2×0.6 3.5 5.4 90 32 53
15 30 WGF 1530-3 15.75 12.5 2×1.6 8.1 14.5 220 32 53
WHF 1530-3.4 15.75 12.5 2×1.7 8 14.4 195 32 53
40 WGF 1540-1.5 15.75 12.5 2×0.75 3.9 7.4 110 32 53
WHF 1540-3.4 15.75 12.5 2×1.7 7.7 16.3 209 34 57
Note) Models MDK0401, 0601 and 0801 is not provided with a labyrinth seal.
Models MDK0401, 0601, 0801, model WHF, model WGF and Large Lead Precision Ball Screw model BLK cannot be attached with seal.
A15-216 THK
To download a desired data, search for the corresponding model number in the Technical site
https://tech.thk.com
Static Safety Factor
The basic static load rating (Coa) generally equals to the permissible axial load of a Ball Screw. Depending on the conditions, it is necessary to take into account the following static safety factor against the calculated load. When the Ball Screw is stationary or in motion, unexpected external force may be applied through an inertia caused by the impact or the start and stop.
Fa = Coa / fs ·····(26)
Fa : Permissible Axial Load (kN)
Coa : Basic static load rating* (kN)
fs : Static safety factor (see Table21)
Table21 Static Safety Factor (fs)
Machine using the LM system
Load conditions
Lower limit of fs
General industrial machinery
Without vibration or impact 1 to 1.3
With vibration or impact 2 to 3
Machine tool
Without vibration or impact 1 to 1.5
With vibration or impact 2.5 to 7
The basic static load rating (Coa) is a static load with a constant direction and magnitude whereby the sum of the permanent deformation of the rolling element and that of the raceway on the contact area under the maximum stress is 0.0001 times the rolling element diameter. With the Ball Screw, it is defined as the axial load. (Specific values of each Ball Screw model are indicated in the specification tables for the corresponding model number.)
Ball Screw
Permissible Axial Load
[Buckling Load on the Screw Shaft]
With the Ball Screw, it is necessary to select a screw shaft so that it will not buckle when the maximum compressive load is applied in the axial direction.
Fig.12 on B15-31 shows the relationship between the screw shaft diameter and a buckling load.
If determining a buckling load by calculation, it can be obtained from the equation (5) below. Note that in this equation, a safety factor of 0.5 is multiplied to the result.
Pc = η1·π²·E·I / la² × 0.5 = η2 · d1⁴ / la² · 10⁷ ·····(5)
Pc : Buckling load (N)
la : Distance between two mounting surfaces (mm)
E : Young's modulus (2.06×10⁴ N/mm²)
I : Minimum geometrical moment of inertia of the shaft (mm⁴)
I = π/64 · d1⁴ d1: screw-shaft thread minor diameter (mm)
η1, η2=Factor according to the mounting method
Fixed - free η1=0.25 η2=1.3
Fixed - supported η1=2 η2=10
Fixed - fixed η1=4 η2=20
[Permissible Tensile Compressive Load on the Screw Shaft]
If an axial load is applied to the Ball Screw, it is necessary to take into account not only the buckling load but also the permissible tensile compressive load in relation to the yielding stress on the screw shaft.
The permissible tensile compressive load is obtained from the equation (6).
Pt = σ · π/4 · d1² = 116d1² ·····(6)
Pt : Permissible tensile compressive load (N)
σ : Permissible tensile compressive stress (147 MPa)
d1 : Screw-shaft thread minor diameter (mm)
Distance between two mounting surfaces (mm)
Fixed - free
Fixed - supported
Fixed - fixed
Mounting method
Axial load (kN)
Fig.12 Permissible Tensile Compressive Load Diagram
Permissible Rotational Speed
[Dangerous Speed of the Screw Shaft]
When the rotational speed reaches a high magnitude, the Ball Screw may resonate and eventually become unable to operate due to the screw shaft's natural frequency. Therefore, it is necessary to select a model so that it is used below the resonance point (dangerous speed).
Fig.9 on A-716 shows the relationship between the screw shaft diameter and a dangerous speed.
If determining a dangerous speed by calculation, it can be obtained from the equation (8) below. Note that in this equation, a safety factor of 0.8 is multiplied to the result.
Nc = 60·λ1²/(2π·la²) × √(E×10⁷·I/(γ·A)) ×0.8 = λ2 · d1/la² · 10⁷ ·····(8)
Nc : Permissible rotational speed determined by dangerous speed (min⁻¹)
la : Distance between two mounting surfaces (mm)
E : Young's modulus (2.06×10⁴ N/mm²)
I : Minimum geometrical moment of inertia of the shaft (mm⁴)
I = π/64 · d1⁴ d1: screw-shaft thread minor diameter (mm)
γ : Density (specific gravity) (7.85×10⁻⁶kg/mm³)
A : Screw shaft cross-sectional area (mm²)
A = π/4 · d1²
λ1, λ2 : Factor according to the mounting method
Fixed - free λ1=1.875 λ2=3.4
Supported - supported λ1=3.142 λ2=9.7
Fixed - supported λ1=3.927 λ2=15.1
Fixed - fixed λ1=4.73 λ2=21.9
[DN Value]
The permissible rotational speed of the Ball Screw must be obtained from the dangerous speed of the screw shaft and the DN value.
The permissible rotational speed determined by the DN value is obtained using the equations (9) to (14) below.
● Ball Screw with Ball Cage
■Models SBN and HBN
Nc = 130000/D ·····(9)
Nc : Permissible rotational speed determined by the DN value (min⁻¹(rpm))
D : Ball center-to-center diameter (indicated in the specification tables of the respective model number)
■Model SBK
Nc = 160000/D ·····(10)
● Precision Ball Screw (DIN Standard Compliant Ball Screw)
Nc = 100000/D ·····(11)
● Precision Ball Screw
Nc = 70000/D ·····(12)
● Rolled Ball Screw (excluding large lead type)
Nc = 50000/D ·····(13)
● Large-Lead Rolled Ball Screw
Nc = 70000/D ·····(14)
Of the permissible rotational speed determined by dangerous speed (Nc) and the permissible rotational speed determined by DN value (Nc), the lower rotational speed is regarded as the permissible rotational speed.
If the working rotational speed exceeds Nc, a high-speed type Ball Screw is available. Contact THK for details.
Distance between two mounting surfaces (mm)
Fixed - free
Fixed - supported
Fixed - fixed
Mounting method
Rotational speed (min⁻¹)
or

Appendix B

Gait Cycle Plots

B.1 0.447 m/s (1 mph) Walking Gait

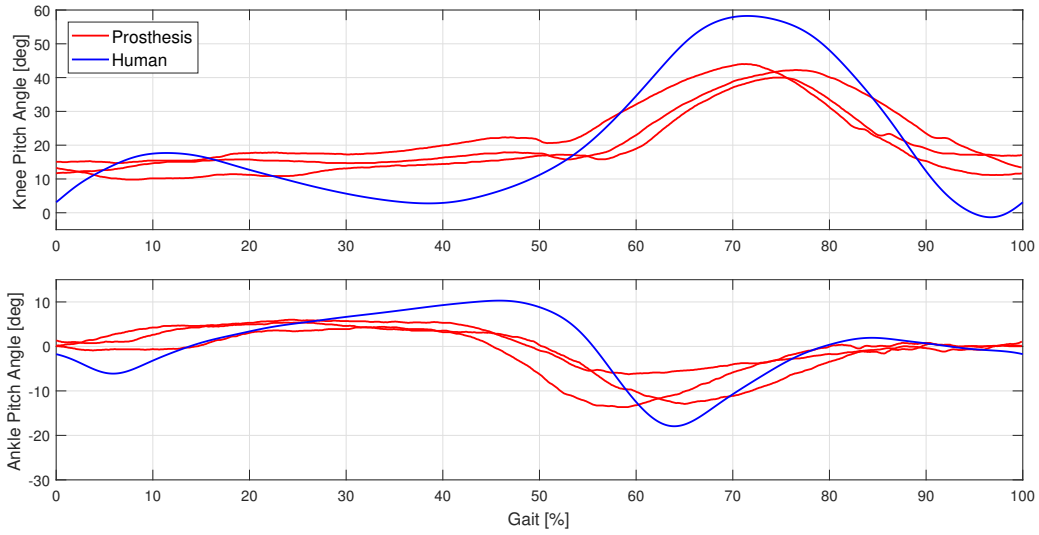

Figure B.1: Top: Knee pitch angle vs. gait percent. Bottom: Ankle pitch angle vs. gait percent

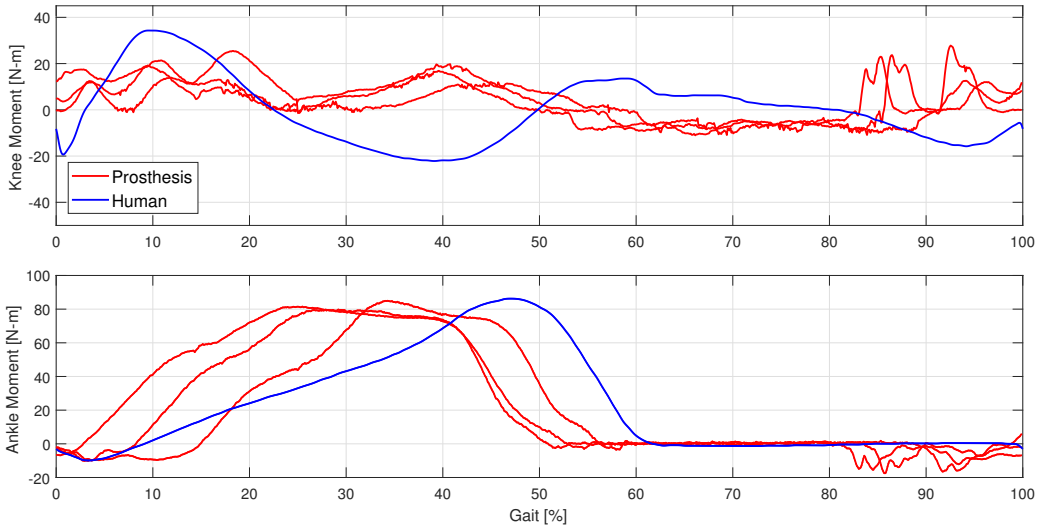

Figure B.2: Top: Knee joint moment vs. gait percent. Bottom: Ankle joint moment vs. gait percent.

B.2 0.67 m/s (1.5 mph) Walking Gait with Mode Transitions

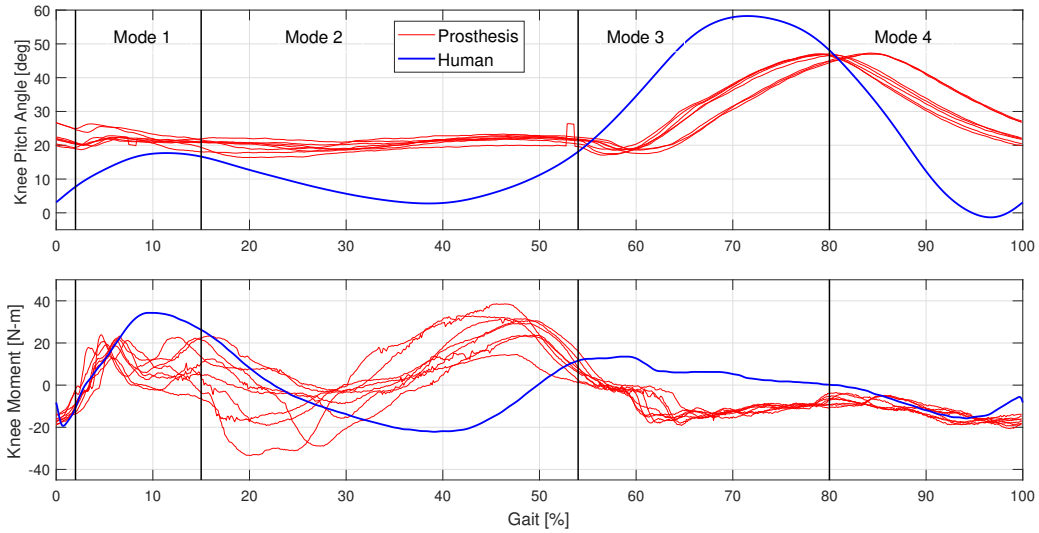

Figure B.3: Top: Knee pitch angle vs. gait percent. Bottom: Knee joint moment vs. gait percent. The transitions are given by the vertical black lines and indicate when each gait mode was entered.

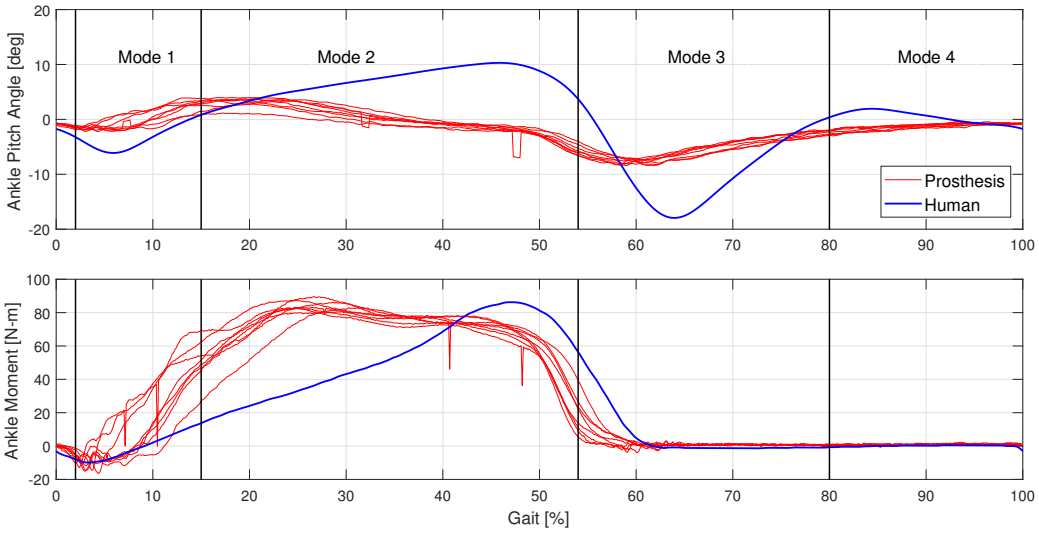

Figure B.4: Top: Ankle pitch angle vs. gait percent. Bottom: Ankle joint moment vs. gait percent. The transitions are given by the vertical black lines and indicate when each gait mode was entered.